POLITECNICO
MILANO 1863

SCUOLA DI INGEGNERIA INDUSTRIALE
E DELL'INFORMAZIONE

Relationship between attenuation and phase delay due to rain in the 10-100 GHz frequency range

Tesi di Laurea Magistrale in
Space Engineering - Ingegneria Aerospaziale

Author: **Salim ABBOUDI**

Student ID: 963735
Advisor: Prof. Lorenzo Luini

Academic Year: 2021-2022

Abstract

The aim of this dissertation is to present an analytical relationship linking attenuation to phase delay due to rain based on a statistical model of the horizontal rain rate structure -EXCELL and depending on the link parameters.

The EXCELL model constitutes a simple but solid model to represent the rain structure: by simulating the different scenarios between the station and the satellite, and using a combination of exponential cells, results can be used to derive the fitting relationship between phase delay and attenuation.

This relationship is investigated to derive an analytical global model linking attenuation to phase delay along the path as a function of three main parameters : frequency, projection of the slant path on the ground L_H involving the rain height and the elevation angle θ and finally μ value characterising the gamma drop size distribution

Keywords: EXCELL, attenuation, phase delay, frequency, horizontal slant path, drop size distribution

Abstract in lingua italiana

Lo scopo di questa tesi è presentare una relazione analitica che lega l'attenuazione al ritardo di fase dovuto alla pioggia, basata su un modello statistico della struttura orizzontale del tasso di pioggia -EXCELL e dipendente dai parametri del collegamento. guida

Il modello EXCELL costituisce un modello semplice ma solido per rappresentare la struttura della pioggia: simulando i diversi scenari tra la stazione e il satellite e utilizzando una combinazione di celle esponenziali, i risultati possono essere utilizzati per ricavare la relazione di adattamento tra ritardo di fase e attenuazione.

Questa relazione viene studiata per ricavare un modello analitico globale che collega l'attenuazione al ritardo di fase lungo il percorso in funzione di tre parametri principali: la frequenza, la proiezione del percorso obliquo sul terreno L_H che coinvolge l'altezza della pioggia e l'angolo di elevazione θ e infine il valore μ che caratterizza la distribuzione delle dimensioni delle gocce gamma.

Parole chiave: attenuazione , ritardo di fase, frequenza, percorso obliquo orizzontale, distribuzione delle dimensioni delle gocce

Contents

List of Figures

List of Tables

Nomenclature

$\boldsymbol{A}$	Attenuation due to rain [db]	$\boldsymbol{\tau}$	Phase delay due to rain [ps]
$\boldsymbol{\gamma_R}$	Specific attenuation [db/Km]	$\boldsymbol{\varphi_R}$	Specific phase delay [ps/km]
$\boldsymbol{R}$	Rain rate [mm/h]	$\boldsymbol{R_M}$	Cell's peak rain rate [mm/h]
$\boldsymbol{\rho_0}$	Cell's effective radius [Km]	$\boldsymbol{R_{th}}$	Threshold rain rate [mm/h]
$\boldsymbol{f}$	Link frequency [GHz]	$\boldsymbol{\theta}$	Elevation angle [deg]
$\boldsymbol{\psi}$	Polarisation angle [deg]	$\boldsymbol{H_R}$	Rain height [Km]
$\boldsymbol{L_H}$	Horizontal path [Km]	$\boldsymbol{L}$	Slant path [Km]
$\boldsymbol{\mu}$	Gamma distribution parameter[–]	$\boldsymbol{r_{cell}}$	Cell radius [Km]
$\boldsymbol{dx}$	Map resolution [Km]	$\boldsymbol{N_{pixels}}$	Number of map pixels [–]
$\boldsymbol{k, \alpha, h, \beta}$	Experimental coefficients [–]	$\boldsymbol{h_0}$	Isothermal layer height [Km]
$\boldsymbol{N(D)}$	Drop Size distribution $[m^{-3}mm^{-1}]$	$\boldsymbol{rms}$	Root mean square
$\boldsymbol{x, y}$	Map coordinates [Km]	$\boldsymbol{k}$	Propagation constant $[m^{-1}]$
$\boldsymbol{ccdf}$	Cumulative distribution function [–]	$\boldsymbol{P}$	Probability [–]
$\boldsymbol{D}$	Drop size diameter [mm]	$\boldsymbol{v(D)}$	Terminal velocity of drops [m/s]

Acknowledgements

I would like to thank Prof. Lorenzo Luini for giving me the opportunity to do this work with him, for his patience , his availability and for his help. For just being an invaluable companion during all the process.

Symbolically, to me, the present work is more than "just" a Master's Thesis. It represents the final milestone of my university studies,and the best way to end a track lasted almost 20 years ever since I enrolled to school, an important phase of my life whose epitome is hard work , determination and dedication , This road has been sometimes very treacherous but very amazing , I learnt many things , I raised myriad challenges and I thrived personally before professionally So I would like to take this chance to thank all the people who have been part of that journey.

I want to thank all the professors I have had during university, here in Politecnico di Milano and in Centrale Marseille , and my teachers of CPGE who had a huge impact on my personality and my career , But I want to extend it with enthusiasm to those teachers who set my foundation as a student before university, since I was a child. It is thanks to them that I made it here and I cherish their memories.

But most of all, I want to thank my parents , my brother and my sister for their unconditional love and support but also for the inspiration , the motivation and the power they inculcated in me .

Milano , October 2022 *S.A*

Introduction

Shifting to new high frequency bands typically above 10 GHz like Ka, Q or even V bands has became recently vital to comply with the increasing demands in high bandwidth, data rate and availability but more importantly to overcome the lower frequency bands 's crowding, the next future wireless telecommunications systems are expected to provide reel time multimedia availability to meet with ever increasing customer services [18]. However the higher frequencies are considerably affected by rainfall; attenuation and phase delay are major aspects putting in jeopardy the user requirements meeting, therefore it is necessary to mitigate rain attenuation to ensure the quality of the link, to this purpose, dynamic attenuation mitigation methods or fade mitigation techniques(FMT)[2] are implemented alongside attenuation prediction models to predict the projected attenuation of the link. Many studies have been conducted on this issue worldwide,where by investigating geographically distributed locations, we can develop and analyze rain attenuation models applicable over a wide frequency range, apply FMT first, plan the link budget and finally design the system ensuring the best quality for the service.
It was shown that rain attenuation could reduce the throughput of a link compared to sunny weather conditions [8], likely by deploying an appropriate rain attenuation model, even in the rain, a terrestrial link's throughput can be kept unchanged compared to a case without deploying any FMT and with the condition that other parts are usually working, an appropriate model requires the collection of factors impacting attenuation like path length, frequency, elevation angle, polarisation angle, rain drop size distribution (DSD)... Thus, rain attenuation models play a significant role in the FMT operation in a transmission system, the reader can find in [19] a holistic and critical review of 18 well-known rain attenuation prediction models assessed,classified,evaluated,compared, and summarized .
At high frequencies the most serious problems in system design come from attenuation, depolarization and scattering interference by precipitation particles along the radio path. The statistical description of these effects, which is needed by system engineers, can be obtained by two different approaches: direct measurements of the quantities of interest or their evaluation through simulations or models taking into account the characteristics of precipitation. Since Radar measured data are not always available ,the second reason

behind developing rainfall models is to aggregate those characteristics and build a suitable rain framework capable of escaping the necessity of radar measurements.

Several measurements and modeling of rain attenuation exist in the literature, and [19] summarizes the majority of models that have been used, this abundance unlikely is faced by a rarity of phase delay models, the reason why deriving a relationship linking the latter to attenuation is crucial as a solid baseline to extend the model for several sites, thus with reference to [14] where an analytical model is developed based on the synthetic storm technique(SST), the SST can generate rain attenuation and phase delay (or phase) time series at any frequency and polarization, for any slant path above about 10 degrees, at any site. A synthetic storm is obtained by converting a rain rate time series, recorded at a point by a rain gauge, to a rain rate space series along a line, by using an estimate of the storm translation speed to transform time to distance, .This thesis work uses therefore the EXCELL model [5] to establish a similar analytical relationship, but includes moreover the drop size distribution as one of its parameters.

EXCELL, unlike the other radar-measured ground rain models, is used to devise and assess its use in some of the future telecommunication applications. The model is based on cells of exponential profile (which is shown to reproduce best the point rain rate cumulative distribution function CDF); both rotational and bi axial symmetries are considered for the horizontal cross sections.

Past works have shown that the relationship between the specific rain attenuation γ_R in dB/km and the rain rate (R) can be modelled using a simple power-law expression [13]. The same is valid for the relationship between the phase shift φ_R in degrees/km and rain rate (R).

The EXCELL model was then used to calculate both attenuation and phase delay and dissect their relationship dependency on the link main parameters : frequency- DSD- rain height- elevation angle, the last two parameters were combined in a new variable: the projection of the slant path on the ground, which is the key parameter for a horizontal rain rate profile (EXCELL).

Notwithstanding the few studies on rain attenuation and phase delay conducted in the past, no comprehensive models are available to describe analytically the specific attenuation due to rain and phase delay relationship using a physical model EXCELL and as a function of frequency, horizontal path and different DSDs.

This work aims then at filling the gap in the literature by presenting an analytical model for the attenuation and delay due to rain relationship as a function of different drop size distributions in the 10-100 GHz range. The procedure analyzes at first different parameters affecting attenuation and phase delay, then once identified, the attenuation-phase delay data is fitted with an analytical model depending on three main parameters. In order to compute its error ,two different approach were used, once is numerical and the other is statistical using the cumulative distributed function generated considering the SC-EXCELL given site and the given parameters. The model is tuned iteratively until its error is accepted. Finallly, the final model found is compared to Matricciani's one [15].

1 | Effect Of Rain On Telecommunications Systems

To be successful, a satellite service must be competitive with a terrestrial alternative if one is available. The level of service must equal or exceed the terrestrial service at a comparable cost if the satellite solution is to gain acceptance among potential customers. When there are two alternatives, the choice of a satellite system will involve considerations of cost, the amount of user equipment, ease of use and reliability. For example, a potential broadband customer would have an expectation of an affordable subscription rate, convenient installation, superior performance and high availability. One of the factors that affects availability in a satellite communication link is rain.An electromagnetic wave, propagating in rainy conditions is affected in three different ways :

- The wave is attenuated
- The wave polarisation is changed

Both mechanisms can be combined simultaneously causing a degradation in the received signal quality. At C-band (4-8 GHz) the effects are minor and at Ku-band(11-20 GHz), while they are noticeable, can be accommodated. But at higher frequencies, such as Ka-band (27-40 GHz) or V-band (40-70 GHz), the degradation can be so great that it simply cannot be compensated for to reach the level of availability usually expected for lower frequencies.

1.1. Attenuation

The first, and most well known, effect of rain is that it attenuates the signal. The attenuation is caused by the scattering and absorption of electromagnetic waves by drops of liquid water [16]. The scattering diffuses the signal, while absorption involves the penetration of the wave within the drops, with following dissipation of the EM energy into heat. Absorption increases the molecular energy, corresponding to a slight increase in temperature, and results in an equivalent loss of signal energy. Attenuation is negligible

for snow or ice crystals (up to the W band), in which the molecules are tightly bound and do not interact with the waves.

The attenuation increases as the wavelength approaches the size of a typical raindrop, which is about 1.5 millimeters. Wavelength in a hydrometeor depends on the phase constant β

$$\lambda = \frac{2\pi}{\beta}$$

The propagation constant γ depends also on the attenuation constant α

$$\gamma = \alpha + i\beta \tag{1.1}$$

We recall the Helmolthz equation for the electric field E, derived from Maxwell's equations in a lossy medium :

$$\nabla^2 E = \gamma^2 E \tag{1.2}$$

Where :

$$\gamma^2 = i\frac{2\pi}{f}\mu(\sigma + i\frac{2\pi}{f}\epsilon) \tag{1.3}$$

f is the frequency, σ is the medium conductivity, ϵ is medium's permittivity and μ is the medium's permeability.eq. (1.3) depicts the relationship between the wavelength and frequency and for example, at the C-band downlink frequency of 4 GHz, the wavelength is 75 millimeters. The wavelength is thus 50 times larger than a raindrop and the signal passes through the rain with relatively small attenuation. At the Ku-band downlink frequency of 12 GHz, the wavelength is 25 millimeters. Again, the wavelength is much greater than the size of a raindrop, although not as much as at C-band. At Ka-band, with a downlink frequency of 20 GHz, the wavelength is 15 millimeters and at V-band, at a downlink frequency of 40 GHz, it is only 7.5 millimeters. At these frequencies, the wavelength and raindrop size are comparable and the attenuation is quite large.

Considerable research has been carried out to model rain attenuation mathematically and to characterize rainfall throughout the world. For example, experimental measurement and methods of analysis are discussed in the book Radiowave Propagation in Satellite Communications by Louis J. Ippolito [9]. The standard method of representing rain attenuation is through an integration along the slant path L of an equation of the form

$$A = \int_{x,y \in L} aR^b(x,y) \tag{1.4}$$

which can be simplified as:

$$A = aR^b L_{equ} \tag{1.5}$$

where A is the rain attenuation in decibels (dB), R is the rain rate in millimeters per hour, L_{equ} is an equivalent path length (km), and a and b are empirical coefficients that depend on frequency, elevation angle... The equivalent path length depends on the angle of elevation to the satellite, the height of the rain layer, and the latitude of the earth station.

The rain rate enters into this equation because it is a measure of the average size of the raindrops. When the rain rate increases, i.e. it rains harder, the raindrops are larger and thus there is more attenuation. Rain models differ principally in the way the effective path length L is calculated. Two authoritative rain models that are widely used are the Crane model and the ITU-R (CCIR) model.

The original Crane model is the global model. A revision of this model that accounts for both the dense center and fringe area of a rain cell is the so-called two component model. These models are discussed in detail in the book Electromagnetic Wave Propagation Through Rain by Robert K. Crane [7] which is accompanied by spreadsheet add-in software.

In the design of any engineering system, it is impossible to guarantee the performance under every conceivable condition. One sets reasonable limits based on the conditions that are expected to occur at a given level of probability. For example, a bridge is designed to withstand loads and stresses that are expected to occur in normal operation and to withstand the forces of wind and ground movement that are most likely to be encountered. But even the best bridge design cannot compensate for a tornado or an earthquake of unusual strength.

Similarly, in the design of a satellite communications link one includes margin to compensate for the effects of rain at a given level of availability. The statistical characterization of rain begins by dividing the world into rain climate zones. Within each zone, the maximum rain rate for a given probability is determined from actual meteorological data accumulated over many years.

For a digital signal, the required signal power is determined by the bit rate, the bit error rate, the method of coding, and the method of modulation. The performance objective is specified by the bit error rate. If the maximum allowed rain rate is exceeded, the bit error rate would increase at the nominal bit rate, or else the bit rate would have to decrease to maintain the required bit error rate.

At C-band, the rain attenuation for an elevation angle of 40 degrees and a maximum rain rate of 22.3 mm/h in Washington, DC is 0.1 dB. This is practically a negligible effect. At Ku-band, under the same conditions, the attenuation is 4.5 dB. This is a large but manageable contribution to the link budget. However, at the Ka-band downlink frequency of 20 GHz, the attenuation is 12.2 dB. This would be a significant effect, requiring over 16 times the power called for in clear sky conditions. At the uplink frequency of 30 GHz, the attenuation would be 23.5 dB, requiring over 200 times the power. At the V-band downlink frequency of 40 GHz, the attenuation would be 34.6 dB and at the uplink frequency of 50 GHz the attenuation would be 43.7 GHz. These losses simply cannot be accommodated and thus the availability would be much less.

In practice, these high rain attenuations are sometimes avoided by using site diversity, in which two widely separated earth stations are used. The probability that both earth stations are within the same area of rain concentration is small. Alternatively, a portion of spectrum in a lower frequency band may be used where needed. For example, a hybrid Ka-band/Ku-band system might be designed in which Ka-band provides plentiful spectrum in regions of clear weather, but Ku-band is allocated to regions in which the rain margin at Ka-band is exceeded

1.2. Depolarisation

Rain also changes the polarization of the signal somewhat. Due to the resistance of the air, a falling raindrop assumes the shape of an oblate spheroid. Wind and other dynamic forces cause the raindrop to be rotated at a statistical distribution of angles. Consequently, the transmission path length through the raindrop is different for different signal polarizations and the polarization of the received signal is altered.

For a satellite communication system with dual linear polarizations, the change in polarization has two effects. First, there is a loss in the signal strength because of misalignment of the antenna relative to the clear sky orientation given by

$$L = 20log(cos(t)) \tag{1.6}$$

where t is the tilt angle relative to the polarization direction induced by the rain. Second, there is additional interference noise due to the admission of a portion of the signal in the opposite polarization. The average canting angle with respect to the local horizon can be taken to be 25 degrees.

It is an interesting property of earth-satellite geometry that a linearly polarized signal is not oriented with the local horizontal and vertical directions, even though a horizontally polarized signal is parallel to the equatorial plane and a vertically polarized signal is perpendicular to the equatorial plane when transmitted from the satellite. Thus the optics of the earth station antenna must be correctly rotated in order to attain the appropriate polarization alignment with the satellite. The earth station feed rotation angle q is :

$$tan(q) = G\frac{sin\delta l}{tanf} \tag{1.7}$$

where f is the latitude of the earth station, δl is the difference in longitude, and G is a geometrical factor that for a geostationary satellite is nearly unity. For example, in Milan , at a latitude of 45.46 degrees, the antenna polarization must be rotated by about 9.7 degrees if the difference in longitude between the earth station and satellite is 10 degrees.

Since in this thesis work we focus only on the first aspect i.e attenuation and phase delay , in the next subsection we will introduce some theoretical aspects to investigate the reason behind both attenuation and phase delay .

1.3. Specific Attenuation and phase delay

When a plane electromagnetic wave with polarization vector $\hat{\mathbf{e}}$ is incident on a raindrop at the origin, it induces a transmitted field in the interior of the drop and a scattered field. Assuming that the incident wave with unit amplitude and frequency f is propagating in direction $\hat{\mathbf{K}}_1$, the scattered electric field, $\mathbf{E}^s$, toward direction $\hat{\mathbf{K}}_2$ may be written in the far-field region as:

$$\mathbf{E}^s = \mathbf{f}\left(\hat{\mathbf{K}}_1, \hat{\mathbf{K}}_2\right)\frac{1}{r}\exp\left(-\gamma_0 r\right) \tag{1.8}$$

where vector function $\mathbf{f}\left(\hat{\mathbf{K}}_1, \hat{\mathbf{K}}_2\right)$, often referred to as "scattering amplitude", denotes the amplitude, phase, and the state of polarization of the scattered field, r is the distance from the origin to the observation point, and γ_0 is the free-space propagation constant defined by $i2\pi f/c_0$, where c_0 is the speed of light in free space. An $\exp(+i2\pi ft)$ time convention is assumed and is suppressed.

The propagation constant, γ, in a space containing many raindrops is given by :

$$\gamma = \gamma_0 + \frac{2\pi}{\gamma_0}\int_D \hat{\mathbf{e}}\cdot\mathbf{f}\left(\hat{\mathbf{K}}_1, \hat{\mathbf{K}}_1, D\right)n(D)dD \tag{1.9}$$

where $\mathbf{f}\left(\hat{\mathbf{K}}_1, \hat{\mathbf{K}}_1, D\right)$ denotes the forward scattering amplitude of a raindrop with diameter D, and $n(D)dD$ is the number of drops per cubic meter in space with diameter D in range dD and is a function of rainfall rate R. Since the propagation factor in a rain medium is $\exp(-\gamma r)$, the real $\Re$ and imaginary part $\Im$ of γ are respectively responsible for attenuation and phase shift of the wave propagating in the rain medium.
The specific attenuation due to rain γ_R, and specific phase delay due to rain φ_R, are then given in dB/km and deg/km and can written

$$\gamma_R = \Re(\gamma) = 2\pi\ \Re(\int_D \frac{\hat{\mathbf{e}} \cdot \mathbf{f}\left(\hat{\mathbf{K}}_1, \hat{\mathbf{K}}_1, D\right)}{\gamma_0} n(D)dD) \tag{1.10}$$

$$\varphi_R = \Im(\gamma) = \frac{2\pi f}{c} + 2\pi\ \Im(\int_D \frac{\hat{\mathbf{e}} \cdot \mathbf{f}\left(\hat{\mathbf{K}}_1, \hat{\mathbf{K}}_1, D\right)}{\gamma_0} n(D)dD) \tag{1.11}$$

Hence eqs. (1.10) and (1.11) give theoretical hints on the specific attenuation and specific phase delay calculations , further explanations can be found in [17].
Drop-size distribution $n(D)$ can be obtained by measuring the size distribution of raindrops reaching the ground, and converting it to a distribution in space with the aid of the fall velocity of raindrops. The drop-size distribution is a function of the rainfall rate, and depends on rain types. Although the measurements were made more than sixty years ago, the distribution by Laws and Parsons, among others, is considered to be typical of the average distribution both for widespread rain (in the lower rainfall-rate range) and for convective rainfall (in the higher rainfall-rate range).Nowadays measurements of drop sizes are extrapolated with enhanced distributions like the Gamma distribution or lognormal distribution , These distributions gave a more accurate description of the real drop size distribution. Especially they solve the former problem of the overestimation of the number of small drops with exponential approaches. Disdrometers measure DSDs of hydrometeors during a rain event in real time. Modern systems operate in the optical regime (Rogers 1976). Furthermore, since the terminal velocity varies with drop size, Doppler spectra of electromagnetic signals show the size distribution by applying this relation of drop radius to terminal velocity
[13] provides an empirical procedure based on the approximate relation between γ (dB/km) and rain rate R (mm/h), which is fitted by L-P distribution, the relationship between specific attenuation γ and rain rate R with a power-law is:

$$\gamma_R = kR^{\alpha} \tag{1.12}$$

Phase delay results mainly from the imaginary part of the propagation constant ; eq. (1.11) ,the phase delay can be inherently translated to a delay in picoseconds , which is the typical order of magnitude for terrestrial link delay due to atmospheric propagation .
[13] provides similarly an empirical procedure based on the approximate relation between φ_R (deg/km) and rain rate R (mm/h), which is fitted by L-P distribution, the relationship between the phase P and rain rate R with a power-law is:

$$\varphi_R = hR^{\beta} \tag{1.13}$$

1.4. Specific phase delay and attenuation parameters

In eqs. (1.12) and (1.13) there are 4 coefficients: k, α, h, β, since attenuation and delay are simply the integration of their specific quantities along the slant path, and since our goal is to link attenuation to delay, it is vital to visualize how the coefficients k, α, h, β vary with frequency f , elevation angle θ of the link...
In fact, this work was developed in the thesis *An analytical model for the attenuation and phase delay due to rain in the 6-100 GHz range* by Guanjun Li, [11]. Therefore it's interesting to present some of its important results.
This study presents the analytical model as a function of different drop size distribution (DSDs) in the 6-100 GHz range. The values of specific attenuation and phase delay for horizontal and vertical polarizations are obtained using the T-Matrix method to calculate the rain drop scattering amplitude and considering different Gamma DSDs. For each frequency, elevation angle and DSD type, the results obtained for various rain rates are fitted using the customary power law expression and, finally, such coefficients are studied as a function of frequency to provide a fully analytical model receiving as input the frequency and the DSD type.
Values of the coefficients k and α are determined as function of frequency, f(GHz), ranging from 1 to 1000GHz. In recommendation ITU-R P.838-3 [10], coefficients k and α are calculated by vertical and horizontal polarizations, the formulas are

$$\log_{10} k = \sum_{j=1}^{4} a_{jk} \exp\left[-\left(\frac{\log_{10} f - b_{jk}}{c_{jk}}\right)^2\right] + m_k \log_{10} f + c_k \tag{1.14}$$

$$\alpha = \sum_{j=1}^{5} a_{j\alpha} \exp\left[-\left(\frac{\log_{10} f - b_{j\alpha}}{c_{j\alpha}}\right)^2\right] + m_\alpha \log_{10} f + c_\alpha \tag{1.15}$$

Similarly for h and β we can write :

$$\log_{10} h = \sum_{j=1}^{4} a_{jh} \exp\left[-\left(\frac{\log_{10} f - b_{jh}}{c_{jh}}\right)^2\right] + m_h \log_{10} f + c_h \tag{1.16}$$

$$\beta = \sum_{j=1}^{5} a_{j\beta} \exp\left[-\left(\frac{\log_{10} f - b_{j\beta}}{c_{j\beta}}\right)^2\right] + m_\beta \log_{10} f + c_\beta \tag{1.17}$$

where f is frequency (GHz), k is either k_H or k_V, α is either a_H or a_V.for horizontal and vertical polarisations respectively,
The coefficients $a_{jk}, b_{jk}, c_{jk}, m_k, c_k, a_{j\alpha}, b_{j\alpha}, c_{j\alpha}, m_\alpha, c_\alpha, a_{jh}, b_{jh}, c_{jh}, m_h, c_h, a_{j\beta}, b_{j\beta}, c_{j\beta}, m_\beta, c_\beta$ are constants that depend on the drop size distribution . The latter is a gamma distribution whose main parameter is μ varying in the range {-3,-2,...8} The coefficients k_H and k_V, a_H and a_V can be converted into k and α using the following equations:

$$\begin{aligned} k &= \frac{[k_H + k_V + (k_H - k_V)\cos^2\theta \cos 2\psi]}{2} \\ \alpha &= \frac{[k_H\alpha_H + k_V\alpha_V + (k_H\alpha_H - k_V\alpha_V)\cos^2\theta \cos 2\psi]}{2k} \end{aligned} \tag{1.18}$$

Similarly , the coefficients h_H and $_V, \beta_H$ and β_V can be converted into m and β

$$\begin{aligned} h &= \frac{[h_H + h_V + (h_H - h_V)\cos^2\theta \cos 2\psi]}{2} \\ \beta &= \frac{[h_H\beta_H + h_V\beta_V + (h_H\beta_H - h_V\beta_V)\cos^2\theta \cos 2\psi]}{2h} \end{aligned} \tag{1.19}$$

Table 1.1: Coefficients in horizontal and vertical polarization

μ	f(GHz)	α_H	α_V	k_H	k_V	β_H	β_V	m_H	m_V
−3	10	1.18636	1.10570	0.01912	0.01687	0.81640	0.77993	1.55130	1.50701
0	10	1.21836	1.17192	0.01158	0.01161	0.88791	0.85845	1.24040	1.23360
3	10	1.13989	1.12094	0.01112	0.01044	0.92987	0.91704	1.15828	1.13195
5	10	1.10068	1.08864	0.01084	0.01000	0.94308	0.93444	1.14611	1.11340
8	10	1.06484	1.05692	0.01053	0.00971	0.95431	0.94903	1.14289	1.10719
−3	30	0.94778	0.92119	0.19791	0.17887	0.65309	0.67604	4.80198	4.54586
0	30	1.02064	0.99834	0.18239	0.17000	0.73860	0.74919	4.44365	4.18556
3	30	1.06418	1.04816	0.15987	0.14987	0.86380	0.86262	3.84752	3.68708
5	30	1.06467	1.05229	0.15338	0.14386	0.90231	0.89895	3.70679	3.56385
8	30	1.05809	1.04842	0.14830	0.13907	0.93202	0.92839	3.62167	3.48999

Where θ is the link elevation angle and ψ is the wave polarisation angle. Hence, the coefficients k, α, h, β depend mainly on frequency, elevation angle, polarisation angle, and the parameter μ characterizing the gamma drop size distribution which is detailed in section 3.1.8. The table 1.1 shows vertical and horizontal coefficients variation with the parameter μ, for 2 frequencies: 10 GHz and 30 GHz

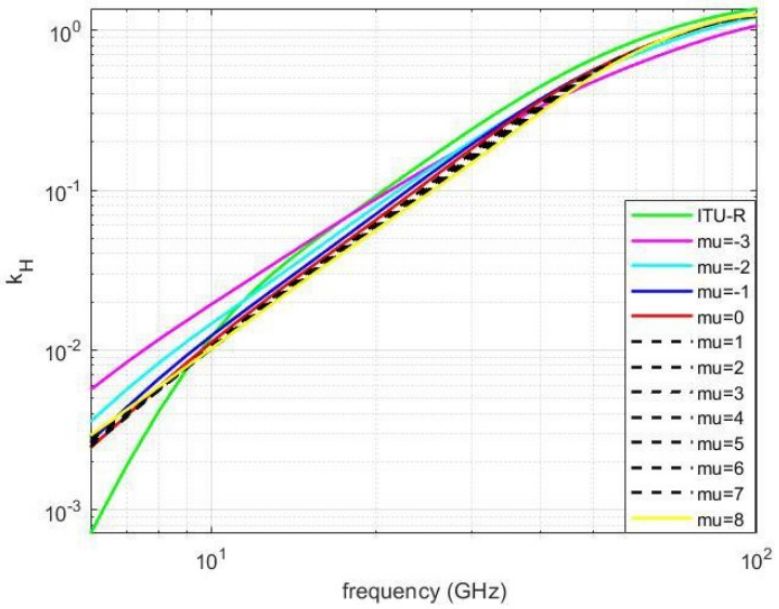

Figure 1.1: k_H Variation with frequency

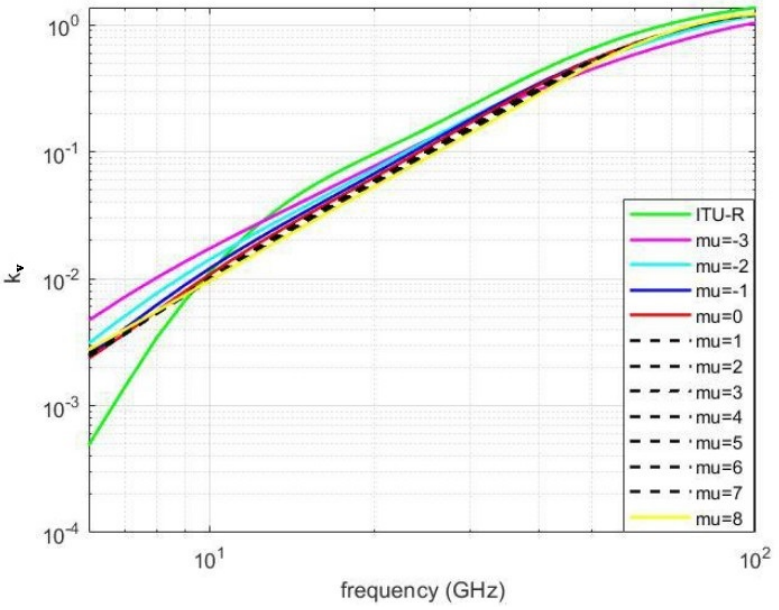

Figure 1.2: k_V Variation with frequency

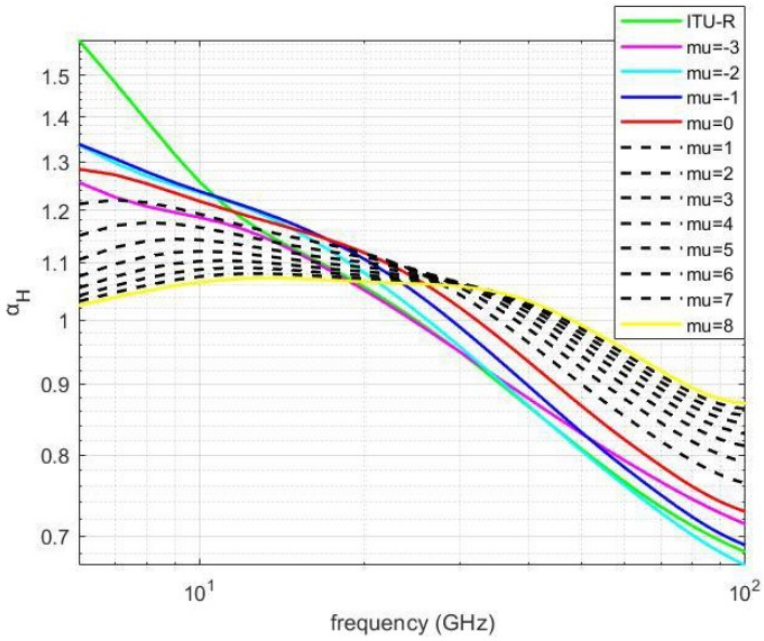

Figure 1.3: α_H Variation with frequency

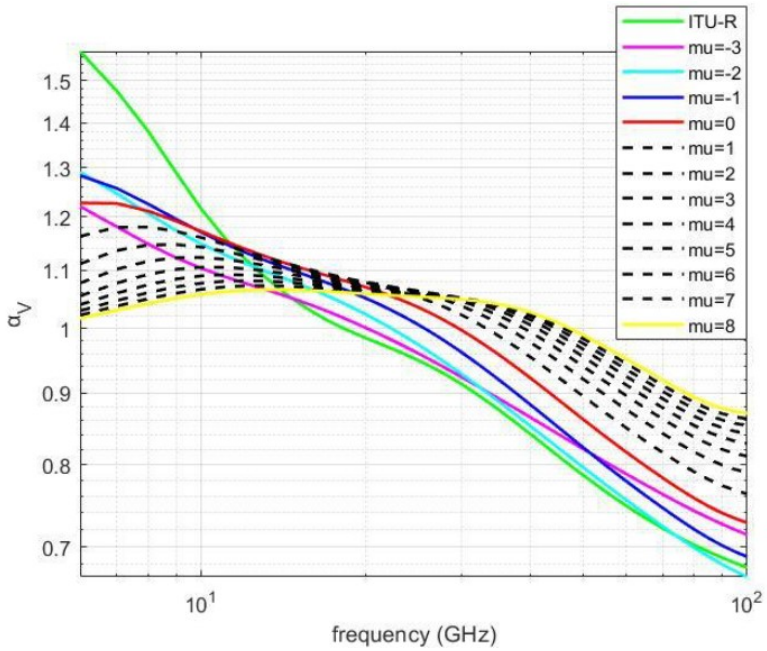

Figure 1.4: α_V Variation with frequency

It's also interesting to present the dependency of these coefficients, in order to avoid being cumbersome, we plot only the frequency dependency of k, α in horizontal and polarisations figs. 1.1 to 1.4, but the reader is addressed to [11] for further plots and elaborations. For each plot, we can see how the value μ changes the results, the ITU-R 838-3 model[10] has been plotted also for comparisons.

1.5. Rain Mitigation Techniques

As mentioned in the introduction, rain effect on telecommunications can be sometimes critical, the reason why developing mitigation techniques is crucial for better services. Rain loss at Ka-band can be mitigated, but it cannot be totally compensated. Few commons techniques are used :

- One technique is site diversity. Two earth stations separated by a distance of about 15 km to 30 km and connected by a terrestrial link can be used. It is unlikely that both earth stations would experience the same rain intensity simultaneously.
- Another technique is to reserve bandwidth to permit more robust Forward error correction coding that will maintain the same bit error rate at the specified bit rate at a lower carrier power. In addition, the bit rate itself may be lowered below the nominal value during periods of heavy rain.
- Another possibility is the selective allocation of an alternative frequency, such as Ku-band, as needed in areas encountering rain at a particular time. The rain degradation at Ku-band could be within the allocated margin even though the margin was exceeded at Ka-band.

The reader is addressed to [12] for further details on rain mitigation techniques .

2 | Rainfall Models

Rain rate is the most familiar measure for rain. This value is both made public by the weather services and used by scientists of weather-related subjects.
table 2.1 classifies different rain rates together with their common terms

Table 2.1: Rain categories and corresponding rates in mm/h.

Rain Rate	
0.25	Drizzle
1	Light Rain
4	Moderate Rain
16	Heavy Rain
100	Extremely Heavy Rain

A lot of work in the literature has been dedicated to developing rain attenuation models , these models no matter how different they are , can be classified into 5 categories

- **Empirical Model** : The model is based on experimental data observations rather than input-output relationships that can be mathematically described. The model is then classified as an empirical category
- **Physical Model** : The physical model is based on some of the similarities between the rain attenuation model's formulation and the physical structure of rain events
- **Statistical Model** : This approach is based on statistical weather and infrastructural data analysis, and the final model is built as a result of regression analysis in most cases.
- **Fade Slope Model** : In the fade slope model, the slope of attenuation from the rain attenuation versus time data was developed with a particular experimental setup. Later, these data were used to predict rain attenuation.
- **Optimization-based Model** ; In this type of model, the input parameters of some of the other factors that affect the rain attenuation are developed through optimization (e.g., minimum error value) process

The Models considered in this thesis work belong to physically based/statistical models , The method is based on a recently devised statistical model of the rain horizontal structure [4], whose parameters can be determined on the basis of the local statistical distribution of the point rainfall intensity. A test of the ability of this method in predicting attenuation statistics is performed using data collected in Europe with the satellites SIRIO and OTS (COST 205, 1985). The excellent results obtained encourage the application of the model to the statistical prediction of other parameters pertaining to propagation

2.1. EXCELL

The parameters of the EXCELL model [4],[5] for the horizontal rain structure can be determined based on the local statistical distribution of the point rainfall intensity. The model was validated using the COST 205, 1985 database. This model consists of several rain cell structures, collectively refereed to as kernels. In such a rain cell, the rainfall rate at a distance l from the center is given by:

$$R = R_{\text{peak}}\, e^{-l/l_0}. \tag{2.1}$$

Where R_{peak} is the cell's peak rain rate, and l_0 is an equivalent radius i.e for which the rain rate decreases by a factor of e^{-1}.
The probability of attenuation equation:

$$P(A) = \int_{R_E}^{\infty} E \cdot \left[0.5 \ln^2 \left(R_{\text{peak}} / R_E\right) + r \ln \left(R_{\text{peak}} / R_E\right)\right] \cdot \left[-P\left(R_p\right)'''\right] d\left(\ln R_{\text{peak}}\right) \tag{2.2}$$

Where $r = 1/4\pi\bar{l}_0$ Rain distribution can be modeled as:

$$P(R) = P_0 \ln^n \left(\frac{R^*}{R}\right). \tag{2.3}$$

A simplified version of the model with the point rain intensity at point (x, y) can be defined ine biaxial case as

$$R(x, y) = R_M e^{-\sqrt{\left(\frac{x}{l_x}\right)^2 + \left(\frac{y}{l_y}\right)^2}} \tag{2.4}$$

along a monoaxial cell radius:

$$R(x, y) = R_M e^{-\frac{\sqrt{x^2+y^2}}{l_0}}. \tag{2.5}$$

In the sense of the rain attenuation model, this model does not provide attenuation. However, it facilitates the generation of a synthetic rain rate from which attenuation , phase delay can be predicted using a suitable prediction model [13] . There are critics that the exponential rain peak is not present in nature, and the model does not differentiate between stratiform and convective rain.

2.2. SC Excell

An upgraded version of the exponential cell (EXCELL) rain attenuation model called sc-Excell was developped to predict attenuation through a cellular representation of precipitation, but, in addition, is able to discriminate between stratiform and convective rain by means of an embedded algorithm. Accordingly, two separate physical rain heights, derived from the ERA-15 database, are used to calculate stratiform and convective rain attenuation and.Eventually, the predicted cumulative distribution function (CDF) of excess attenuation is the combination of the contributions due to stratiform and convective precipitation types. The complete procedure for estimating attenuation due to rain in the sc-excell framework includes the following steps:

1. The yearly cumulative distribution function (CCDF)$P(R)$ of the rain rate can be discriminate between stratiform and convective rain, the equation is given by:

$$P(R)_{\text{year}} = P(R)_{str} + P(R)_{cnv} \tag{2.6}$$

2. The bright band effect should be considered in stratiform rain, from the calculation of [6], the average equivalent bright band height, H_{BB} is:

$$H_{BB}(f) = 4.58e^{-0.0675f} + 0.51(\text{ km}) \tag{2.7}$$

3. The ERA-15 database, which is provided by the ECMWF(European Centre of Medium-Range Weather Forecast), derives the new mean physical rain height. The monthly mean values of the 0°C isothermal height of stratiform (h_{str}) and convective (h_{cnv}) are calculated.

4. Considering the melting layer, the effective rain height of stratiform is defined:

$$H_{\text{strRain}} = h_{\text{str}} + H_{BB}(f)(km) \tag{2.8}$$

5. The effective convective rain height considered increasing 20% by the value of h_{cnv}, which defined as:

$$H_{cnv\ \mathrm{Rain}} = 1.2h_{cnv}(\ \mathrm{km}) \tag{2.9}$$

6. Through the EXCELL model, the stratiform and convective cells contribution to attenuation $P_C(A)_{str}$ and $P_C(A)_{cnv}$ can be estimated by using $P(R)_{str}$, H_{strRain} and $P(R)_{cnv}, H_{cnv\ \mathrm{Rain}}$ respectively.

7. Add the plateau contribution to attenuation for stratiform and convective attenuation CDFs respectively:

$$P(A)_{\mathrm{str}} = P_C(A)_{str} + P_P(A)_{\mathrm{str}} \tag{2.10}$$

$$P(A)_{cnv} = P_C(A)_{cnv} + P_P(A)_{cnv} \tag{2.11}$$

8. Summing the probability values of stratiform and convective contributions:

$$P(A)_{tot} = P(A)_{str} + P(A)_{cnv} \tag{2.12}$$

starting from new analytical model in this study, which provides the specific phase in terms of deg /km, the SC EXCELL model will give the phase ϕ in deg by integrating along the path. Conversion from phase ϕ in deg to the phase delay τ in picoseconds is well explained in chapter 3

NOTE that the same procedure can be followed to derive the CDF of phase delay .

For further details and explanations , the reader is addressed to [6] on the SC EXCELL model.

2.3. MultiEXCELL

MultiEXCELL, a new rainfall model oriented to the analysis of radio propagation impairments which was developed on the basis of a comprehensive rain field database collected by the weather radar sited in Spino d'Adda (Italy), Single rain cells are modeled by an analytical exponential profile which best represents real single-peaked rain structures. The rain cells' probability of occurrence is analytically derived from the local rainfall statistics. The spatial features of the rain field at midand large-scale are investigated through their natural aggregative process. The clusters (aggregates) of cells are studied in terms of distance between individual cells, number of cells per aggregate, and distance between

aggregates. Finally, the fractional area covered by rain, on which the rainfall spatial correlation strongly depends , is derived from radar data through the comparison with the same quantity provided by global long-term numerical weather products. The MultiEXCELL procedure for the generation of spatially correlated synthetic rain fields is duly presented and the model's accurateness is preliminary assessed against the available radar dataset. Although MultiEXCELL is mainly oriented to propagation-related applications, its cellular approach may reveal useful also in hydrology, for the prediction/management of water resources, and in meteorology, for the nowcasting of the temporal evolution of rain structures. The MultiEXCELL model assumes that the exponential profile has a global validity, what changes from site to site is the rain cells' probability of occurrence, so that, for instance, in tropical areas, convective cells prevail over stratiform ones, whereas in temperate sites, their relative occurrence is more balanced. Accordingly, the following relationship expresses the superposition of the cells' contributions to generate the $P(R)$ and links the rain cells' probability of occurrence, $N(R_M, \rho_0)$, to the local rainfall statistic (for clarity's sake, although $N(R_M, \rho_0)$ is identified as a probability, its dimensions are $\left[1/\left(\mathrm{km}^2 \cdot \mathrm{km} \cdot \mathrm{mm/h}\right)\right]$)

$$P(R) = \int_R^\infty \int_a^b A(R_M, \rho_0, R)\, N(R_M, \rho_0)\, d\rho_0 dR_M \qquad R_M \geq 5 \text{ mm/h} \tag{2.13}$$

where $A(R_M, \rho_0, R) = \pi \left[\rho_0 \ln(R_M/R)\right]^2$ is the area of the exponential cell derived from eq. (3.2) The rain rate probability can be fitted into the following law :

$$P(R) = P_0 \ln^n \left(\frac{R_a + R_{\text{low}}}{R + R_{\text{low}}} \right) \tag{2.14}$$

The probability of occurrence for a certain cell (R_M, ρ_0) is then deduced by inverting eq. (2.13)

$$\begin{aligned} N(R_M, \rho_0) = &- \frac{1}{\pi (\psi_m - \psi_M) \exp\left(2\sigma^2(R_M) + 2\mu(R_M)\right)} \\ &\times \left. \frac{d^3 P(R)}{d \ln(R)^3} \right|_{R=R_M} \cdot \frac{1}{\rho_0 \sigma(R_M) \sqrt{2\pi}} \\ &\times \exp\left[- \left(\frac{\ln(\rho_0) - \mu(R_M)}{\sqrt{2}\sigma(R_M)} \right)^2 \right] \end{aligned} \tag{2.15}$$

where

$$\begin{aligned} \psi_m &= \psi\left[\frac{\mu\left(R_M\right)+2\sigma^2\left(R_M\right)-\ln(a)}{\sqrt{2}\sigma\left(R_M\right)}\right] \quad \text{and} \\ \psi_M &= \psi\left[\frac{\mu\left(R_M\right)+2\sigma^2\left(R_M\right)-\ln(b)}{\sqrt{2}\sigma\left(R_M\right)}\right] \end{aligned} \tag{2.16}$$

For further details and explanations , the reader is addressed to[12] on the multi-EXCELL model

fig. 2.1 shows a typical rain field observed by the radar located at Spino d'Adda: the inner ellipse on the left identifies a single rain cell, the two small circles in the bottom right corner indicate two of the cells pertaining to the same aggregate, and, finally, the large ellipses delimit two aggregates. It appears from the figure that rain is organized on three spatial scales

- The small-scale (up to approximately 20 km) which involves single rain cells
- The mid-scale (roughly from 20 km to 50 km) that is related to how cells cluster together to form an aggregate, and finally
- The large-scale (from 50 km to about 300 km) which is related to the mutual position of the aggregates on the map.

,

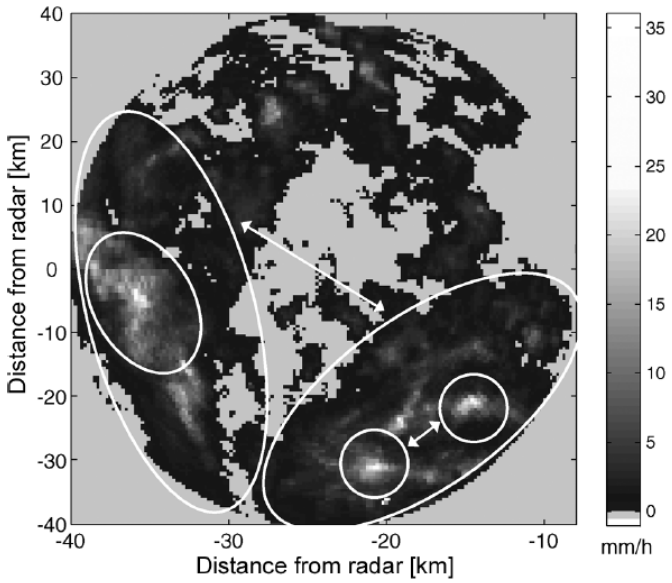

Figure 2.1: Aggregates of rain cells in the multi Ex-cell

3 | Analytical Model For Path Attenuation And Delay

This chapter defines the core of the thesis work, for the seek of clarity, we present the chapter map in fig. 3.1. At first, we will exploit the EXCELL model to generate some data for both attenuation and phase delay. The next step is to see how does their relationship change varying some parameters like: frequency and elevation angle, once identified, the main features are used to fit the data generated with an analytical formula. The error of the model is computed using the data used in the fitting, and the data emerging from the SC-EXCELL model based on the measured ccdfs of attenuation and delay, the delay-attenuation relationship is derived from an iterative process until the the error is accepted .

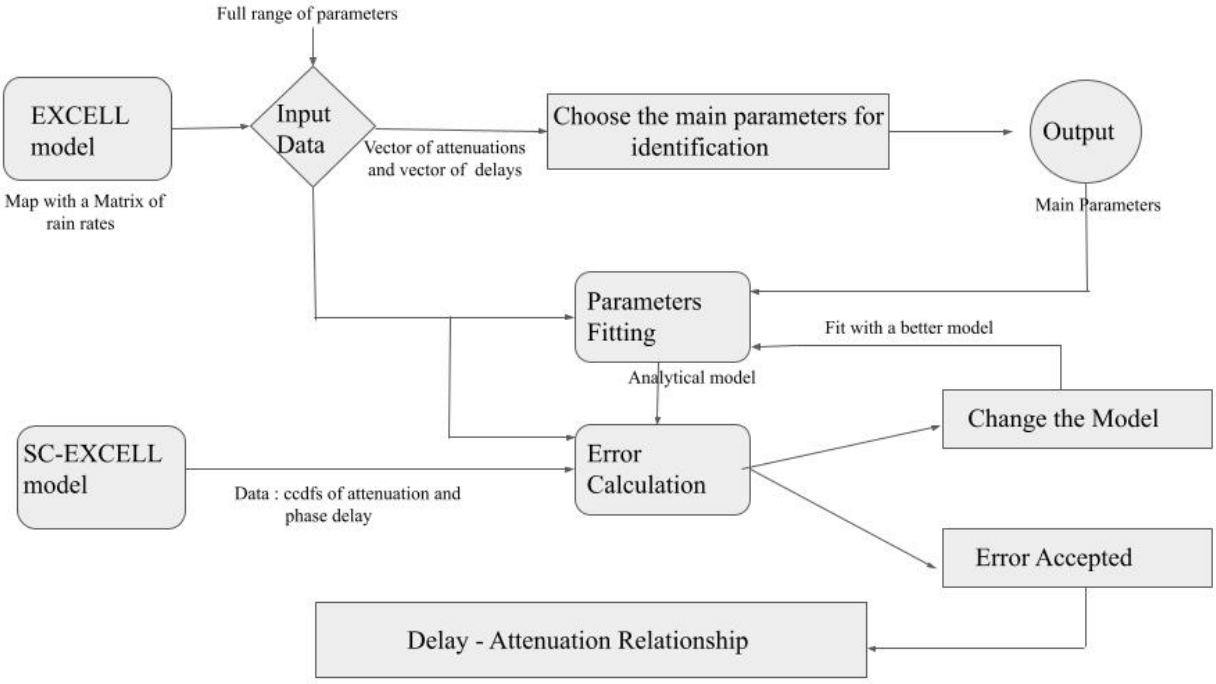

Figure 3.1: Map of the Chapter

3.1. Parameters Identification

3.1.1. EXCELL generation

In this section we generate a numerical representation of the analytical profile in fig. 3.2, the exponential cell is characterized by 2 parameters R_M and ρ_0 representing the maximum rain rate inside the cell and its equivalent radius i.e the radius for which the rain rate decreases by a factor of e^{-1}. The rain rate profile inside one cell can be expressed as :

$$R(\rho) = R_M \exp\left[-\rho/\rho_0\right]. \tag{3.1}$$

The radius of the cell is constrained by a threshold value R_{th} since the most commonly accepted definition of rain cell is "*the continuous area inside which the rain rate is higher than a given threshold* ", we fix then this threshold to $R_{th} = 0.5mm/h$. The radius of the cell can be written :

$$R_{cell} = \rho_0 \, log(\frac{R_M}{R_{th}}) \tag{3.2}$$

Working in the cartesian framework, we can write the cell radius as :

$$\rho = \sqrt{x^2 + y^2} \tag{3.3}$$

NOTE that the coordinate x and y have to be sampled in accordance to the radius of the cell because smaller cells entail a refined sampling to explicitly exhibit their variation on the map . For this reason it has been decided that a sampling pace of $r_{cell}/30$ (section 3.1.2) is suitable for the cells generation .

REMARKS

- In fig. 3.2, the rain cell modeling clearly depicts the exponential profile for a value of $R_M = 10mm/h$ and an effective radius of $\rho_0 = 5km$ we get a cell radius of 15 Km chosen to not exceed the boundary R_{th} .

- We can see also that the sampling distance gives a smooth plot for the cell's rain rate

- NOTE that the rain rate is stored as a 2d matrix and since the exponential profile is rotational (invariant) with respect to the azimuth , the path attenuation and delay are thereby be independent on the azimuth angle

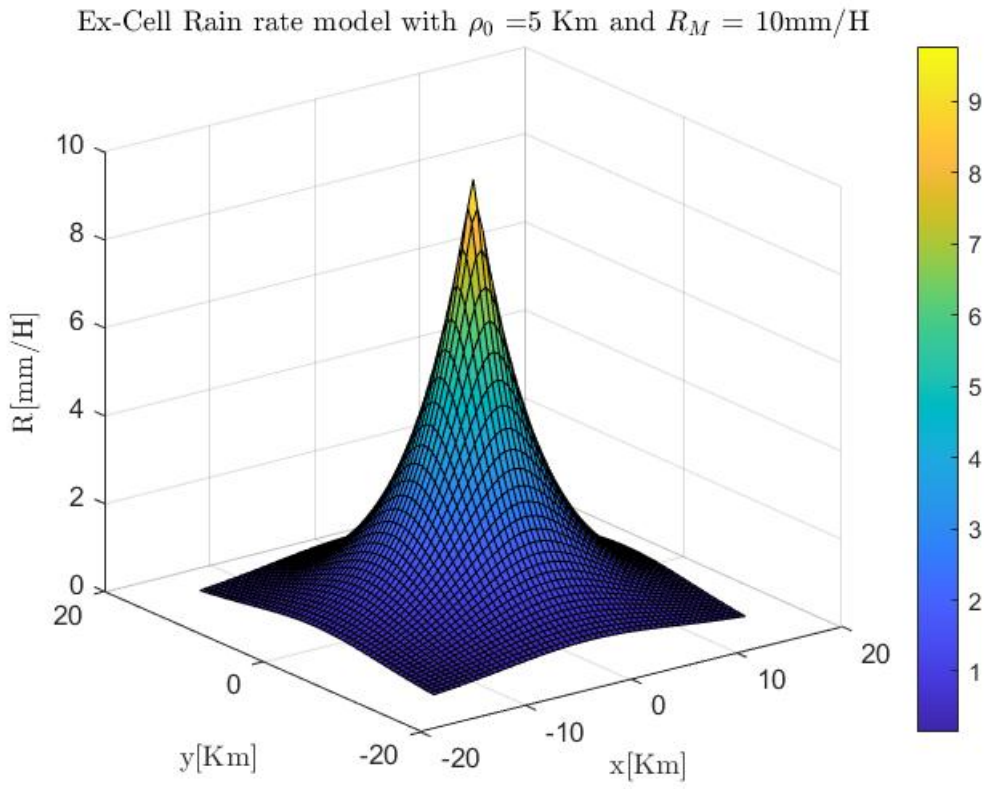

Figure 3.2: Excell rain rate Profile

3.1.2. Attenuation And delay

[13] provides an empirical procedure based on the approximate relation between γ (dB/km) and rain rate R (mm/h), which is fitted by Laws and Parsons (L-P) distribution, the relationship between specific attenuation γ and rain rate R is described with a power law:

$$\gamma_R = kR^{\alpha} \tag{3.4}$$

Similarly, an empirical procedure based on the approximate relation between φ_R (deg/km) and rain rate R (mm/h) can be used, which is fitted by L-P distribution, the relationship between the phase and rain rate R with a power-law is:

$$\varphi_R = hR^{\beta} \tag{3.5}$$

Finally, the phase can be linked to the phase delay in picoseconds and frequency f in GHz through

$$\tau_R = \frac{1000}{360f}\,\varphi_R \tag{3.6}$$

The attenuation along the slant path can be written as :

$$A = \int_{Slantpath} \gamma_R = \int_{Slantpath} kR^{\alpha} \tag{3.7}$$

Whilst the delay can be written as

$$\tau = \frac{1000}{360f} \int_{Slantpath} \varphi_R = \frac{1000}{360f} \int_{Slantpath} hR^{\beta} \tag{3.8}$$

Let θ be the elevation angle of the link, H_R the rain height, L the slant path , L_H the horizontal path length, from fig. 3.3 we can write :

$$tan(\theta) = \frac{H_R}{L_H} \qquad cos(\theta) = \frac{L_H}{L} \tag{3.9}$$

Since the EXCELL model hinges only on the horizontal variation on the path (no dependence on the height), eqs. (3.7) and (3.8) can be written :

$$cos(\theta)A = \int_{L_H} \gamma_R = \int_{L_H} kR^{\alpha} \tag{3.10}$$

$$cos(\theta)\tau = \frac{1000}{360f} \int_{L_H} \varphi_R = \frac{1000}{360f} \int_{L_H} hR^{\beta} \tag{3.11}$$

Remark : Since the goal is to find an analytical formula linking attenuation to phase delay, and since the term $cos(\theta)$ is present for both , we can forget it henceforth.

Data Generation Refering to the map of this work: fig. 3.1, we will explain how we generate the data i.e vector of attenuations and phase delays starting from the EXCELL map of rain rates fig. 3.2, since this is a critical procedure and the most important one, and for the seek of clarity we will present the general picture of the data generation .
In fact, in fig. 3.4 we can see the rotational profile of the EXCELL model, whose peak is in the center,and cell radius covers the map dimension. Simulating two random positions of the satellite and the station inside the EXCELL cell, we can perform integration along their relative distance (horizontal path length L_H) eqs. (3.10) and (3.11)
Thus, for a fixed L_H, the one cell approach leads to a couple (τ, A). In order to simulate all the scenarios, i.e all the possible L_H between the ground station and the satellite , we move the satellite mapping all the possible points in the map, for each scenario we get a couple (τ, A), hence for each EXCELL map (R_M, ρ_0), we get a vector of attenuations and phase delays that we can plot in a scatter plot fig. 3.6

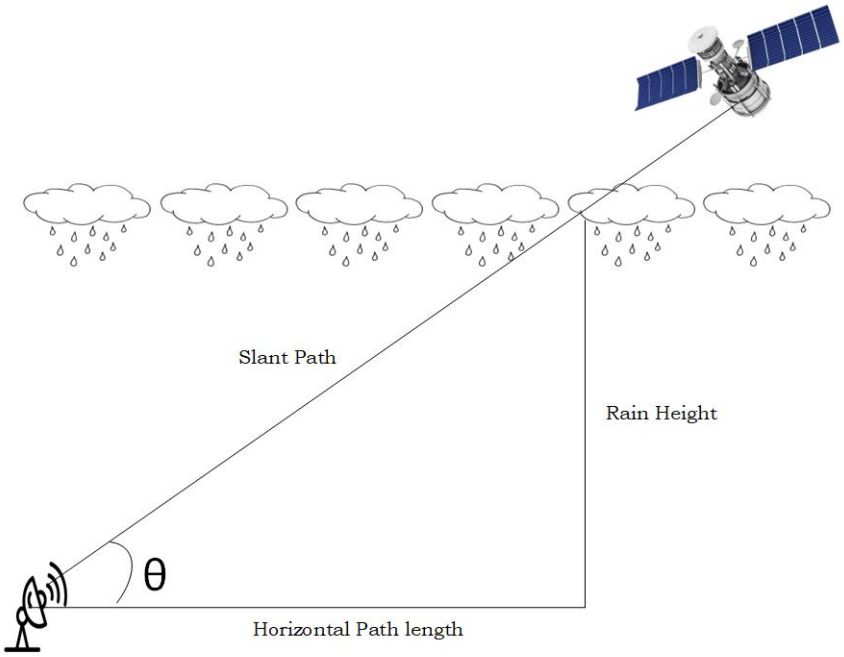

Figure 3.3: Sketch slant path and elevation angle

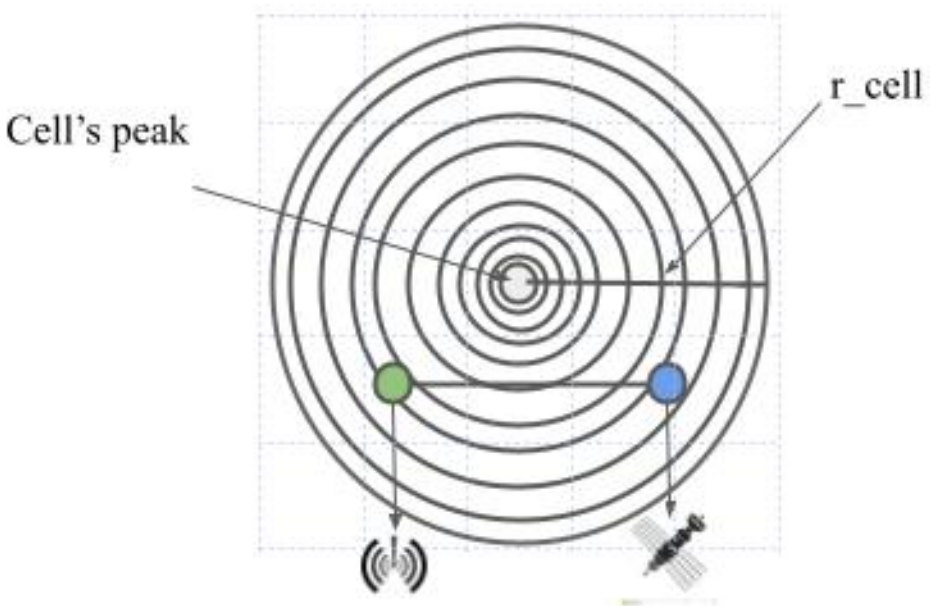

Figure 3.4: satellite and station positions inside the cell

Space resolution effect The map resolution : dr is the space sampling distance used to generate the rain rate map in fig. 3.2, in cartesian coordinates we choose the same resolution for both x and y i.e :

$$dr = dx = dy \tag{3.12}$$

The choice of the map resolution is critical since all the results and their accuracy depend on this step , in order to first visualize its effect , we generate an EXCELL profile and a link with the following properties

Cell properties				**Link properties**			
R_M [mm/h]	ρ_0 [Km]	r_{cell} [Km]	R_{th} [mm/h]	f [Ghz]	θ [deg]	H_R [km]	μ [—]
20	2	7.37	0.5	10	30	4	0

Table 3.1: One Cell and Link properties

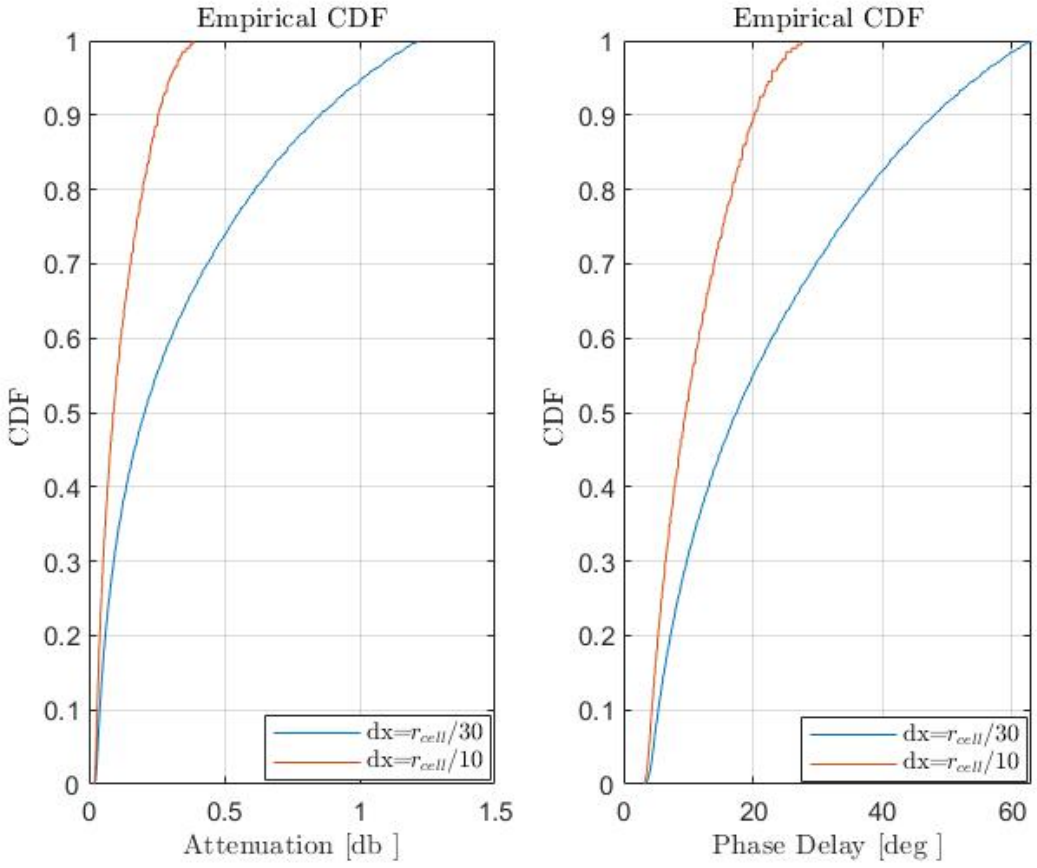

Figure 3.5: Effect of the map resolutio dx

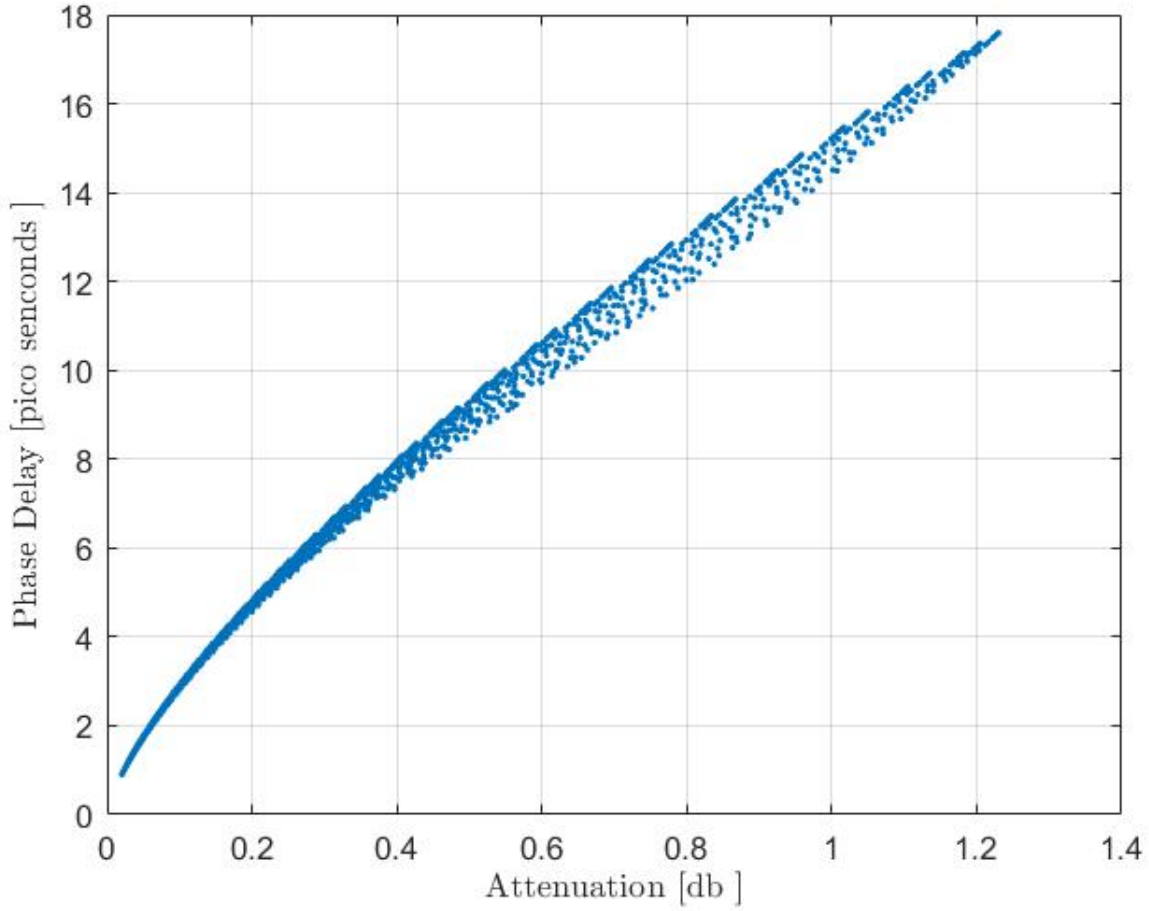

Figure 3.6: One cell results

As we can notice ,fig. 3.5 shows the effect of the map resolution, in fact, for a sufficiently small resolution results are smooth, while for the second case ($dx = r_{cell}/10$) there are some *jumps* in the probability levels.
NOTE that lower resolution dr means more calculations (higher number of pixels) but we found that the best compromise between accuracy and time consumption is for a resolution :

$$dr = \frac{r_{cell}}{30} \tag{3.13}$$

fig. 3.6 shows that with the chosen resolution, we get a good scattering plot that follows the trend of a powerlaw .Recall that each point of this scatter plot corresponds to a certain scenario (relative distance between the station and the satellite but also its location within the EXCELL map) fig. 3.4

Multiple cells generation The first curiosity that arises when generating a single cell profile, and dissecting the given results, is whether the scatter plot $\tau = f(A)$ depends on the couple (R_M, ρ_0) characterizing an EXCELL cell, which leads us to investigate the multi cells approach . In order to do that, we conserve the link properties of table 3.1 but this time we generate a grid 20x 20 of exponential cells where $R_M \in [15, 100]$ mm/h and $\rho_0 \in [0.6, 20]$ Km, thus for a fixed horizontal path and for every couple $(R_M^{(i)}, \rho_0^{(j)})$ we get a certain scatter plot fig. 3.6. But this is only possible when :

$$H_{Hor} < r_{cell}^{(i,j)} = \rho_0^{(i)} \, log(\frac{R_M^{(j)}}{R_{th}}) \tag{3.14}$$

We recall also that for every $r_{cell}^{(i,j)}$ the map generation is changed accordingly .

$$dr^{(i,j)} = dx^{(i,j)} = dy^{(i,j)} = \frac{r_{cell}^{(i,j)}}{30} \tag{3.15}$$

Now, following the same procedure explained in the previous section for the one cell approach, but this time plotting all the plots together(for all 20x20 cells) we can see how the curve changes slightly with each profile $(R_M^{(i)}, \rho_0^{(j)})$

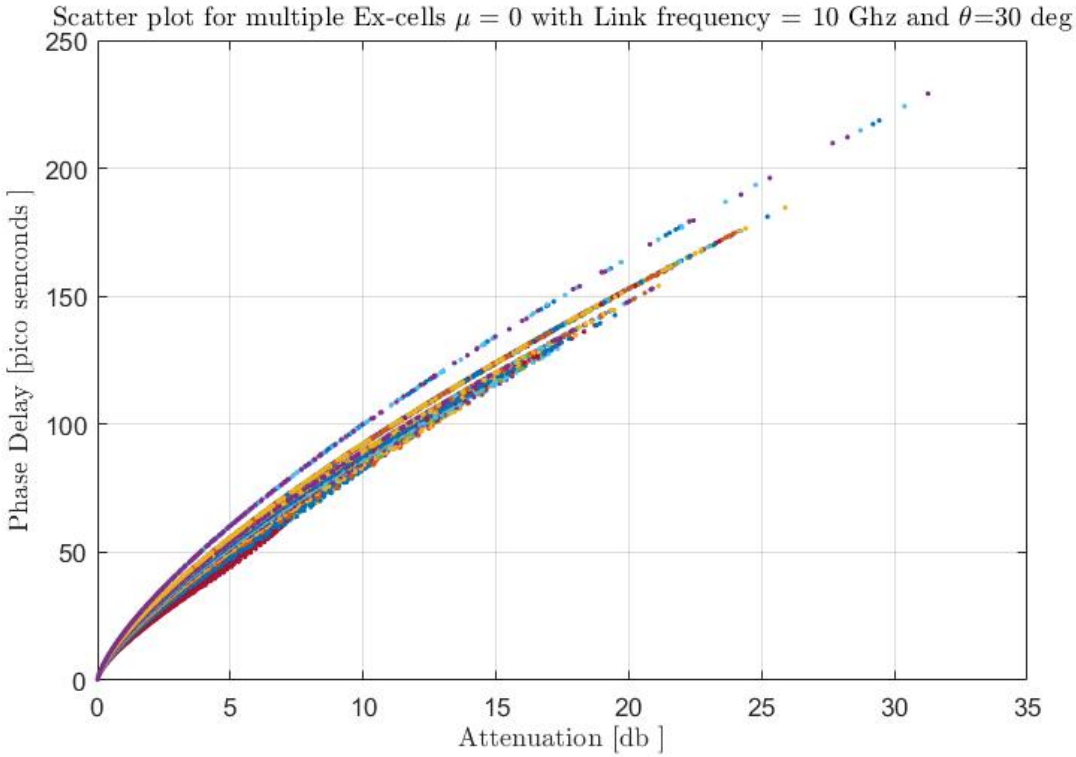

Figure 3.7: Multi-cell approach

In fig. 3.7 the global trend is always a power law, for higher rain rates, we can see the divergence of the plots for different cells. with reference to the chapter's map fig. 3.1, we are still in the data generation block, but as we can see in fig. 3.7, having data that depends on 400 cells and involve many parameters is cumbersome, we decide then to fit all of these scatter-plot with one single plot for two reasons :

1. Since the EXCELL model is used only to generate data for attenuation and delay,it should not be a fitting parameter, thus we have to retain data that best represent any scenario for the rainfall
2. By fitting all the cells with one single plot, i.e one single vector of attenuations + one single vector of phase delays, we can first identify clearly the parameters changing the plot and second, fit it easily to the main parameters.

3.1.3. Multi exponential cell fitting

As explained in the previous section, we are trying to fit all the 400 scatter plots with a single plot that best represents the data, for this purpose we will use the least square approach, we would like to present its theoretical milestones.

Least Square approach Least square method is the process of finding a regression line or best-fitted line for any data set that is described by an equation. This method requires reducing the sum of the squares of the residual parts of the points from the curve or line and the trend of outcomes is found quantitatively. The method of curve fitting is seen while regression analysis and the fitting equations to derive the curve is the least square method. The objective consists of adjusting the parameters of a model function to best fit a data set. A simple data set consists of n points (data pairs) $(x_i, y_i), i = 1, \ldots, n$, where x_i is an independent variable and y_i is a dependent variable whose value is found by observation. The model function has the form $f(x, \boldsymbol{\beta})$, where m adjustable parameters are held in the vector $\boldsymbol{\beta}$. The goal is to find the parameter values for the model that "best" fits the data. The fit of a model to a data point is measured by its residual, defined as the difference between the observed value of the dependent variable and the value predicted by the model:

$$r_i = y_i - f(x_i, \boldsymbol{\beta}).$$

The least-squares method finds the optimal parameter values by minimizing the sum of squared residuals

$$S = \sum_{i=1}^{n} r_i^2.$$

An example of a model in two dimensions is that of the power law. the model function is given by $f(x, \boldsymbol{\beta}) = \beta_1 x^{\beta_2}$. The sum S is minimized then for

$$\begin{aligned} \beta_1 &= \frac{\sum_{i=1}^{n} (\ln y_i) - b \sum_{i=1}^{n} (\ln x_i)}{n} \\ \beta_2 &= \frac{n \sum_{i=1}^{n} (\ln x_i \ln y_i) - \sum_{i=1}^{n} (\ln x_i) \sum_{i=1}^{n} (\ln y_i)}{n \sum_{i=1}^{n} (\ln x_i)^2 - (\sum_{i=1}^{n} \ln x_i)^2} \end{aligned} \tag{3.16}$$

In Matlab , the command fitobject = fit(x,y,fitType) creates the fit to the data in x and y with the model specified by fitType (power law in our case) has been used in this step . Henceforth , all the 400 cells will be represented by the fitting curve fig. 3.8 that regardless

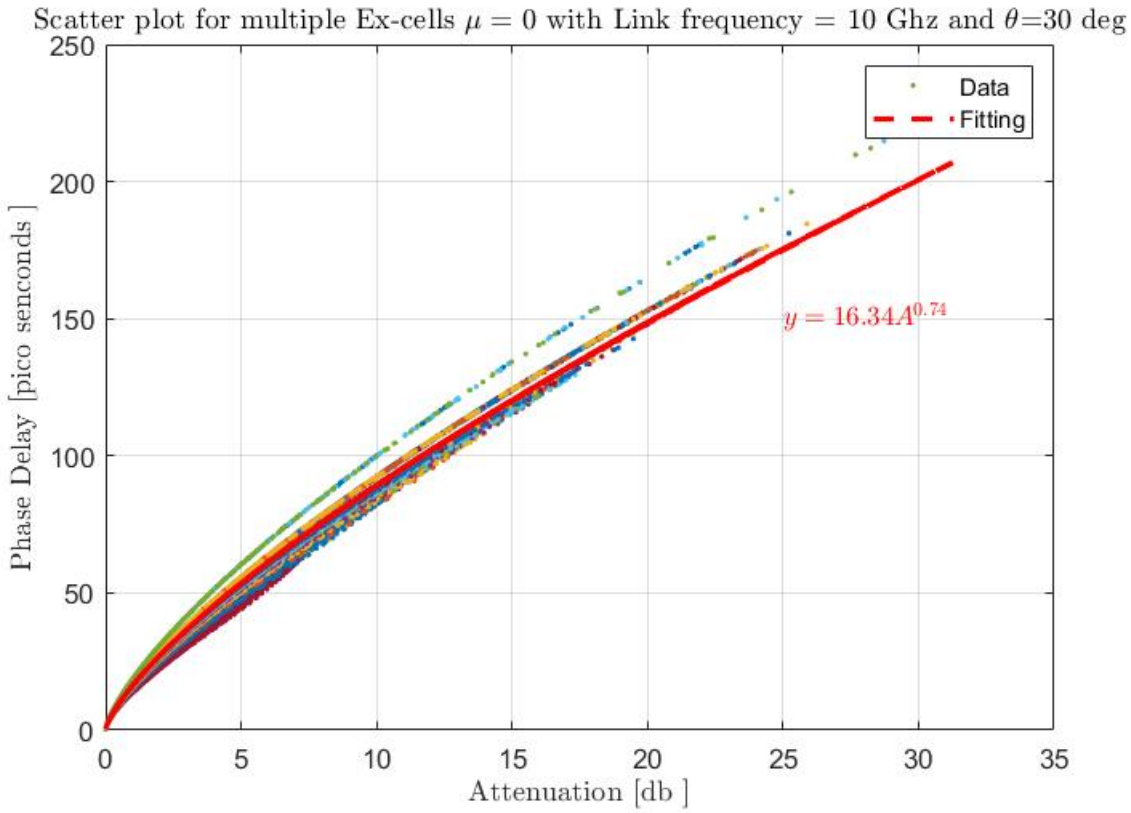

Figure 3.8: Multi-cell approach Fitting

the EXCELL profile , depends mainly on the horizontal path . We can also see that the relation between attenuation and delay for the parameters f=10 GHz , θ=30 deg , μ=0 is

$$\tau = 16.34A^{0.74} \tag{3.17}$$

Which gives already an idea about the power law linking attenuation to phase delay.

3.1.4. Parameters variation

In this section, we dissect the full range of parameters involved, in order to select the most important ones (fig. 3.1). As explained in section 1.3 and since this thesis work uses the analytical model developed in [11] for the coefficients k, α, h, β eqs. (3.6) and (3.7) The full range of parameters *potentially* influencing the relationship $\tau = f(A)$ can be listed below :

- **Frequency** f : used in [11]
- **Elevation Angle** θ used in [11]
- **Rain Height** H_R influencing attenuation and delay through L_H eqs. (3.10) and (3.11)
- **Gamma DSD parameter** μ used in [11]
- **Polarisation Angle** ψ used in [11]

For each parameter, we generate data fixing all the other parameters and using the multi-cell approach,we fit it as explained in the previous section, we plot finally the delay-attenuation $\tau = f(A)$ scatter plot varying the parameter selected .

3.1.5. Frequency

Frequency,as explained in chapter 1, is a critical parameter on which attenuation and delay intrinsically depend. In this thesis work frequencies are limited in the range 10-100 GHz. In order to depict this effect along frequency, we choose 3 frequencies 20, 50 and 90 GHz , we represent the cluster of the multi-cells curves and their fitting curve as well .

Comments

- Referring to fig. 3.9 we can first see that the frequency changes drastically the coefficients a and b ($\tau = aA^b$)
- As we discussed inchapter 1 , higher frequency leads to higher attenuation and lower phase delay thanks to eq. (3.6)
- As frequency increases, the coefficient a tends to decrease so does b, thus we can say that the functions linking a and b to frequency are decreasing functions, this part is going to be investigated in the parameters fitting section 3.2

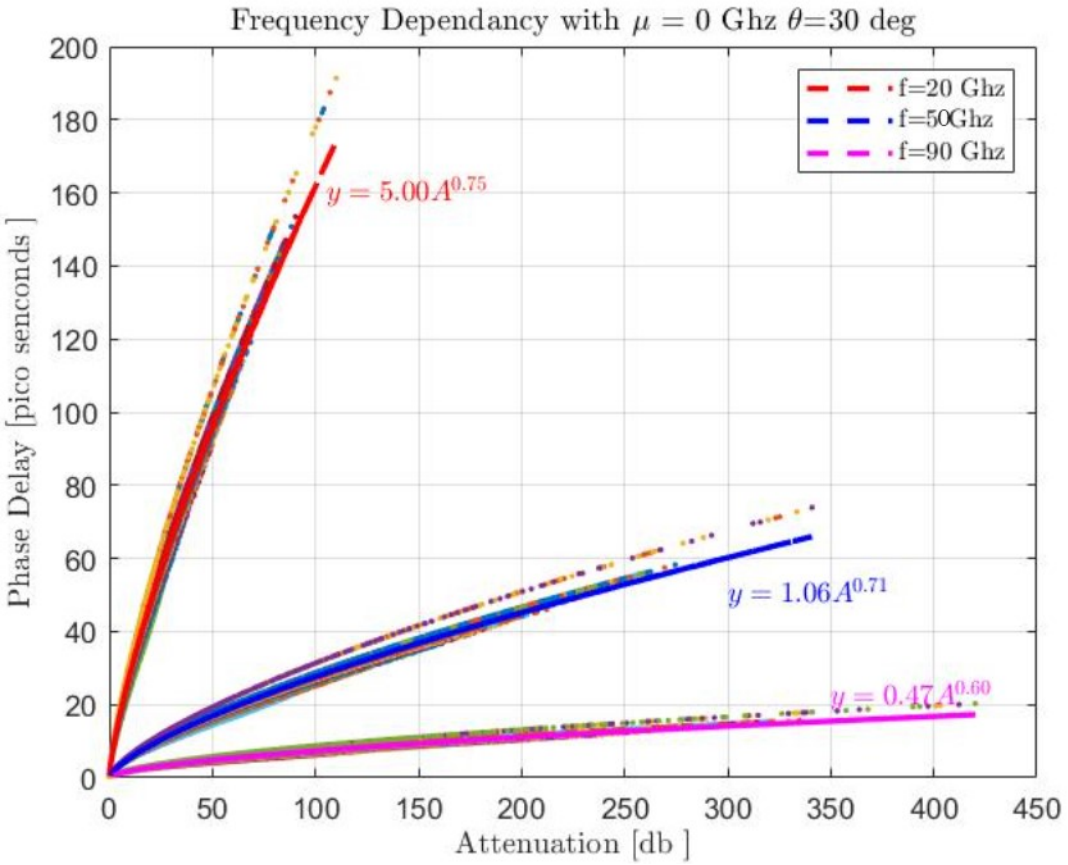

Figure 3.9: Frequency Effect on τ-A plot

3.1.6. Elevation Angle

Here we present the results of changing the elevation angle along the slant path , fixing always the frequency , rain height and drop site distribution .
In fact as we can see in fig. 3.10

$$\theta_1 < \theta_2 \Rightarrow H_p^{(2)} < H_p^{(1)} \tag{3.18}$$

The smaller the angle of elevation is , the larger is the distance that a propagated wave must pass through the Earth's atmosphere. As distance increases, the signal quality deteriorates , thus we must set a lower limit for the elevation angle i.e like in [15] we choose to limit θ to $\theta_{min} = 20°$. And since the EXCELL profile depends only on the horizontal path, we expect higher elevation angles to be less attenuated and less delayed .
Indeed , fig. 3.11 shows clearly that higher elevation angle attenuates and delays the signal less reaching the limit of zero delay and attenuation due to rain for a station pointing

upwards with an angle of $\theta = 90°$

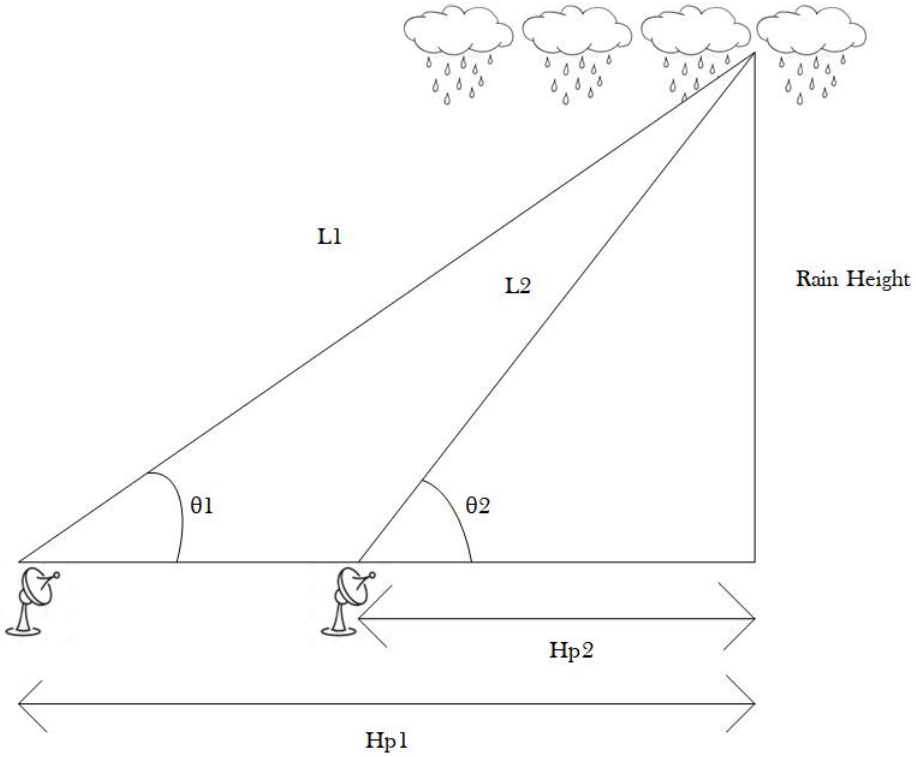

Figure 3.10: Elevation angle change Sketch

Comments

- The first thing we can notice , is how close are all the plots i.e the elevation angle variation is less influencing the τ-A plot than frequency , i.e θ is not a genuine variable of the problem since it changes merely the results , though must be taken into account probably once combined with other variables can constitute a real variable of the problem
- The elevation angle variation basically doesn't act on the exponent as we can notice the fitting of the three elevation angles plots , leads to the same exponent ≈ 0.74
- As we can see in fig. 3.11 and referring to the scheme fig. 3.5 ,the longer is the horizontal path (low elevation angle) the less are the points used in theτ-A plot , i.e less are the possibilities for the relative positions between the station and the satellite . That's why we expect for higher elevation angles (lower horizontal path) denser plots . The zoomed figure in the plot shows a different thing which brings us to understand the reason behind .

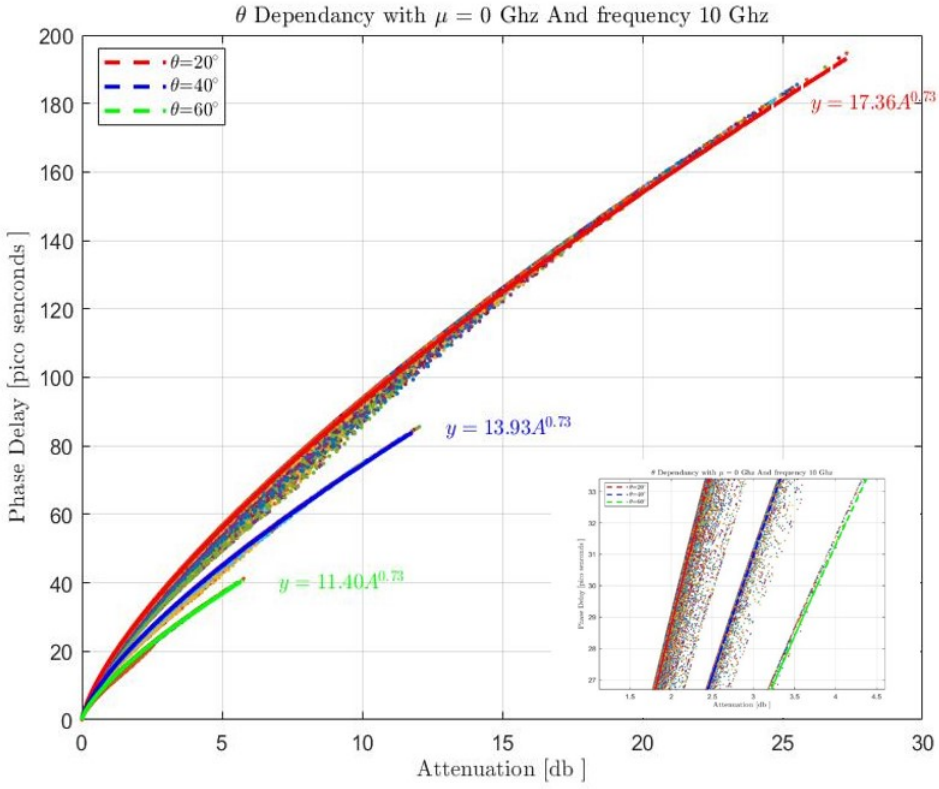

Figure 3.11: Elevation Angle Variation Effect

In fact , since we are using 20x20 cells ,as the cell's radius increases the number of pixels used for the integration decreases for a fixed H_{Hor}

$$N_{pixels} = \frac{H_{Hor}}{dx} = \frac{H_{Hor}30}{r_{cell}} \tag{3.19}$$

Let's take for example 2 cases $\theta_1 = 20°$ and $\theta_2 = 30°$ since $H^{(1)}_{Hor} > H^{(2)}_{Hor}$ for a given rain cell , we have

$$N^{(1)}_{pixels} = \frac{H^{(1)}_{Hor}30}{r_{cell}} > N^{(2)}_{pixels} = \frac{H^{(2)}_{Hor}30}{r_{cell}} \tag{3.20}$$

As the cell radius increases , the higher value of $H^{(1)}_{Hor}$ makes that it compensates the denominator r_{cell} so that the number of pixels remains sufficiently enough to perform integration $N^{(1)}_{pixels} \geq 2$ whilst for $N^{(2)}_{pixels}$ the decrease due to $1/r_{cell}$ leads many times to $N^{(2)}_{pixels} \leq 1$ the point is then discarded from the scatter plot ,since the station and the satellite positions can't occur in the same pixel leading to zero attenuation , at this stage it should be clear why for higher elevation angles , the plots are less dense

3.1.7. Rain Height

Rain height is also an important feature to study the τ-A. In recommendation ITU-R P.839-4 [20], the mean yearly rain height above mean sea level:

$$h_R = h_0 + 0.36 \text{ km} \tag{3.21}$$

where h_0 is the height of the 0°C isothermal layer, values of h_0 corresponding to different latitude and longitude which can be found in [20], which also reports the yearly average 0°C isothermal height above mean sea level as in the figure above. Typically we can set H_{Rain} to vary in the range [1.5km,5km] , since the extreme cases correspond either polar regions or in north China .

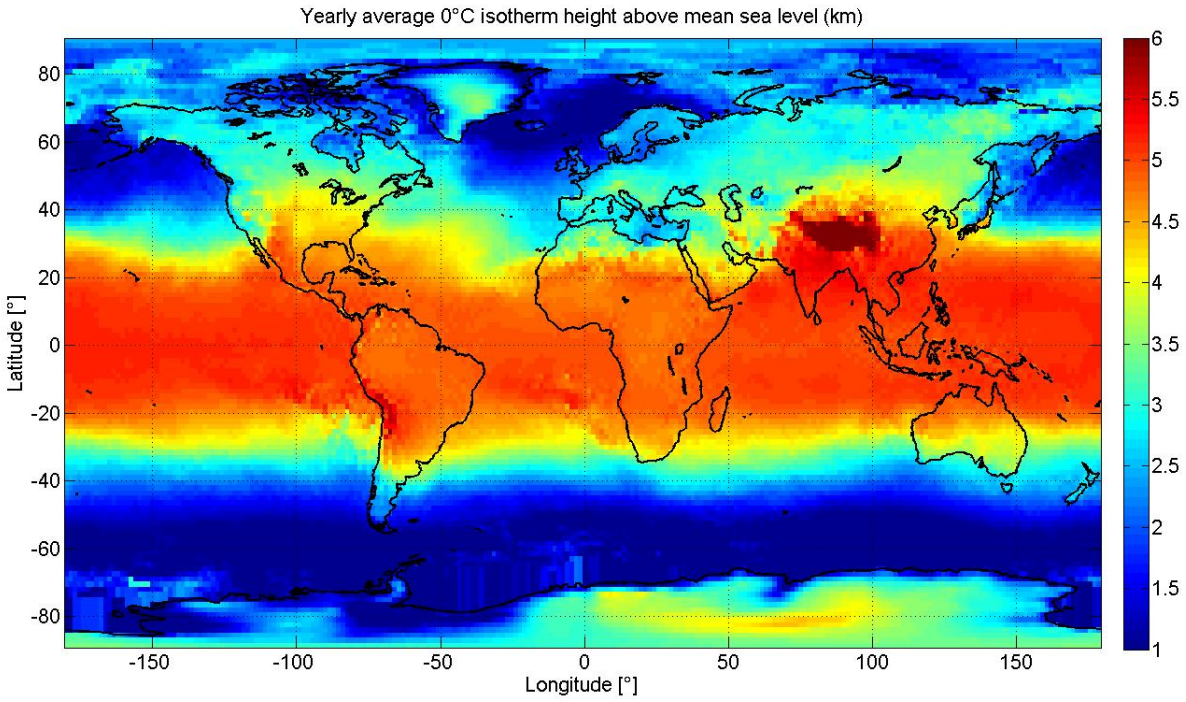

Figure 3.12: Isothermal Layer latitude

Comments In fig. 3.13, we notice that the rain height likewise elevation angle θ is not a real variable since it only drives small changes in the Attenuation-Delay power law, we can still notice the density of points for higher rain heights likewise the elevation angle plots, and the highest attenuation and delay are for higher rain altitudes for the same reason explained in the previous section.

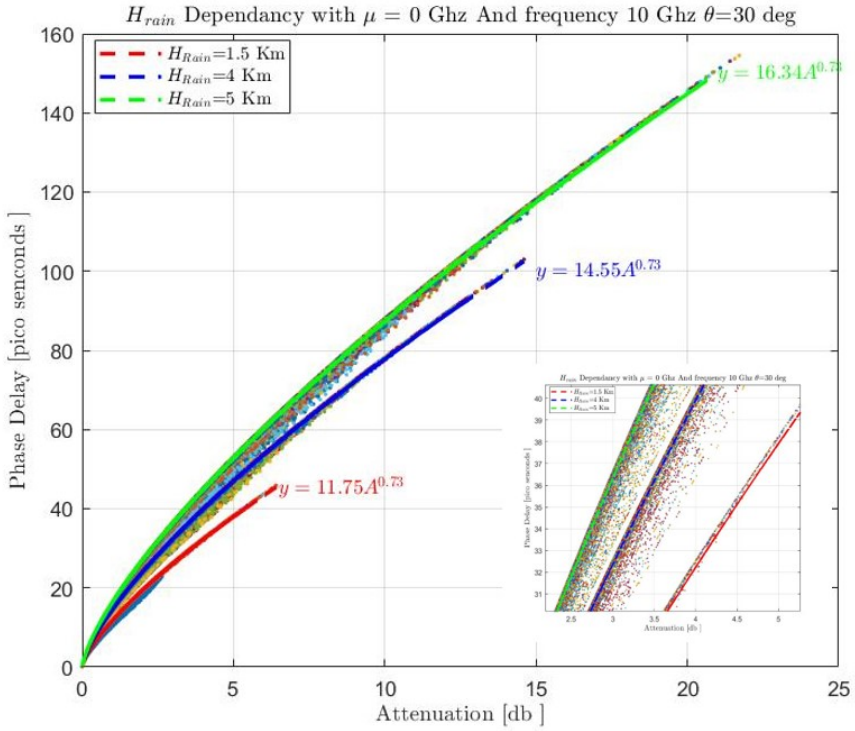

Figure 3.13: Rain Height Variation Effect

3.1.8. Drop size distribution

The Drop Size Distribution (DSD) represents the number of raindrops in a unit volume and for a given size. DSD is an important information to study the effects of drops on electromagnetic waves. There exist different DSD such as : Laws-Parson distribution , Marshell-Parson(MP) distribution , Gamma distribution , Joss distribution , log-normal distribution , Weibull distribution... Theoretically, rainfall rate is a function of DSD and rain drop terminal velocity [3], the equation is:

$$R = 6 \times 10^{-3} \pi \int_0^{\infty} N(D) v(D) D^3 dD \quad \left(\frac{\text{mm}}{\text{h}}\right) \tag{3.22}$$

where $v(D)$ is the terminal velocity of drops, the equation is:

$$v(D) = 9.65 - 10.3e^{-600D} \quad \left(\frac{\text{m}}{\text{s}}\right) \tag{3.23}$$

In this thesis work ,we pick a gamma distribution since its model was already developed in the thesis work [11]. The Gamma distribution introduces a shape factor μ into the

M-P distribution, its model can be written as :

$$N(D) = N_0 D^{\mu} e^{-\Lambda D} \quad (0 \leq \mathrm{D} \leq \mathrm{D}_{\max}) \tag{3.24}$$

where the value of μ typically falls in the range between -1 and 4 , but values have been also measured in the interval between -3 and $8, N_0$ is the scaling parameter, $\Lambda\,(\mathrm{mm}^{-1})$ is the slope parameter.

REMARK : As the reader might have noticed in the previous sections and also in chapter 1, we say that the value μ is the only parameter characterizing the distribution gamma, in fact in eq. (3.24) N_0 and λ depend on μ and R so that the only free parameter is μ.

Compared with the M-P distribution, thanks to its flexibility, the gamma distribution can fit all kinds of raindrop size distribution well, especially for small droplets. The parameter estimation of the gamma distribution is more complicated than that of the M-P distribution, especially the factor μ. Hence, the gamma distribution hinges mainly on the parameter μ , the relationship τ -A must investigate it as well .

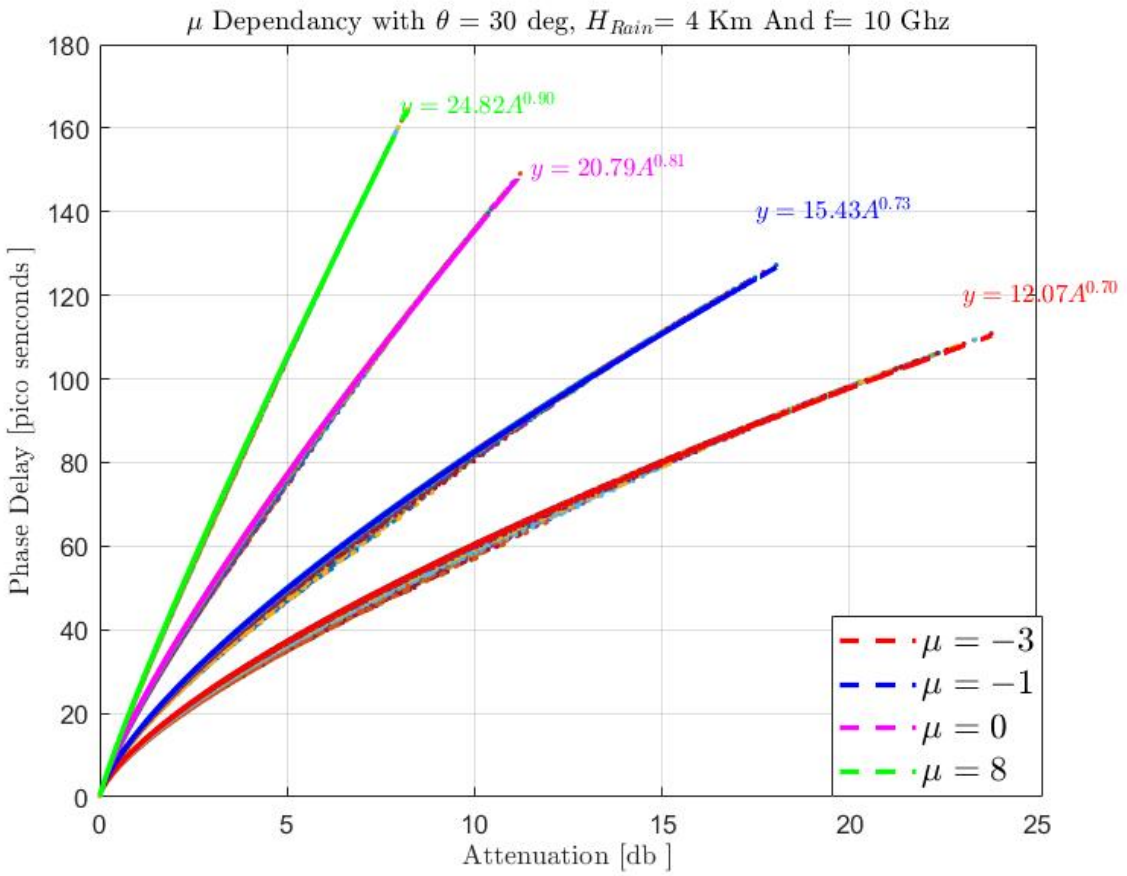

Figure 3.14: DSD Effect varying μ

Comments As we can clearly see in fig. 3.14, changing the parameter μ changes drastically the relationship τ-A , since changing the DSD means, under the hood, increasing or decreasing the number of drops of a given size scattering the signal. Dissecting the results , we can drop some important comments:

- The results show that the highest attenuation is for μ=-3 whilst the highest phase delay is for μ=8
- eq. (3.22) depicts the dependency of the rain rate (mm/h) on the drop size diameter , the latest is exposed to μ+3 inside the integral, thus for $\mu = -3$ N(D) is maximal so is the rain rate the reason why the μ=-3 plot gives the highest attenuation .
- the same thing can be said about the upper case μ= 8 where inside the integral , there is a positive power (μ + 3 =11) of the drop size , since the integral is dominated by smaller rain drops eq. (3.22) then for μ=8 we get a minimum rain rate thus a minimum attenuation

3.1.9. Polarisation angle

Polarization is important in wireless communications systems.Since horizontal and vertical polarisations undergo different propagations, so at least our model should target those two cases, and if it is a main parameter it is important to know its effect on the attenuation and the phase delay relationship Since the polarisation ψ can vary in the range [0,π] we can pick 3 particular cases for the polarisation angle :

- $\psi = 0°$: Vertical linear polarisation
- $\psi = 180°$: Horizontal linear polarisation
- $\psi = 90°$: Circular polarisation
- $\psi = 45°$: random elliptical polarisation

Comments It's important to mention the following aspects about the polarisation angle

- we can notice in figs. 3.15 and 3.16 all the scatter plot follow the same trend
- The linear polarisation ($\psi \equiv 0[\pi]$) knows a slightly higher attenuation while the circular one gives rise to the minimum attenuation
- Conclusion since the polarisation angle doesn't change considerably the τ-A relationship, we can pick a polarisation angle of ψ=45° and thus this variable woun't be investigated in the parameters fitting section 3.2

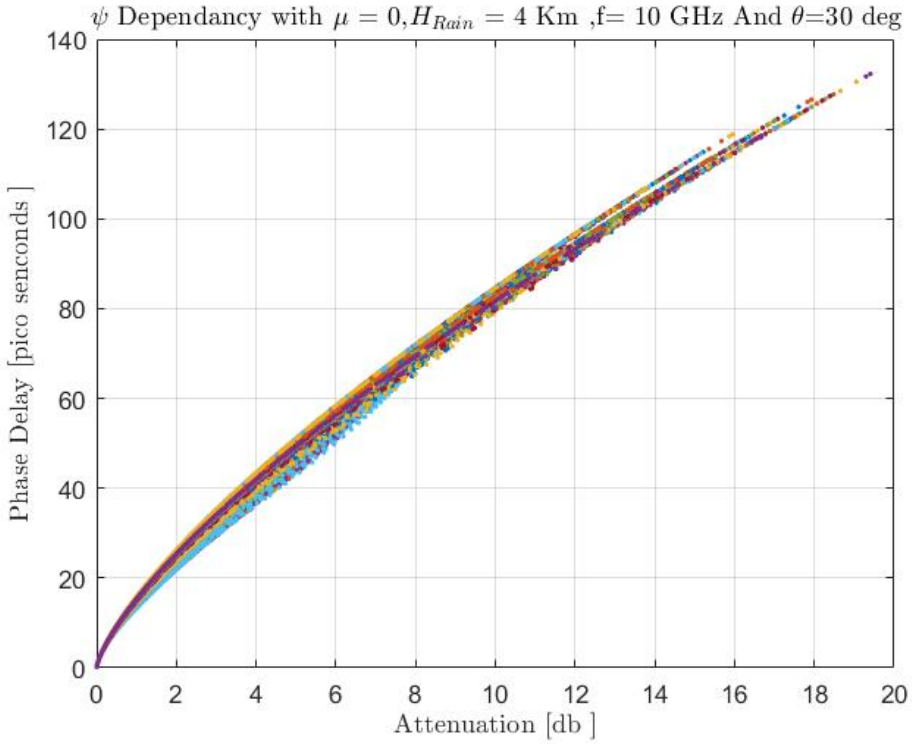

Figure 3.15: ψ Scatter-plot dependency

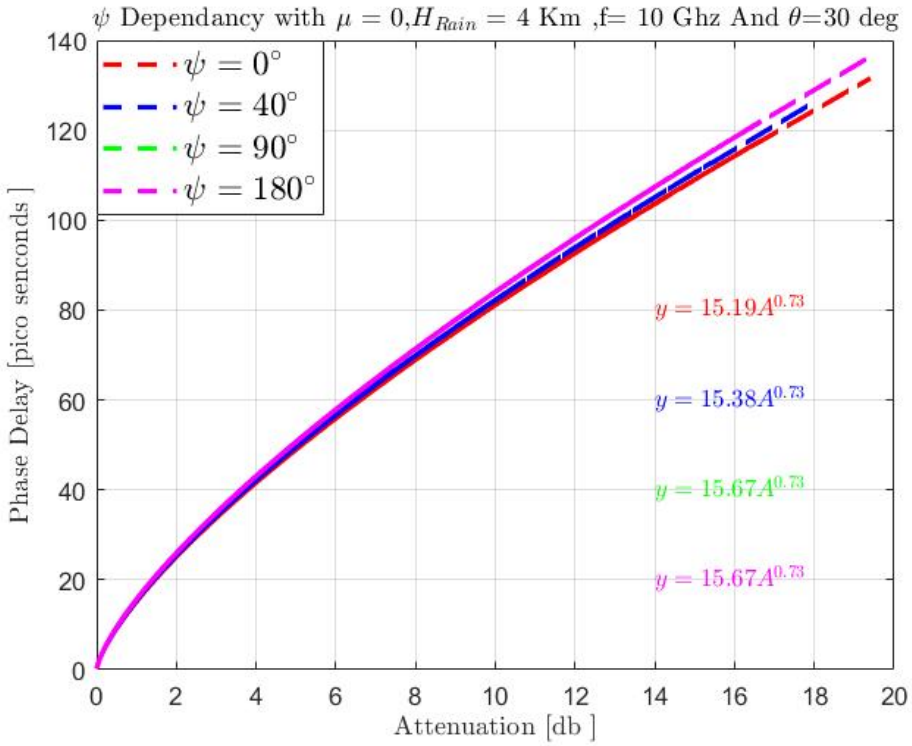

Figure 3.16: ψ Fitting Relationships

3.1.10. Final Parameters

As we have seen, the previous study unveiled that frequency, μ parameter are pivotal variables, while elevation angle θ, rain height H_{Rain} are semi variables, and finally polarisation angle ψ can be fixed henceforth . Since the EXCELL model involves a key parameter which is the horizontal path and considering that cells profile is horizontal and the whole integration is equivalently performed on the horizontal path eqs. (3.10) and (3.11), one way to combine both variables θ and H_{Rain} is then the horizontal path , we recall that

$$L_H = \frac{H_{Rain}}{tan(\theta)}$$

Even though taking L_H as a variable of the problem might look not rigorous because it involves two variables, but since the rain height variation is investigated by the international telecommunications union ITU[20], so the knowledge of the elevation angle is the only thing needed from the user, θ is defined beforehand knowing the station and the satellite positions .

Thus, the choice of L_H is well justified, we can ultimately formulate the following task of fitting as : find the functions a and b such that :

$$\begin{cases} \psi = 45^\circ \\ \\ L_H = \frac{H_{\text{Rain}}}{\tan(\theta).} \\ \\ \tau = a((f, L_H, \mu)\ A^{b(f,L_H,\mu)} \end{cases} \tag{3.25}$$

Where :

- H_{Rain} is the rain height
- θ is the link elevation angle
- f is the link frequency
- L_H is the horizontal path i.e : projection of the slant path on the ground
- μ Gamma distribution parameter for the drop size distribution
- ψ is the fixed polarisation angle

3.2. Parameters Fitting

In this section, we fit the generated curve using multi-cells fitting (section 3.1.3), representing the *Data*, to the parameters defined in the previous section, these parameters are bounded, so, it's important to remind their limits .

3.2.1. Parameters bounding

- **Frequency** The thesis work is limited for frequencies in the range 10-100 GHz, for which atmospheric attenuation is more relevant.
- $\boldsymbol{\mu}$ The parameter μ characterizing the gamma function eq. (3.24) is an integer that varies in the set {-3,-2,..8}
- $\boldsymbol{L_H}$ The horizontal path limits are found from elevation angle and rain height limits respectively , in fact :
  - $\boldsymbol{\theta}$ Most telecommunication links don't go beneath 20° since they have to deal with more attenuation , thus we set θ in the range [20°,90°]
  - $\boldsymbol{H_{Rain}}$ As we discussed in section 3.1.7, the typical rain height is in the range 1.5 Km to 5 Km , and finally recalling eq. (3.9) we can set the horizontal path L_H variable between : 0 and 13.73 Km
- $\boldsymbol{\psi}$ As we discussed in the previous section, ψ doesn't affect the results so we can fix it to $\psi = 45°$, results of other polarisation angles should not be so different from the results shown in this work .

Remark For the seek of simplicity, during all this chapter, we fix μ, since $\mu = 0$ is the most probable one for the gamma distribution, we focus on this case only, but for other values, the reader is addressed to appendix A where important results are shown .

$$\mu = 0 \tag{3.26}$$

3.2.2. Fitting Structure

In order to clarify the procedure used to derive the analytical model linking attenuation to delay.We present the general scheme for fitting. In fact, once fixing μ, the remaining parameters are frequency and horizontal path, as we can see in fig. 3.17, we generate 2 lists for both frequency and horizontal path, then for each couple f, L_H we generate the data (vector of phase delays and attenuations), and we fit both with the known relationship

$\tau = aA^b$, finally we get 2 matrices a(f, L_H) and b(f, L_H).We first fix L_H and we fit the a and b to frequency. Once done , we vary L_H and we fit the coefficients of the first fitting to horizontal path.

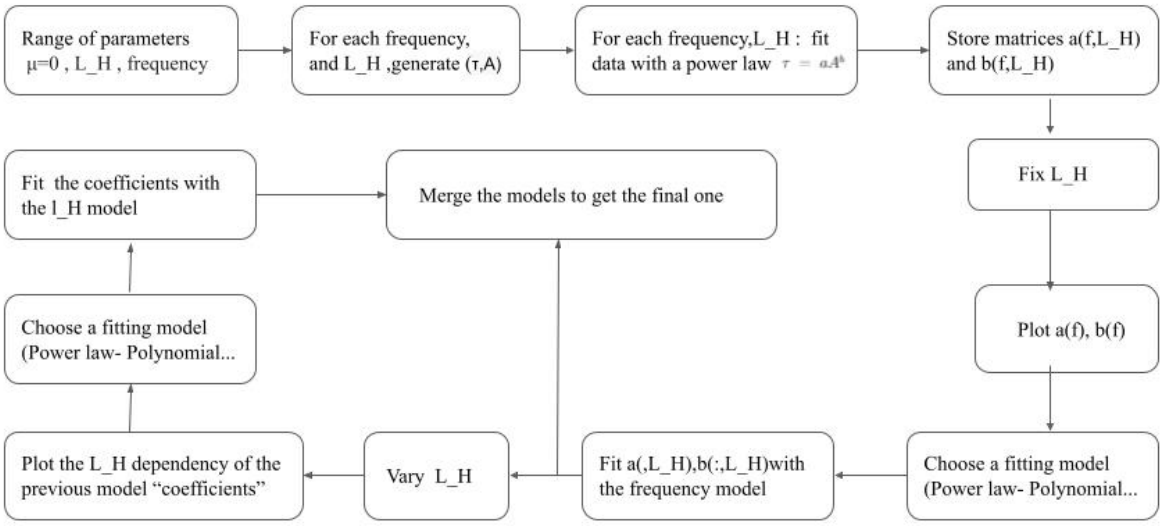

Figure 3.17: Fitting structure

3.2.3. Frequency Mapping

In this first mapping , we fix certain values for (H_{Rain}, θ) i.e a value of L_H and we plot the dependency of both $a((f, L_H, \mu = 0)$ and $b\,(f, L_H, \mu = 0)$. We can see in fig. 3.18 that the a coefficient follows a power law while the frequency trend for b is a polynomial shape. We try therefore to fit a with a power law of frequency, and b with a fourth degree polynomial, we don't know if this is the most accurate model, but the fourth polynomial law already gives good fitting for b. We will confront different models in section 3.2.5 to finally pick up the best one. We can write already :

$$\begin{cases} a(f) = a_1 f^{a_2} \\ b(f) = b_1 f^4 + b_2 f^3 + b_3 f^2 + b_4 f + b_5 \end{cases} \tag{3.27}$$

For the fitting procedure, 100 frequencies spanning the domain 10-100 GHz were used to fit the model, we can see in fig. 3.18 that we have a good fitting especially for the

coefficient a whose dependency follows well a power law, for b there are some inaccuracies for low frequencies but we can say that the model follows roughly a fourth polynomial trend .

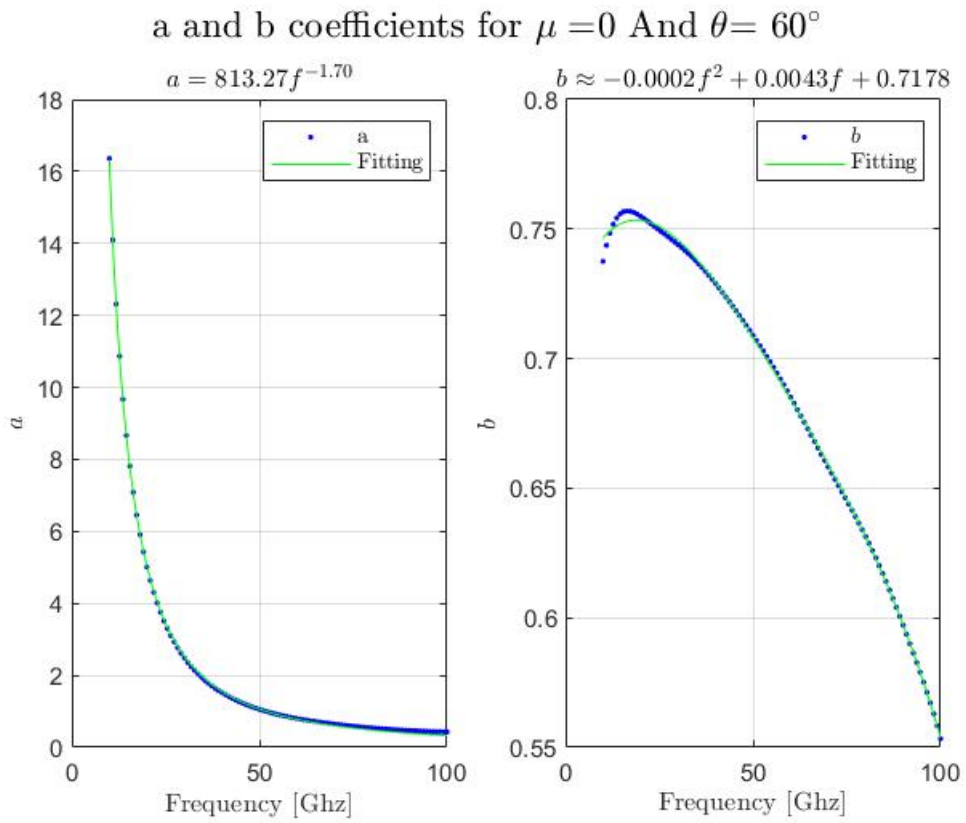

Figure 3.18: Frequency Fitting results

3.2.4. Horizontal Path Mapping

Both elevation angle θ and rain height H_R can be combined as a single variable i.e the slant path L_H. Likewise the frequency , since we don't know beforehand the shape of the dependency on the horizontal path , it's worthwhile to draw the variation of the coefficients found in the first frequency mapping step i.e $a_1, a_2, b_1, b_2, b_3, b_4, b_5$ along the horizontal path L_H.

a coefficients

It appears in figs. 3.19 and 3.20 that a polynomial can fit the data , we can have a pretty good fitting for both a_1 and a_2 using a fifth polynomial ,indeed we can write :

$$\forall i \in \{1,2\} \quad a_i = \sum_{j=0}^{5} a_{ij} L_H^j \tag{3.28}$$

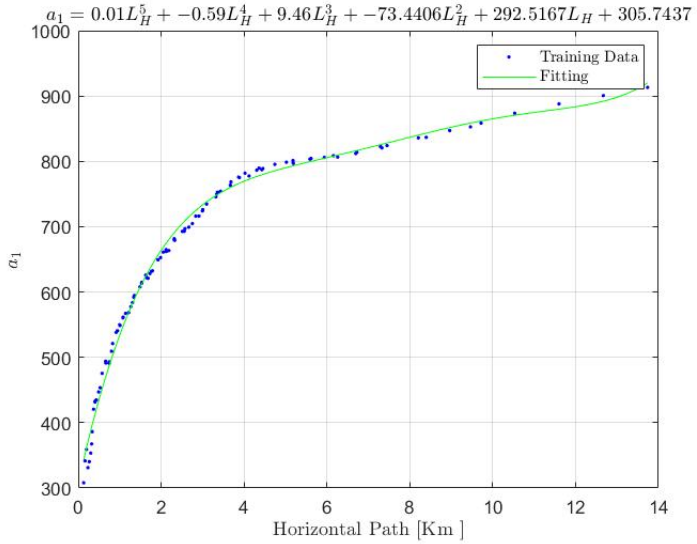

Figure 3.19: a_1 Horizontal Path Fitting results

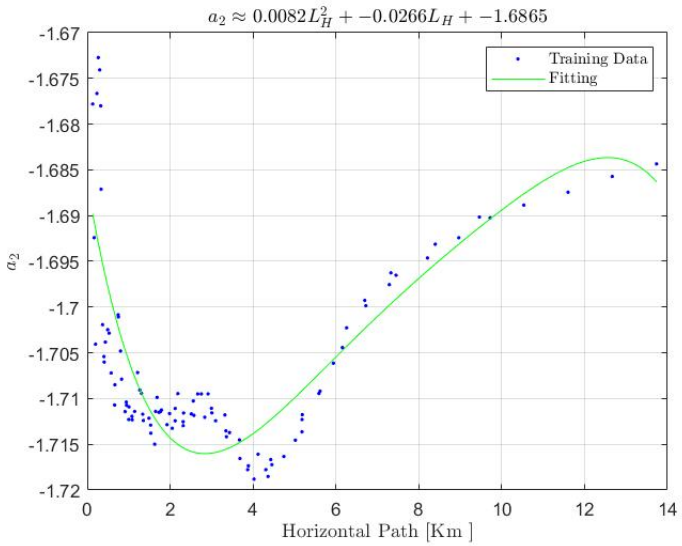

Figure 3.20: a_2 Horizontal Path Fitting results

b coefficients

We can see in fig. 3.21, to fig. 3.25 that a polynomial function is indeed a good candidate to fit the five coefficients b_1,...b_5 dependency to L_H, we can notice that high order coefficients (b_1, b_2) are very small, in fact, in eq. (3.27), they are multiplied by the forth and the third

power of frequencies that are in the range 10 ,10^2 .For example the terms b_1, b_2 bring, in average, a correction in the order of

$$b_1 f^5 \approx 10^{-9}10^5 = 10^{-4} \qquad b_2 f^4 \approx 10^{-6}10^4 = 10^{-2}$$

These terms are therefore adding more corrections to the model , we see also that the dominant part in the exponent is held by the last term b_5 whose average value is around 0.7 . Thus, choosing a fifth degree polynomial we can write :

$$\forall i \in \{1,2,3,4,5\} \quad b_i = \sum_{j=0}^{5} b_{ij} L_H^j \tag{3.29}$$

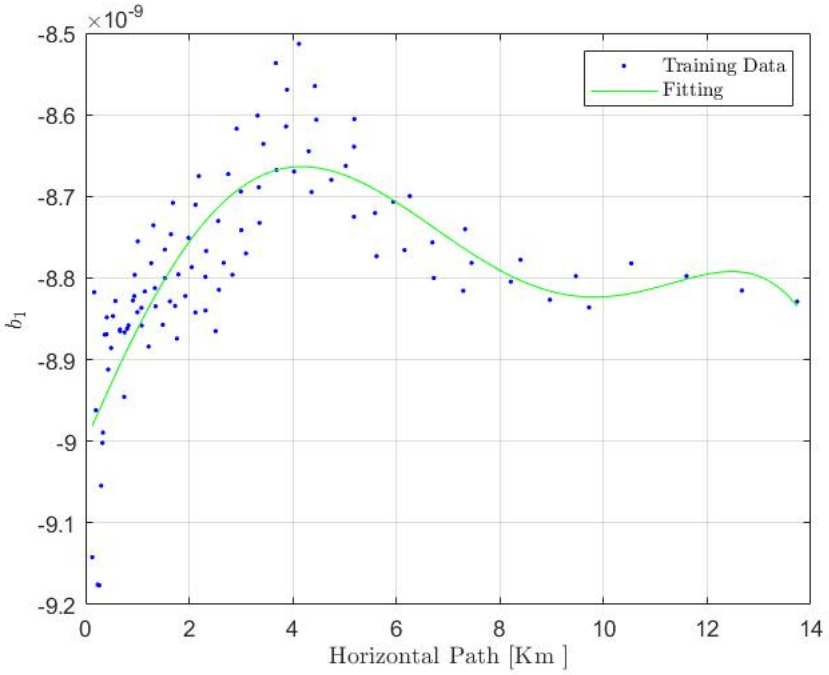

Figure 3.21: b_1 fitting along the Horizontal Path Variation

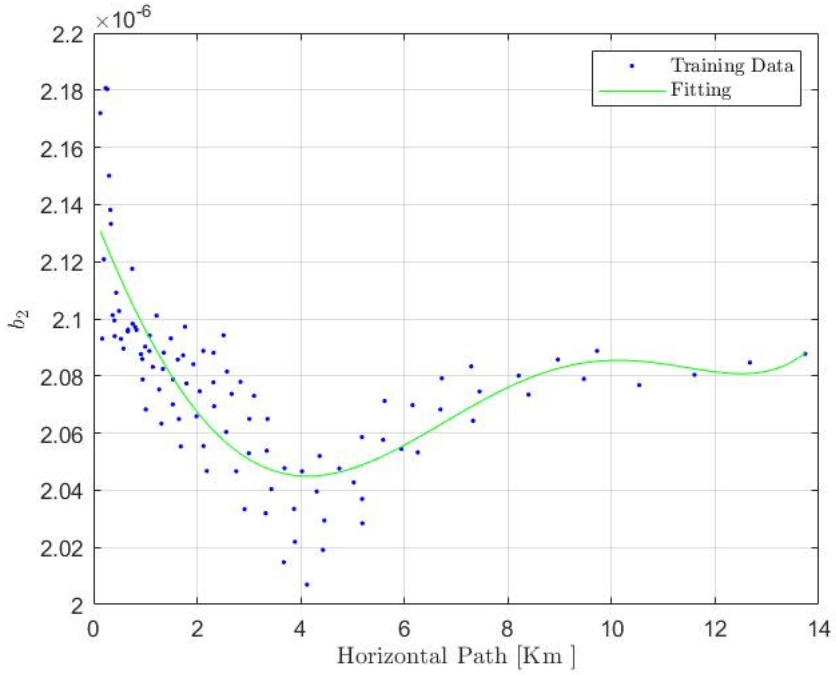

Figure 3.22: b_2 fitting along the Horizontal Path Variation

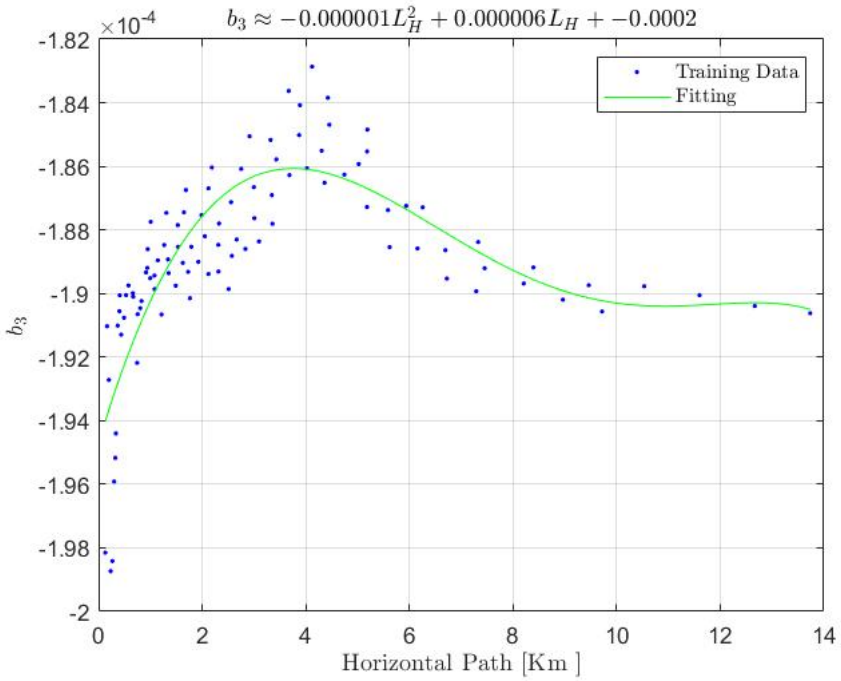

Figure 3.23: b_3 fitting along the Horizontal Path Variation

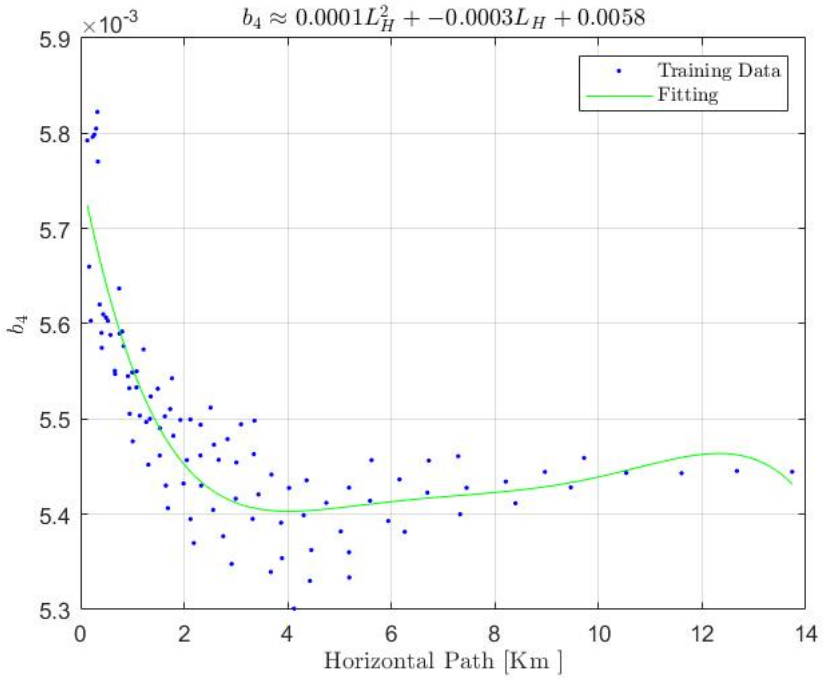

Figure 3.24: b_4 fitting along the Horizontal Path Variation

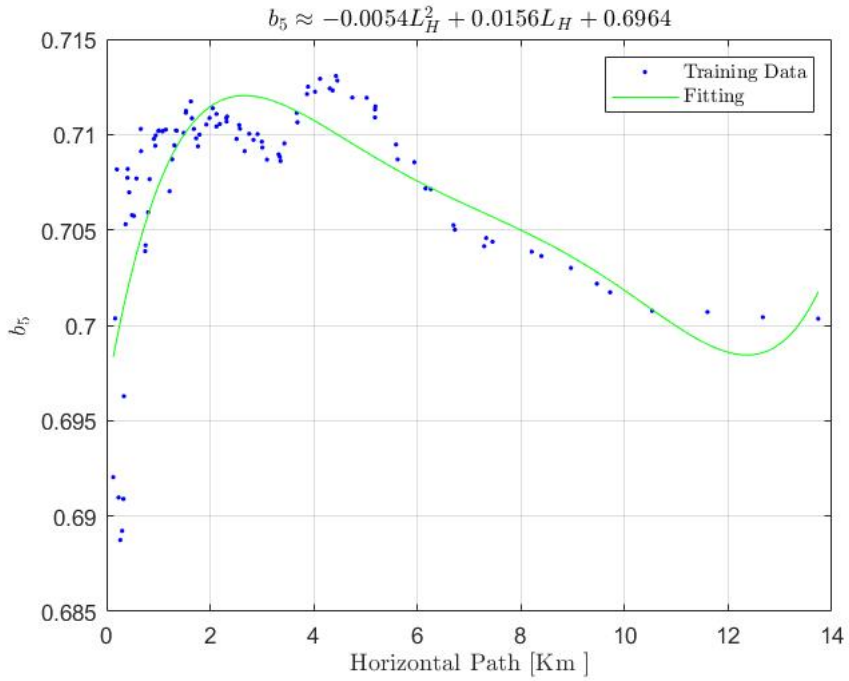

Figure 3.25: b_5 fitting along the Horizontal Path Variation

Model for μ=0

At this stage , for a fixed value $\mu = 0$ we have the complete model involving :

- A power law for a(f) eq. (3.27)
- A fourth polynomial for b(f) eq. (3.27)
- A fifth polynomial for the horizontal path dependency for:$a_1, a_2, b_1, b_2, b_3, b_4, b_5$ eq. (3.28),eq. (3.29)

For the seek of simplicity, this first analytical model will be referred in the rest of this work as *Model 1*, we can explicit all the coefficients involved in table 3.2

Table 3.2: Analytical Model for $\mu = 0$

$\mu = 0$	$\boldsymbol{\tau = aA^b}$						
Model	$\boldsymbol{a = a_1 f^{a_2}}$		$\boldsymbol{b = b_1 f^4 + b_2 f^3 + b_3 f^2 + b_4 f + b_5}$				
	a_1	a_2	b_1	b_2	b_3	b_4	b_5
	$\sum_{j=1}^{j=6} c_j L_H^{j-1}$	$\sum_{j=1}^{j=6} c_j L_H^{j-1}$	$\sum_{j=1}^{j=6} c_j L_H^{j-1}$	$\sum_{j=1}^{j=6} c_j L_H^{j-1}$	$\sum_{j=1}^{j=6} c_j L_H^{j-1}$	$\sum_{j=1}^{j=6} c_j L_H^{j-1}$	$\sum_{j=1}^{j=6} c_j L_H^{j-1}$
$\boldsymbol{c_6}$	0.0142	-1.61 10^{-6}	-2.05 10^{-14}	3.6 10^{-12}	-7.6 10^{-11}	-1.9 10^{-8}	1.56 10^{-6}
$\boldsymbol{c_5}$	-0.589	6.5 10^{-5}	6.09 10^{-13}	-9.82 10^{-11}	-2.68 10^{-11}	7.4 10^{-7}	$-5.78\ 10^{-5}$
$\boldsymbol{c_4}$	9.456	-1.04 10^{-3}	-4.87 10^{-12}	5.36 10^{-10}	6.75 10^{-8}	-1.1 10^{-5}	8 10^{-4}
$\boldsymbol{c_3}$	-73.44	0.008	-4.45 10^{-12}	4.95 10^{-9}	$-1.1\ 10^{-6}$	8.1 10^{-5}	-0.0055
$\boldsymbol{c_2}$	292.5	-0.026	1.46 10^{-10}	-4.6 10^{-8}	5.51 10^{-6}	-2.7 10^{-4}	0.0155
$\boldsymbol{c_1}$	305.7	-1.686	-9 10^{-9}	2.13 10^{-6}	-2 10^{-4}	0.005	0.696

3.2.5. Error of the model

With reference to the map of the chapter fig. 3.1, we arrived at the error computation, in fact, in order to validate Model 1 (section 3.2.4), it's important to compute its error, first, we will observe how close is the analytical formula from "data" (section 3.1.3) for some examples of f and L_H fig. 3.26 and then we will see how this error changes as a matrix of f and L_H fixing always μ to zero. Once the matrix error is computed, we can define a threshold for the error, in order to pick the best model. let's explore how well is the model in 4 cases whose properties are summarized in table 3.5

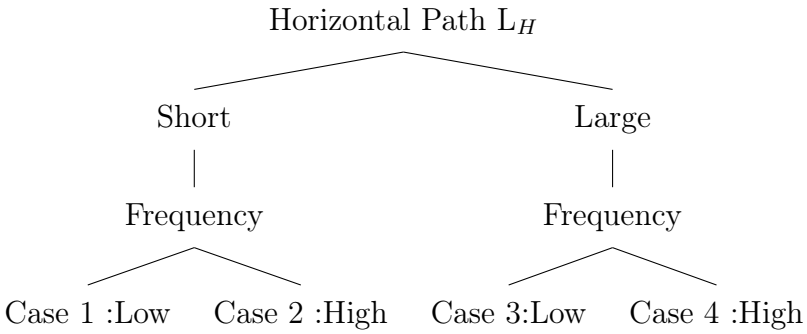

Figure 3.26: 4 different cases

Table 3.3: Link properties

Link properties						
	$\boldsymbol{f}$	$\boldsymbol{\theta}$	$\boldsymbol{H_R}$	$\boldsymbol{\mu}$	$\boldsymbol{\psi}$	$\boldsymbol{L_H}$
Case 1	10 Ghz	60 deg	1.5 Km	0	$\pi/4$	0.86
Case 2	70 Ghz	60 deg	1.5 Km	0	$\pi/4$	0.86
Case 3	10 Ghz	20 deg	5 Km	0	$\pi/4$	13.73
Case 4	70 Ghz	20 deg	5 Km	0	$\pi/4$	13.73

Comments

- At the first glance, fig. 3.27 to fig. 3.30 show that the analytical model follows pretty well the trend of data, with perfect fitting for small attenuation levels, and some divergences (depending on the case) for high attenuations.
- It's also important to notice that only in the fourth case fig. 3.30 that the analytical model underestimates the phase delay (the red curve is below the data curve).
- The 4 cases clearly show that a complete analysis is needed, covering multiple cases and evaluating the error in each case, and that leads us to the next section .

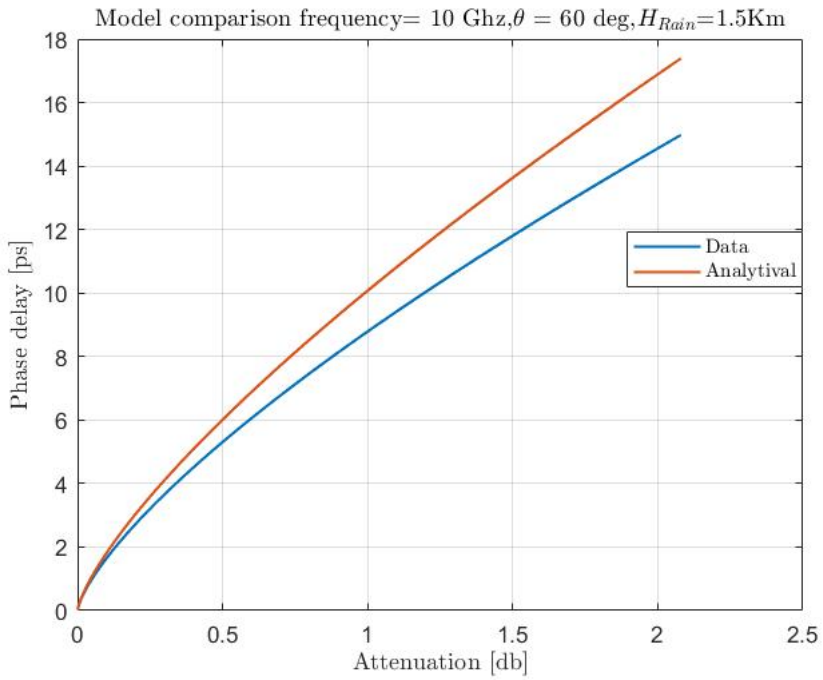

Figure 3.27: Case 1 comparison

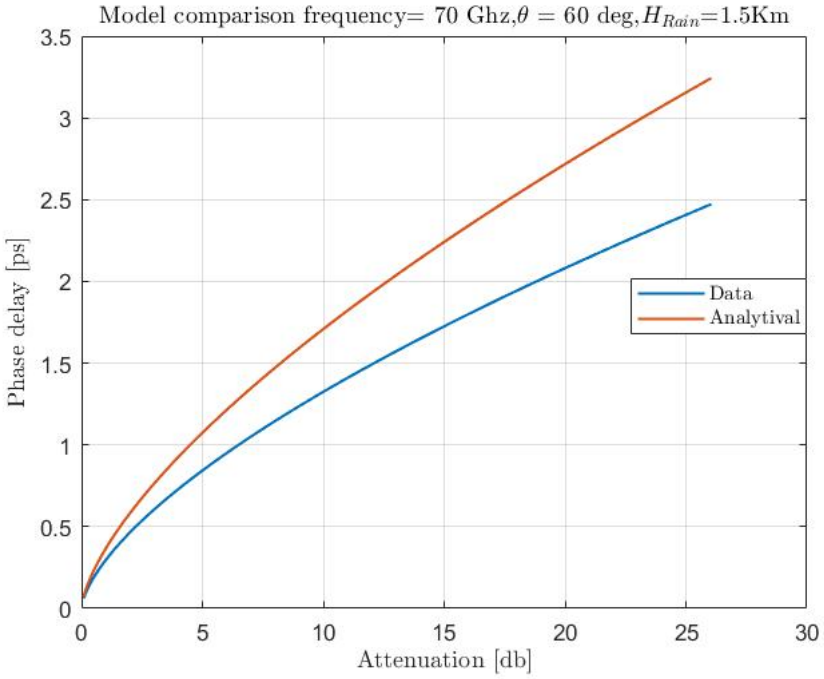

Figure 3.28: Case 2 comparison

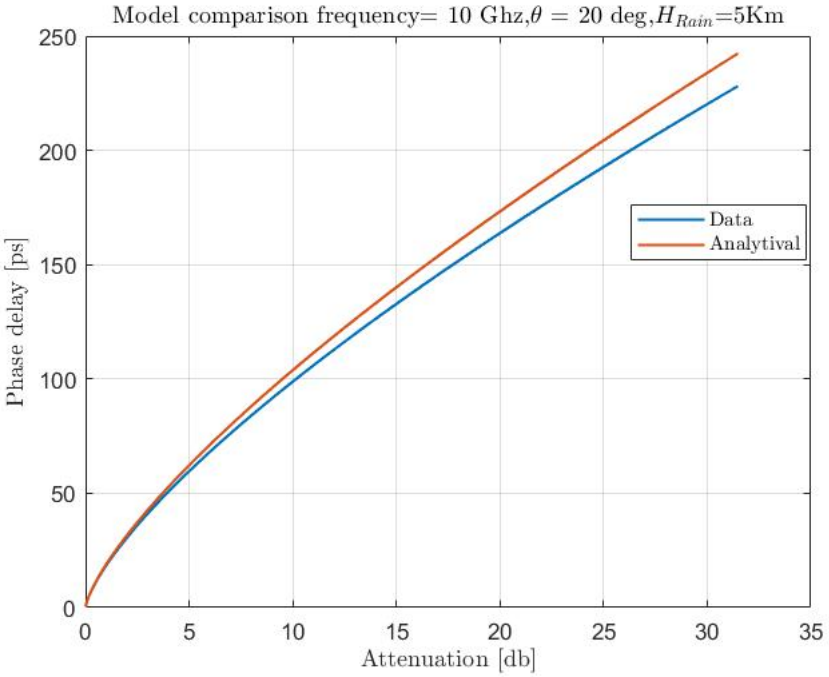

Figure 3.29: Case 3 comparison

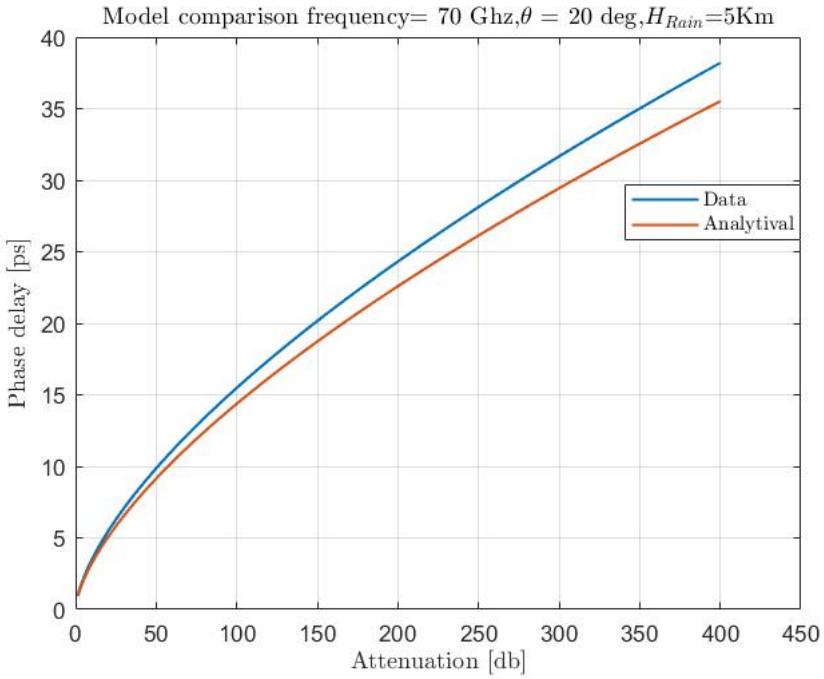

Figure 3.30: Case 4 comparison

Error Analysis

Based on the last figures, we can see that sometimes the analytical curve is much closer to the data curve, while sometimes it's not the case, thus, we need to find a way to quantify

the quality of the fitting i.e define an error figure, the classical way of defining the error between the analytical results and the data is:

$$\epsilon = \tau_{Analy} - \tau_{Data} \tag{3.30}$$

Or similarly, the absolute error in percentage :

$$\epsilon = 100.\frac{\tau_{Analy} - \tau_{Data}}{\tau_{Data}} \tag{3.31}$$

We would better use the error figure in eq. (3.32) which prevents the strong increase in for τ approaching 0 . This error figure has been defined by ITU-R P.311-13 [1] to deal with low value of attenuation, but can be used also for phase delay :

$$\varepsilon = \begin{cases} 100\left(\frac{\tau_{data}}{10}\right)^{0.2}\ln\left(\frac{\tau_{analy}}{\tau_{data}}\right) & \tau_{data} < 10ps \\ 100\ln\left(\frac{\tau_{analy}}{\tau_{data}}\right) & \tau_{data} \geq 10ps \end{cases} \tag{3.32}$$

we can see that for low values of phase delay , the error is compensated by the term $\left(\frac{\tau_{data}}{10}\right)^{0.2}$ to avoid divergence .
Now, having defined the error figure, the idea is to represent every couple (f,L_H) by a value representing how well is the fitting between the analytical model and data, for this purpose, we generate a list of frequencies and a list of horizontal paths, and for each value we evaluate the root mean square (rms) of the *vector* error defined in eq. (3.32).
The first results of fig. 3.31 show that globally the rms is below 10 % with a mean value of 8 %, a maximum of 26.2% and a minimum value of 0.06%, we notice that :

- The plots shows 2 critical regions where the rms of the error is higher than 20 % :
  1. very short horizontal path $L_H \leq 0.7$ Km i.e high elevation angles θ for a fixed rain height and high frequencies (70-100) GHz
  2. High horizontal path $L_H \geq 10$ Km i.e low elevation angles θ for a fixed rain height and very high frequencies (90-100) GHz

  Those regions if kept, might be a shortcoming of the model, thus we need to limit the validity of the actual model if kept or improve it to fit better the data.
- There is a region of green-blue color where the rms is between 10% and 15% where the fitting is not good but not bad, the error in this region might be eliminated increasing the degree of the polynomial used in the fitting.

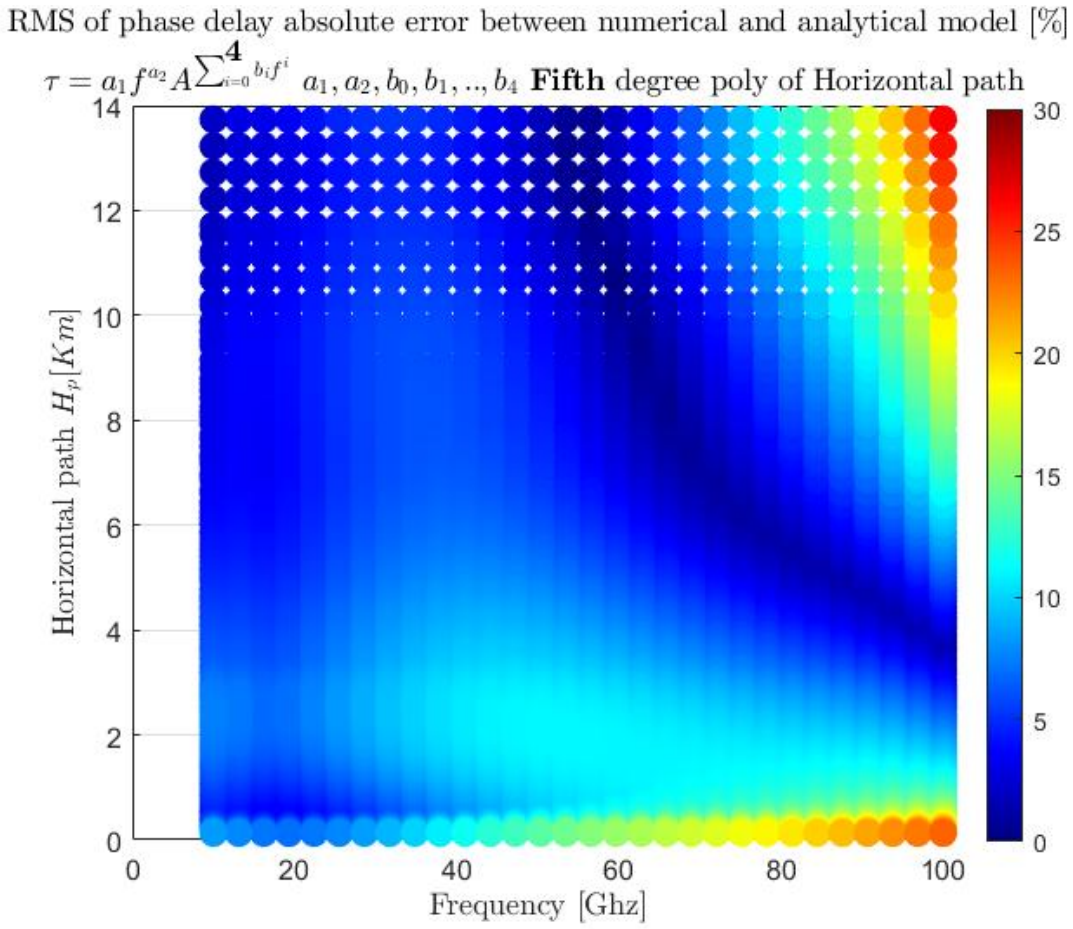

Figure 3.31: Root mean square of the error figure

Let us now see what happens to the error if we use a higher order polynomial for equations eq. (3.27) ,eq. (3.28) ,eq. (3.29) leading to a new model: *Model 2*

- As we saw in previous sections, the power law fits well the data, therefore we keep eq. (3.27) for the coefficient a, i.e $a(f) = a_1 f^{a_2}$
- A ninth degree polynomial for the frequency dependency for the b eq. (3.27) i.e

$$b(f) = \sum_{i=1}^{i=10} b_i f^{i-1} \tag{3.33}$$

- A ninth degree polynomial for L_H for a_1 ,a_2 eq. (3.28) and b_i eq. (3.29)

$$a_1(L_H) = \sum_{j=1}^{j=10} a_{1j} L_H^{i-1} \qquad a_2(L_H) = \sum_{j=1}^{j=10} a_{2j} L_H^{i-1} \qquad b_i(L_H) = \sum_{j=1}^{j=10} b_{ij} L_H^{i-1} \tag{3.34}$$

Defining the same error figure of eq. (3.32) and calculating its rms, we can plot the root mean square of the error figure for the *Model 2*.

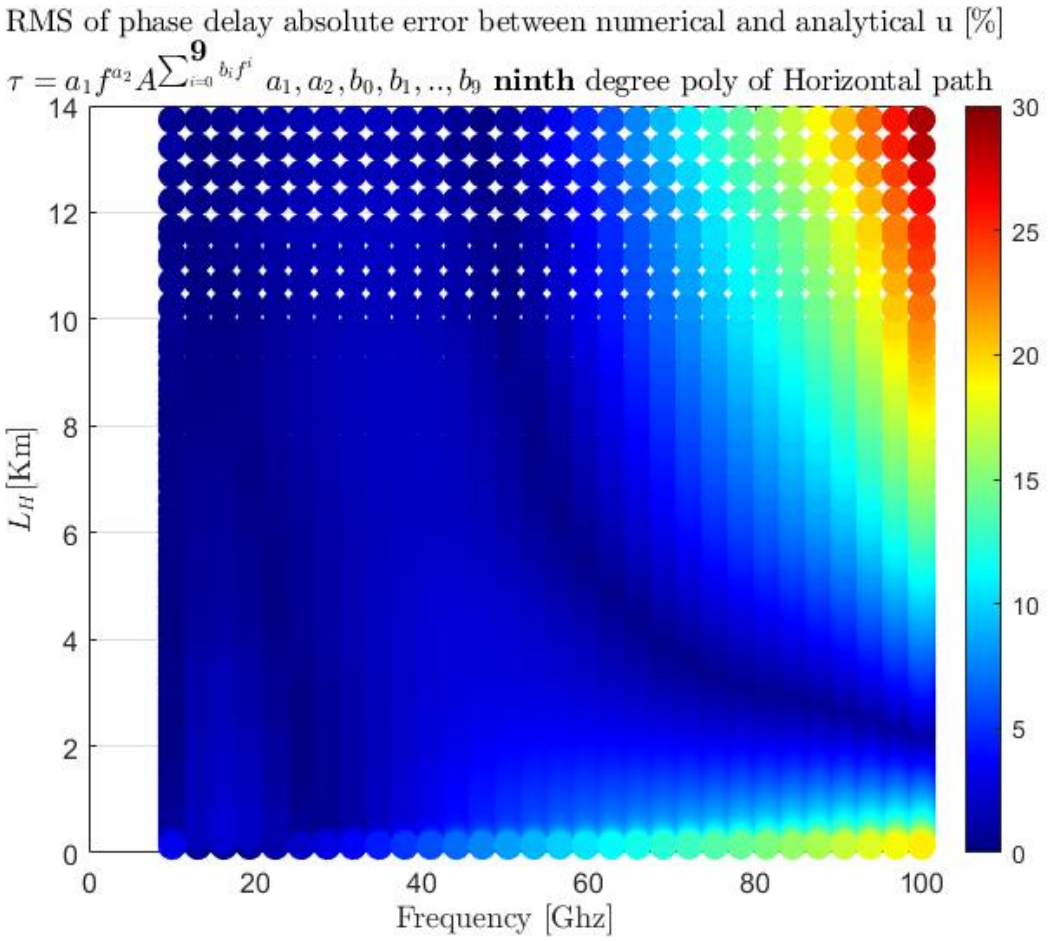

Figure 3.32: Root mean square of the error figure

The results of fig. 3.32 show that globally the rms is much lower than the one in *model 1* with a mean value of 3.5 % , a maximum of 28.3% and a minimum value of 0.06%, we can drop the following comments :

- As expected, the mean value dropped by 5 %, the minimum value did not change and the maximum value increased a little bit , since for higher frequencies and high horizontal path we are overestimating the phase delay.
- We can see that we the region in the middle of *model 1* with a rms between 15-20 % shrunk and now is more accurate the the one in *model 1*
- *model 2* knows also 2 critical regions: the one involving lower horizontal paths is more accurate now, whilst the one in the top right corner is less accurate than before

Generally, we can see that with a developed model we approach more the data, until now we notice that *model 2* is more accurate than *model 1* since its mean value of the error is only of 3% while *model 1* has a 8% mean value, in order to compare the models but using *real data* and as explained in fig. 3.1 , we will use the ccdf of attenuation and phase delay found using the SC-EXCELL model , data measured from real simulation in given sites, to reveal important hints about the *Experimental* accuracy of both models.

Exceedance probability analysis

As explained before, until now we did not compute the accuracy of neither *Model 1* nor *Model 2* once confronted to experimental data. In this framework we would like to to use the output of the SC-EXCELL in terms of cumulative distribution functions for both attenuation and phase delay. In fact, one of the applications of the SC-EXCELL model [6] is the probabilistic analysis of attenuation and phase delay in terms of exceeding a certain probability level, in this section we try to take advantage from this powerful tool emerging from direct measurement using radars to see how good is our analytical model . For this purpose, the steps to derive the probability of exceedance for both attenuation and phase delay are briefly summarized in section 2.2 and fully explained in [6] .
Let's see first an example about the output of the SC-EXCELL cumulative distribution functions for the site : Milan whose characteristics are shown in table 3.4

Table 3.4: Site properties

Link properties				
Latitude	**Longitude**	**Station Height**	**Stratiform rain height**	**Convective rain height**
45.4 °	9.5°	0.081 Km	2.6117 Km	3.3731 Km

The SC-EXCELL model gives the attenuation and phase delay exceedance probability in percent, the function depends among others on the elevation angle, DSD, frequency but also on the site characteristics, we can see in fig. 3.33 that the phase delay and attenuation ccdf follow the same trend. In Milan , the probability to exceed 10 ps in delay is 0.1 % while the probability to exceed 7 db in attenuation is 0.1% , we decide to limit the curve at the probability level 10^{-3} since going below is very low and doesn't have a physical utility .

NOTE that the probability level is presented in logarithmic scale

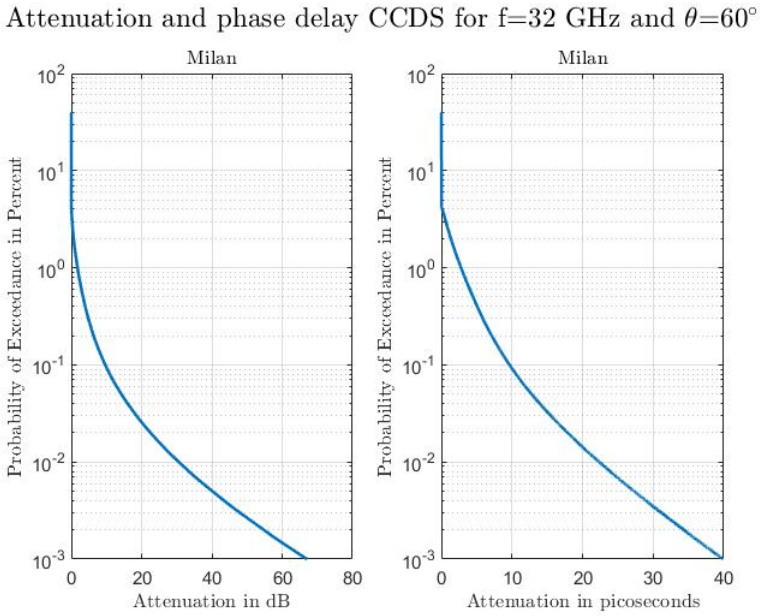

Figure 3.33: Milan phase delay and attenuation ccdf

Before we delve into results and comparison, we must spend few words to explain the procedure used .
For a given site and for certain parameters f, L_H, μ

1. Generate the attenuation cumulative distribution function $F_A(t) = P(A \geq t)$
2. Generate the phase delay cumulative distribution function $F_\tau(t) = P(\tau \geq t)$
3. Use the relationship eq. (3.25) to find the analytical ccdf of phase delay from F_A

For the latter , having the analytical model g for $\mu = 0$, linking phase delay to attenuation

$$\tau = \underset{f,L_H}{g}(A) \qquad eq.\ (3.25)$$

We can write :

$$F_\tau(t) = P(\tau \geq t) = P(\underset{f,L_H}{g}(A) \geq t) \tag{3.35}$$

$$= P(A \geq \underset{f,L_H}{g^{-1}}(t)) \tag{3.36}$$

$$= F_A(\underset{f,L_H}{g^{-1}}(t)) \tag{3.37}$$

Since the model g is a power law , it can be easily inversed , thus we compare the phase delay cumulative exceedance function F_τ and the cumulative exceedance function $F_A \circ \underset{f,L_H}{g^{-1}}$ representing the analytical ccdf

A practical way to this is to set F_A=F_τ= P i.e look at the same probability level P and compare τ giving F_τ which is noted as τ_{data} and $\tau_{analy} = \underset{f,L_H}{g(A)}$ where A giving F_A
The error can be defined in the same way [1], looking at the same probability level P and evaluating the absolute error for between the τ_{analy} and τ_{data}, we can write:

$$\varepsilon(P) = \begin{cases} 100\left(\frac{\tau_{data}(P)}{10}\right)^{0.2} \ln\left(\frac{\tau_{analy}(P)}{\tau_{data}(P)}\right) & \tau_{data}(P) < 10ps \\ 100\ln\left(\frac{\tau_{analy}(P)}{\tau_{data}(P)}\right) & \tau_{data}(P) \geq 10ps \end{cases} \tag{3.38}$$

Then for a couple (f,L_H), we calculate the rms of the error ε taking into account probabilities higher than 10^{-3} since probabilities below are not interesting. At first, we start to explore the first analytical model i.e *Model 1* .

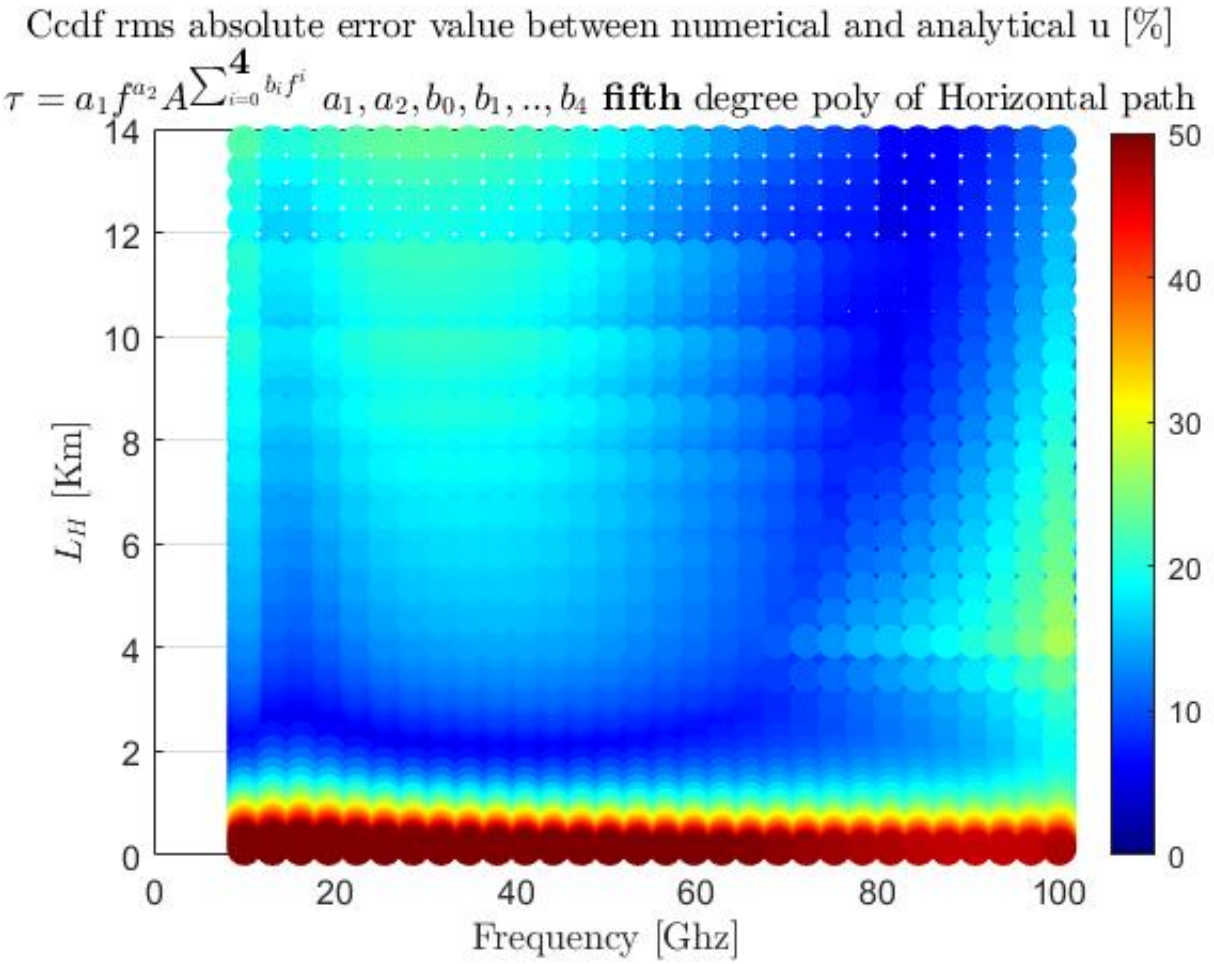

Figure 3.34: CCDF rms of the error between Analytical and experimental phase delay

Comments

- In fig. 3.34, the mean value of the rms is around 13.84 % , the maximum value is 63.55% while the minimum value is 0.88 %
- Likewise the first approach ,The plot shows that for $L_H < 1$ the error is around 45 % which constitute a layer to exclude definitely , the error outside this region has a mean value of only 6% showing thus a great fitting for the analytical model
- In order to visualize how far we are from the data , it's important to visualize the red zone and the blue zone for this purpose we pick the following parameters :

Link properties						
	f	θ	H_R	μ	ψ	L_H
Case 1	20 GHz	45 deg	1.5 Km	0	$\pi/4$	2.8 Km
Case 2	20 GHz	75 deg	1.5 Km	0	$\pi/4$	0.41 Km

Table 3.5: Link properties

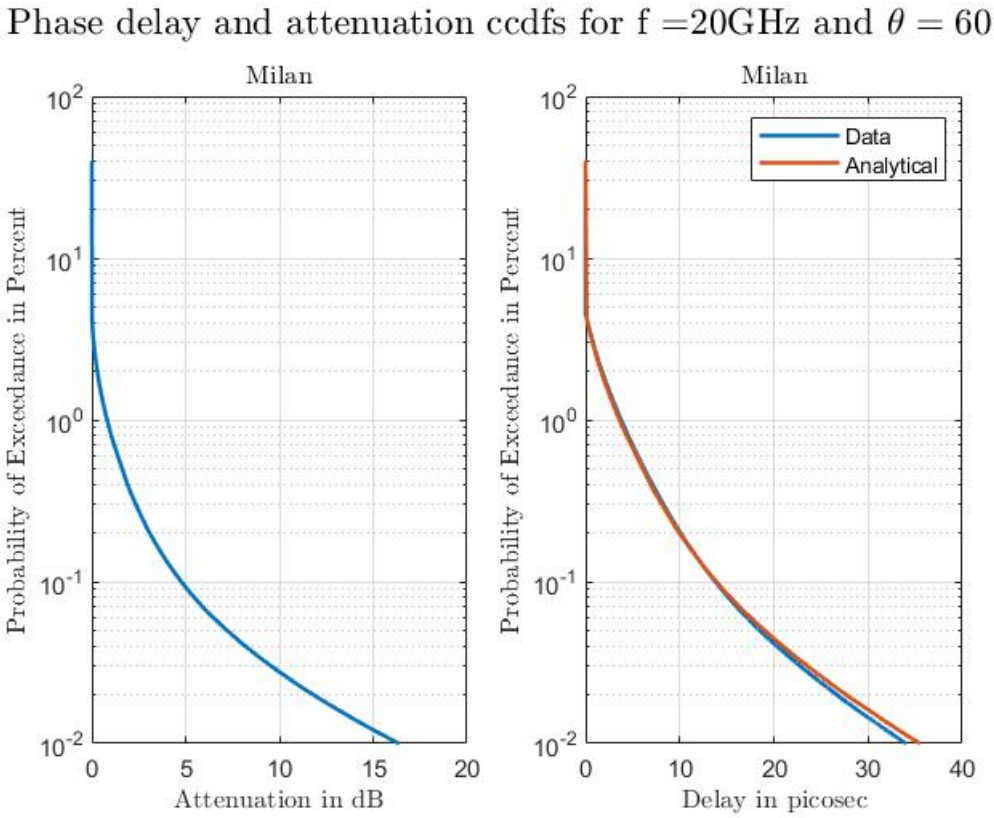

Figure 3.35: Case 1 ccdf plot comaprison vs data

- As we can see from figs. 3.35 and 3.36 the first case represents a good fitting with respect to data , whilst the second one is pretty far from the real ccdf, we can

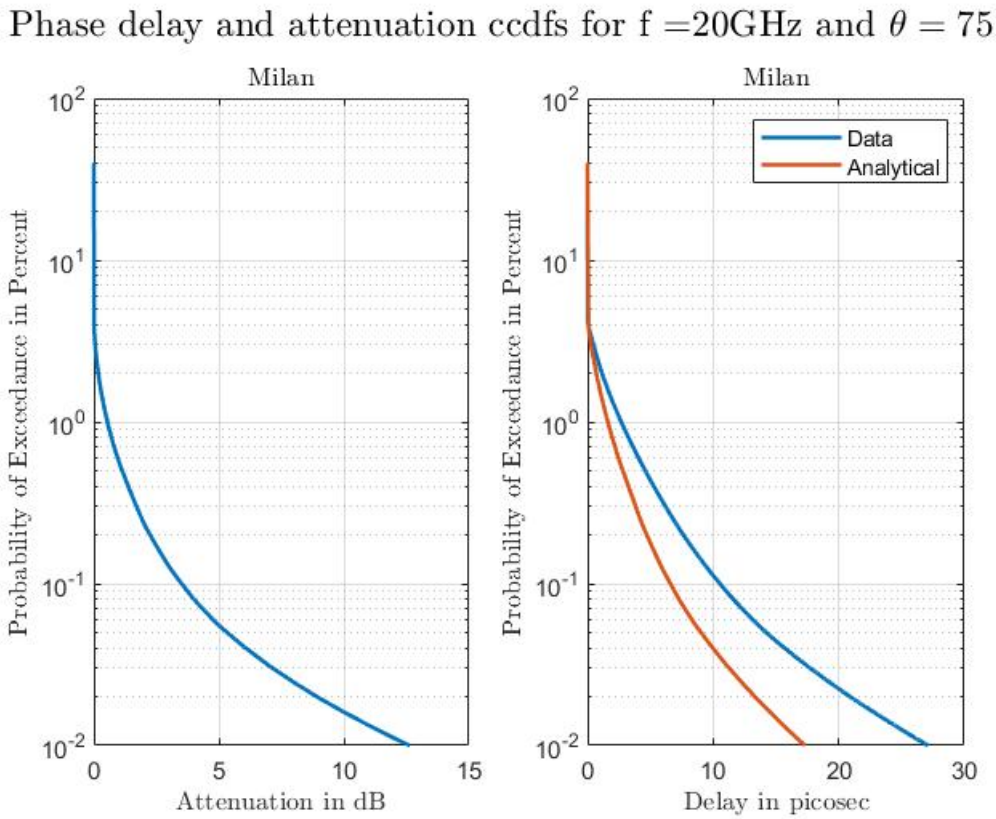

Figure 3.36: Case 2 ccdf plot comaprison vs data

confirm that the reduced model works pretty well for the validation, once the red part is eliminated, the results are pretty satisfying with an mean value of 6%

Let's explore now the results of the full extended model i.e *Model 2* involving a ninth polynomial for the frequency dependency and a ninth polynomial for the horizontal path dependency, limiting always the probability at 10^{-3}, defining the same error figure and calculating its rms for the same values of frequencies and horizontal paths of the first model, we can plot the root mean square of the error figure eq. (3.32) for the extended model .

Comments

- Comparing fig. 3.37 to fig. 3.34 we can clearly notice that the extended model gives less good results with the blue part shrinking and the yellow ,red parts are expanding infig. 3.34 leading to a rms mean value of 21.3 % , a maximum value of 81% and a minimum value of 0.33 %
- The extended model knows also an inaccurate red zone but this time larger $L_H \leq 1.6$ limiting the validity of the model

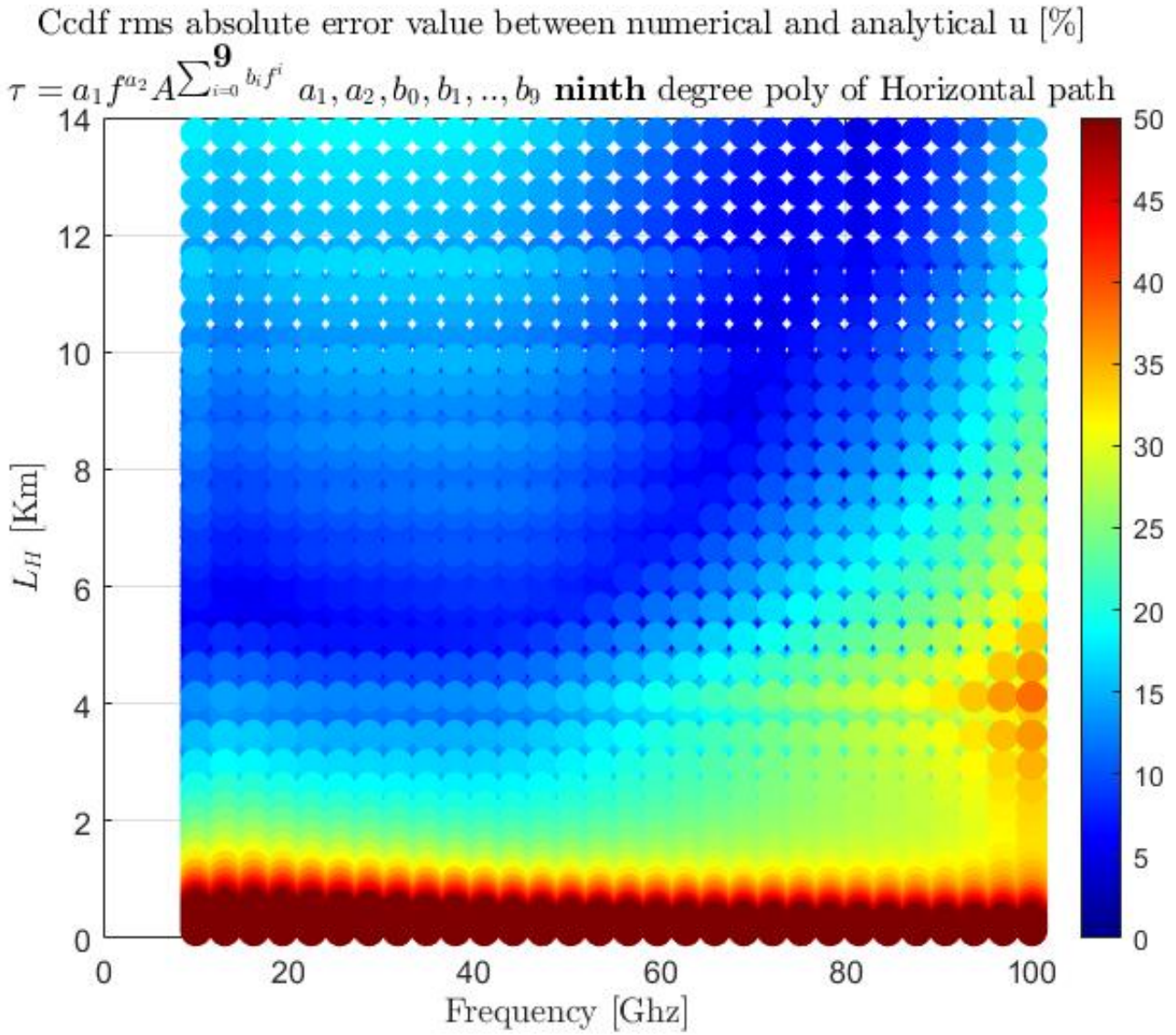

Figure 3.37: CCDF rms of the error between Analytical and experimental phase delay

- The current results show that no matter how the first approach is more accurate for the extended model, the second approach using real data leads us to avoid extending the model

3.2.6. Model Trade-off

Once developing an analytical model fitting some data ,there are always 2 concepts embracing the model development :

- **Complexity** : It means how complex the model is , if it's a formula , how many coefficients are involved to describe the dependency

- **Accuracy**: how accurate is the model, that is to say , how much is the model close from the real data or how small is the model's error

As the reader can notice, we have presented only two analytical models : where Model 1 is less complex involving a fourth degree polynomial depending on frequency "P_f" and a fifth degree polynomial depending on the horizontal path "P_{L_H}" i.e 5x6 coefficients , whilst the second one involves two ninth degree polynomials i.e 10^2 coefficients. Clearly the second model is more *Complex* involving three more times coefficients, but the fitting process idea was to start from a very complex model whose theoretical rms is very small(*Model 2* and then start to reduce the degree of each polynomial P_f and P_{L_H} until the model is no more accurate , i.e until we surpass a certain threshold for the error rms eq. (3.39) , not only for the theoretical approach but more importantly the experimental approach using the ccdf . Two constrains were used to find the thresholds used to limit the model according to eqs. (3.32) and (3.38)

$$mean(rms^{Theo}) \leq 10\% \qquad mean(rms^{Exper}) \leq 10\% \tag{3.39}$$

Decreasing the degrees of P_f and P_{L_H}, we notice that the average theoretical rms goes up whilst the average experimental one goes down, the best trade-off was then found to be the one involving a fourth degree polynomial depending on frequency and a fifth degree polynomial depending on the horizontal path i.e : Model 1

3.2.7. Final Model and Limitations

For the seek of clarity, let's recap what we have done until now : we have started from a *Complex* model(*Model2*): eqs. (3.33) and (3.34) to represent the relationship between delay and attenuation for a given couple (f,L_H). In order to assess the accuracy of the model, 2 approaches were used :

- A theoretical one based on fitting 20 x 20 exponential cells with a curve representing the relation shape τ=f(A) and then validate how well the curve fits with an analytical formula .
- An experimental one based on the SC-EXCELL model , whose outputs are exceedance probabilities for both delay and attenuation , the analytical model helped to transit from A to τ and validate the ccdf of the analytical phase delay

Both approaches were useful to rate the performance of the model through eq. (3.39), once this requirement is not met, we change the model (reduce its complexity) until the

requirement of accuracy eq. (3.39) is met. The attenuation-phase delay relationship is then picked, and this is the last branch of the map fig. 3.1.
At the end, model 1 was chosen, we would like to refine its accuracy by cutting zones where the error is slightly higher than the average error, i.e discard the red zones from both figs. 3.31 and 3.34
Indeed:

1. The region $L_H \leq 1$ in fig. 3.34 has to be discarded since the average rms in there is around 45%
2. The region $f \geq 90$ GHz in fig. 3.31 has to be discarded since the average rms in there is around 20 %

The final figures for both approaches are shown in figs. 3.38 and 3.39, and their properties are depicted in table 3.6

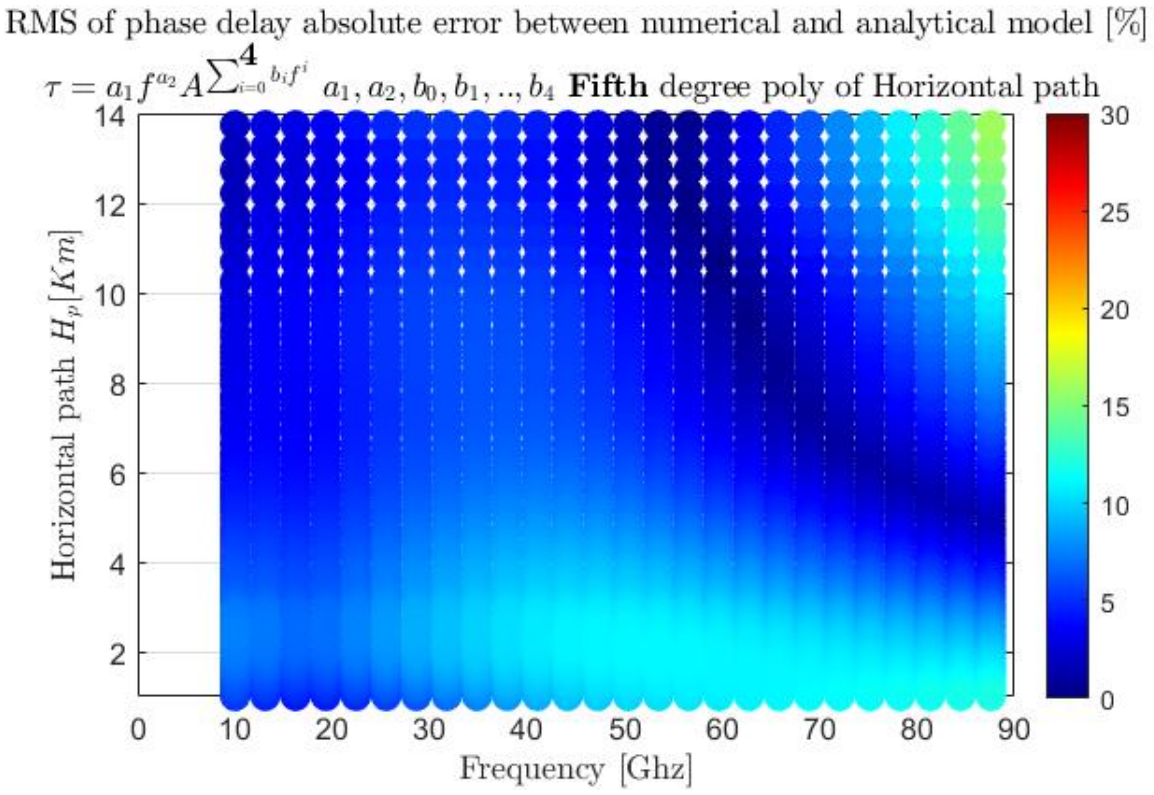

Figure 3.38: Rms of the error between Analytical and experimental phase delay

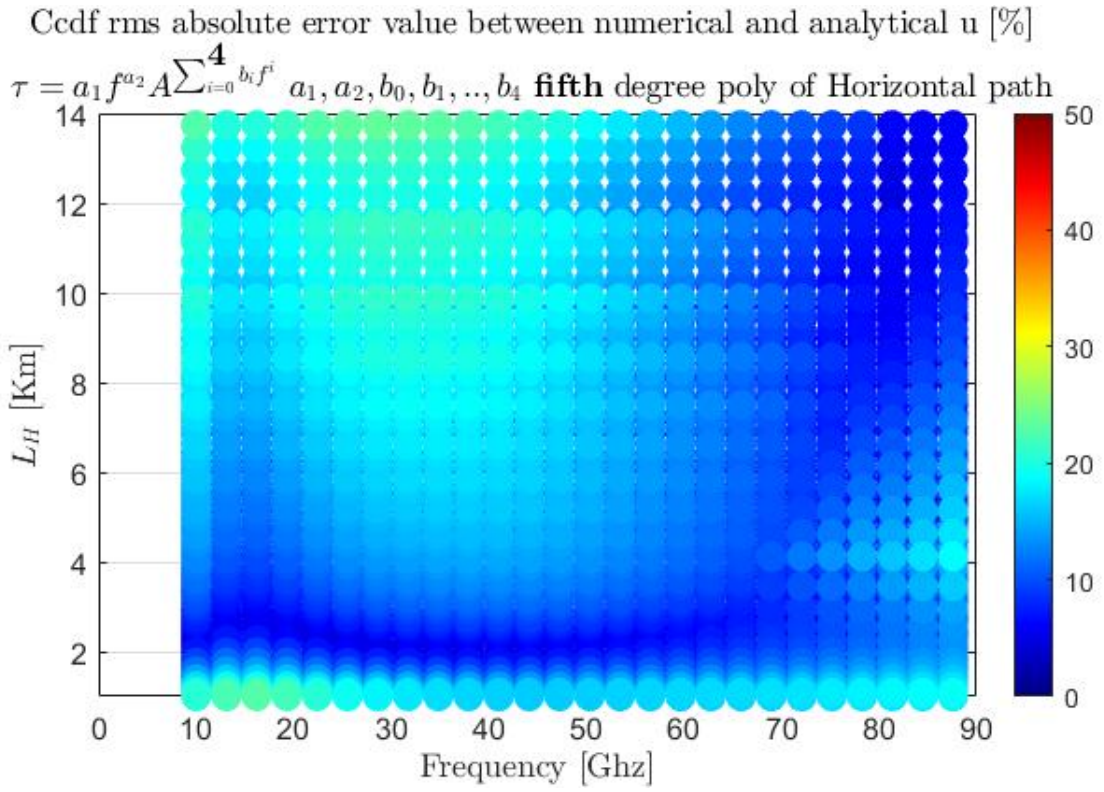

Figure 3.39: CCDF rms of the error between Analytical and experimental phase delay

Table 3.6: Error between the analytical model and data

	Theoretical Approach			**Ccdf Approach**		
	Mean Value	Min	Max	Mean Value	Min	Max
Final Model	**7.36**%	0.06 %	15.92 %	**8.19**%	0.88%	23.55%

As we can see both approaches show similar mean value for the error , with a maximum error 23.55 % for the ccdf approach , finally it's useful to recall the model

$$\begin{cases} \underline{\textbf{Data}} : \psi = 45°, \mu = 0 \\ \underline{\textbf{Model}} \\ \qquad \tau = a_1 f^{a_2} A^{b_1 f^4 + b_2 f^3 + b_3 f^2 + b_4 f + b_5} \\ \qquad a_1(L_H) = \sum_{j=1}^{j=6} a_{1j} L_H^{j-1} \\ \qquad a_2(L_H) = \sum_{j=1}^{j=6} a_{2j} L_H^{j-1} \\ \qquad \forall i \in \{1, 2, ..5\} \;\; b_i(L_H) = \sum_{j=1}^{j=6} b_{ij} L_H^{j-1} \\ \underline{\textbf{Constrains}} : 10GHz \leq f \leq 90GHz, L_H \geq 1Km \end{cases} \tag{3.40}$$

3.2.8. Final Comparison

In this section we compare our model eq. (3.40) to the one developed by Emilio Matricciani [15], since we used two different approachs to accurately define our model section 3.2.5, we have to confront the matricciani's model to both approachs (the one involving the EXCELL model generating data from 20x20 cells and the one involving the SC-EXCELL generating ccdfs for both attenuation and delay). Matrciciani's model can be written :

$$z_{Matri} = \begin{cases} (860, 4 - 4, 82\theta) f^{-1,71} A^{0,73} & \theta \in [20°, 44°] \\ 648, 3 f^{-1,71} A^{0,73} & \theta \in [44°, 90°]. \end{cases} \tag{3.41}$$

Since eq. (3.41) involves only the elevation angle i.e no horizontal path is present, we can compare both models choosing a certain value for H_{Rain} e.g the mean value:

$$H_{Rain} = \frac{1.5 + 5}{2} = 3.25Km \tag{3.42}$$

Thus, for a couple of frequency and elevation angle θ, we compare the phase delay $z_{Matri}(f, \theta)$ in eq. (3.41) to the one in eq. (3.40) : $\tau(f, \frac{3.25}{tan(\theta)})$) eq. (3.9)

EXCELL Data Comparison

In this comparison , we confront the model developed by Emilio Matricciani [15] , to the curve "data" obtained fitting 20x20 exponentiel cells section 3.1.3
The attenuation vector in eqs. (3.40) and (3.41) can be found using the 20x20 exponential cells approach section 3.1.2 and the error between the analytical formula eq. (3.41) and the data can be computed using the error figure used before eq. (3.32)
We can see in fig. 3.40 that we have a pretty good match between the models with the following properties :

Table 3.7: Error between Matricciani's model and data

	Error RMS		
	Mean Value	Min	Max
EXCELL based Comparison	**11.8609**%	0.27 %	31.55 %

Where the error is mostly less than 15% except for :

- High elevation angles i.e low horizontal path which is beyond the limitation , we recall that our model gives high error for $L_H \leq 1$

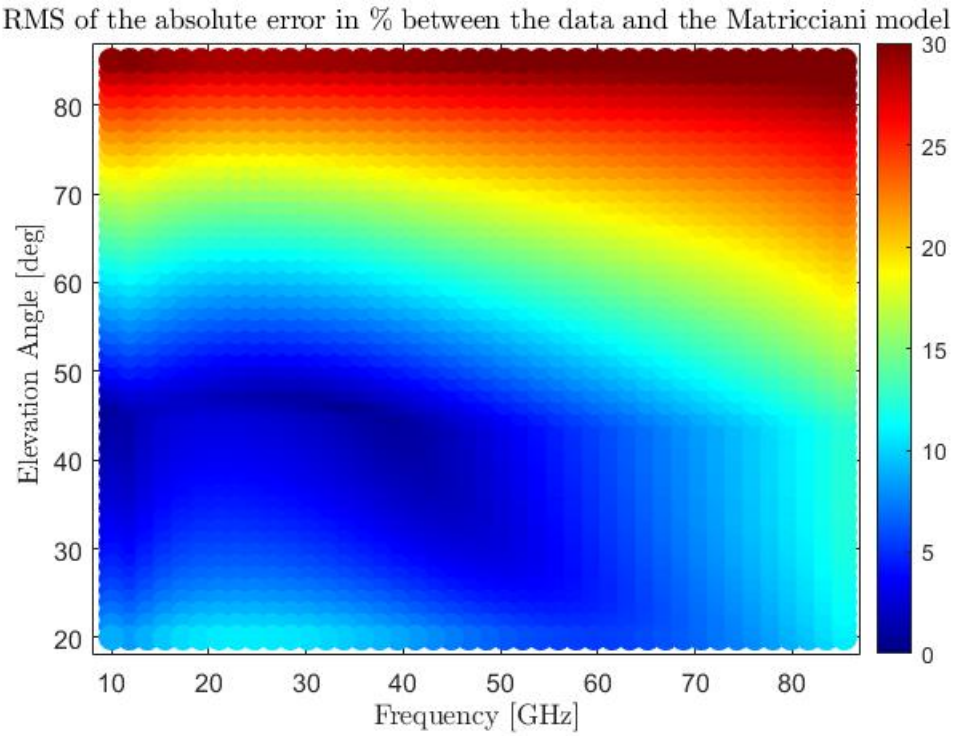

Figure 3.40: Models error comparison

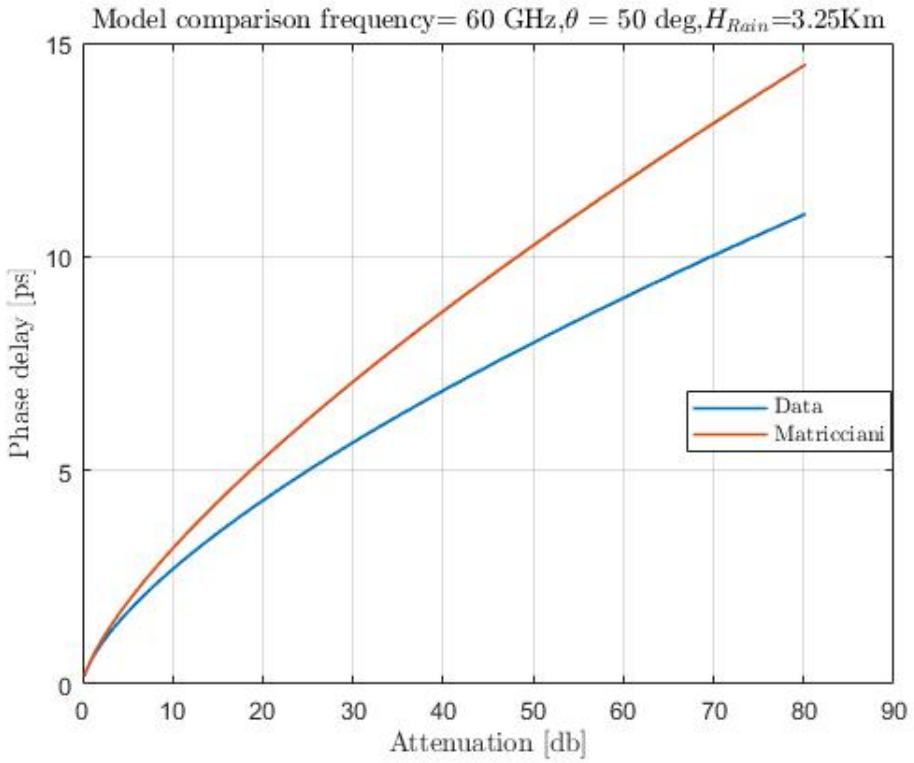

Figure 3.41: Models comparison example

It's important also to notice that

- Comparing fig. 3.41 to fig. 3.31 we can notice that the region $f \geq 90GHz$ is no longer a region of high error for the Matricciani's model.
- Comparing table 3.7 to table 3.6 we can notice the model developed in this thesis eq. (3.40) gives better results.

In fig. 3.41 we plot the data vs Matricciani's model,we can notice some divergences especially for high attenuations.

SC-EXCELL Data Comparison

In this subsection, we confront the Matricciani's model to the output of the SC-EXCELL, we will follow the same procedure for the same site Milan table 3.4 utilized in section 3.2.5 but this time we will utilize eq. (3.41) to transit from attenuation to phase delay(eq. (3.25)

Table 3.8: Error between Matricciani's model and data

	Error RMS		
	Mean Value	Min	Max
SC-EXCELL based Comparison	**12.67**%	0.68 %	32.85 %

Comments

- in fig. 3.42, the error is satisfying, with a mean value of 12.67 %, we can say that the model reproduces well the ccdf of phase delay starting from the ccdf of attenuation. We can see also that for high frequencies that the error gets higher (also encountered for Model 1 fig. 3.39)
- Comparing table 3.8 to table 3.6, we can see that our model eq. (3.40) gives better results also for the experimental data using the ccdf.

Generally the Matricciani's model works well, in order to give an idea about its accuracy in mapping the attenuation ccdf into the phase delay ccdf, we plot the results for certain values of elevation angle and frequency fig. 3.43

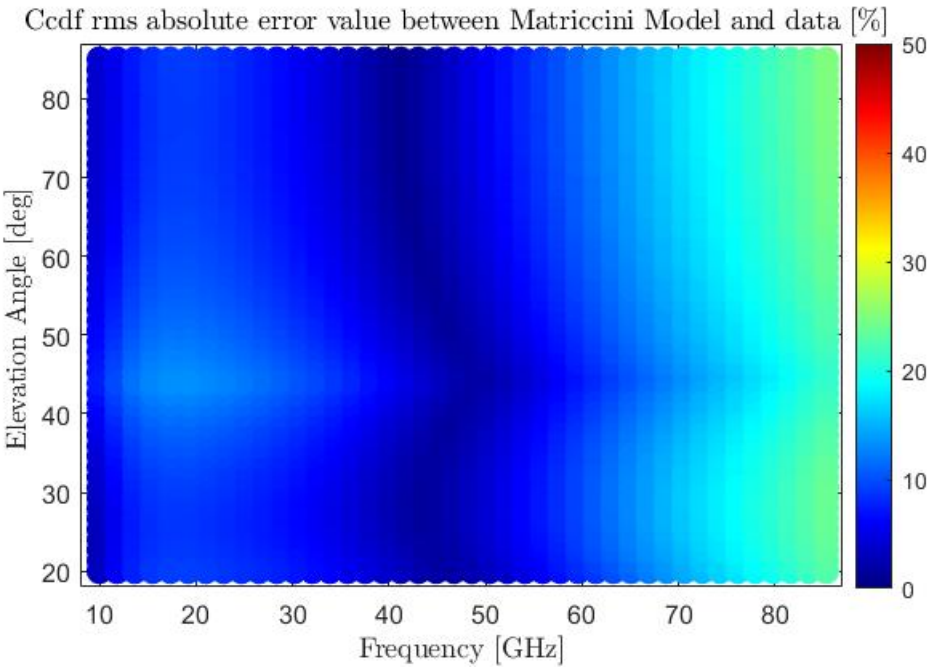

Figure 3.42: Models error comparison

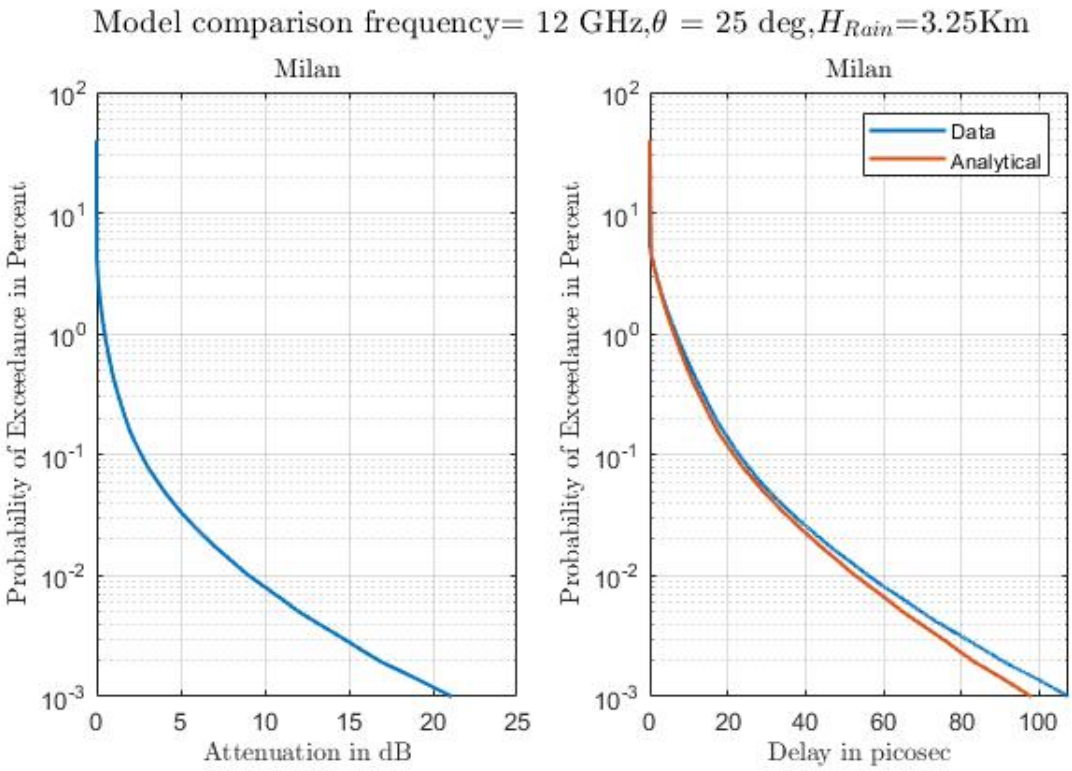

Figure 3.43: Models comparison example

4 | Conclusions and future works

4.1. Conclusions

This thesis work could be one of the applications of the cellular model EXCELL developed in 1981 by capsoni, in fact, we saw that starting from a simple exponential law for rain rate distribution, and simple power laws for specific attenuation and phase delay that we can integrate on the slant path to get both attenuation and delay, we can build a general analytical model linking attenuation to phase delay depending on frequency, horizontal path and DSD. In this work, we generated data for both attenuation and phase delay by using many exponential cells with different peak rain rates R_M and characteristic lengths l_0, we realized that this data follows a power law $\tau = aA^b$, this dependency was then represented by a single curve for a triplet of frequency,horizontal path and DSD,fixed to its most probable value 0.
In the fitting section, we have seen how to fit the curve representing the data with suitable laws constituting the analytical model. The accuracy of this model was computed through two main approachs , one is based intrinsically on the data vs analytical formula error calculation, while the second recalled the SC-EXCELL model deriving experimental ccdfs of attenuation and delay, the analytical model was used to map attenuation ccdf to phase delay ccdf and compare it to the experimental one. Both approaches were useful to choose the best model $\tau = aA^b$ linking attenuation to delay, this model involved :

- A power law dependency of frequency for a i.e $a(f) = a_1 f^{a_2}$
- A fourth degree polynomial for b i.e $b(f) = \sum_{i=1}^{i=5} b_i f^{i-1}$
- A fifth degree polynomial for the dependency on horizontal path for $a_1, a_2$and b_i

The study concluded that the model chosen has a rms error of 7.36 % and 8.19 % for the theoretical and the experimental approach respectively . Finally, a comparison with the Matricciani's model was presented and concluded that the model developped in this thesis gives better results.

4.2. Future Works

This thesis work can be considered a continuation, even though based on a different model " EXCELL" ,of the Matricciani relationship since it includes more parameters and gives better results, but during the elaboration of the work, we noticed different features that can be exploited, here are some recommendations for future add-ons.

- Try to overcome limitations of the developed model especially for high elevation angles and frequencies in the range 90-100 GHz
- Explore different cell models :[19] : MultiEXCELL for example...

Bibliography

[1] P. Acquisition. Analysis of data in studies of tropospheric propagation. *Recommendation ITU-R*, pages 311–10, 2009.

[2] A. V. Alejos, M. G. Sanchez, and I. Cuinas. Propagation impairments mitigation techniques for broadband wlans. In *The Second European Conference on Antennas and Propagation, EuCAP 2007*, pages 1–4. IET, 2007.

[3] D. Atlas and C. W. Ulbrich. Path-and area-integrated rainfall measurement by microwave attenuation in the 1–3 cm band. *Journal of Applied Meteorology and Climatology*, 16(12):1322–1331, 1977.

[4] C. Capsoni, F. Fedi, C. Magistroni, A. Paraboni, and A. Pawlina. Data and theory for a new model of the horizontal structure of rain cells for propagation applications. *Radio Science*, 22(03):395–404, 1987.

[5] C. Capsoni, F. Fedi, C. Magistroni, A. Paraboni, and A. Pawlina. Data and theory for a new model of the horizontal structure of raincells for propagation applications. *NASA STI/Recon Technical Report N*, 89:17785, 1988.

[6] C. Capsoni, L. Luini, A. Paraboni, C. Riva, and A. Martellucci. A new prediction model of rain attenuation that separately accounts for stratiform and convective rain. *IEEE Transactions on Antennas and Propagation*, 57(1):196–204, 2009.

[7] R. K. Crane. *Electromagnetic wave propagation through rain*. Wiley-Interscience, 1996.

[8] A. Hilt. Availability and fade margin calculations for 5g microwave and millimeter-wave anyhaul links. *Applied Sciences*, 9(23):5240, 2019.

[9] L. J. Ippolito. *Radiowave propagation in satellite communications*. Springer Science & Business Media, 2012.

[10] R. Itu. Recommendation itu-r p. 838-2 specific attenuation model for rain for use in prediction methods; 1992199920032. *ITU: Geneva, Switzerland*, pages 1–8, 2005.

[11] G. LI. An analytical model for the attenuation and phase delay due to rain in the 6-100 ghz range. 2022.

[12] L. Luini and C. Capsoni. Multiexcell: A new rain field model for propagation applications. *IEEE Transactions on Antennas and Propagation*, 59(11):4286–4300, 2011.

[13] D. Maggiori. Computed transmission through rain in the 1-400 ghz frequency range for spherical and elliptical drops and any polarization. *Alta Frequenza*, 50:262–273, 1981.

[14] E. Matricciani. Physical-mathematical model of the dynamics of rain attenuation based on rain rate time series and a two-layer vertical structure of precipitation. *Radio Science*, 31(02):281–295, 1996.

[15] E. Matricciani. A relationship between phase delay and attenuation due to rain and its applications to satellite and deep-space tracking. *IEEE transactions on antennas and propagation*, 57(11):3602–3611, 2009.

[16] T. Oguchi and Y. Hosoya. Scattering properties of oblate raindrops and cross polarization of radio waves due to rain. ii-calculations at microwave and millimeter wave regions. *Radio Research Laboratory, Journal*, 21(105):191–259, 1974.

[17] S. Okamura and T. Oguchi. Electromagnetic wave propagation in rain and polarization effects. *Proceedings of the Japan academy, series B*, 86(6):539–562, 2010.

[18] T. Rappaport, R. Heath, R. Daniels, and J. Murdock. *Millimeter wave wireless communications*. Prentice Hall, 2015. ISBN 9780132172288. Includes bibliographical references (pages 585-651) and index.

[19] M. A. Samad, F. D. Diba, and D.-Y. Choi. A survey of rain attenuation prediction models for terrestrial links—current research challenges and state-of-the-art. *Sensors*, 21(4):1207, 2021.

[20] I. Union. Rain height model for prediction methods. *Recommendations ITU-R*, pages 839–4, 2013.

A | Appendix A

In this Appendix we present the analytical model linking phase delay to attenuation for each value of mu, we recall that we adopted the same model as the one presented in the thesis i.e a fourth polynomial for the frequency dependency and a fifth polynomial for the horizontal path dependency .

A.1. μ=-3 analytical model

Table A.1: Analytical Model for $\mu = -3$

$\mu = -3$	$\boldsymbol{\tau = aA^b}$						
Model	$\boldsymbol{a = a_1 f^{a_2}}$		$\boldsymbol{b = b_1 f^4 + b_2 f^3 + b_3 f^2 + b_4 f + b_5}$				
	a_1	a_2	b_1	b_2	b_3	b_4	b_5
	$\sum_{j=1}^{j=6} c_j L_H^{j-1}$	$\sum_{j=1}^{j=6} c_j L_H^{j-1}$	$\sum_{j=1}^{j=6} c_j L_H^{j-1}$	$\sum_{j=1}^{j=6} c_j L_H^{j-1}$	$\sum_{j=1}^{j=6} c_j L_H^{j-1}$	$\sum_{j=1}^{j=6} c_j L_H^{j-1}$	$\sum_{j=1}^{j=6} c_j L_H^{j-1}$
$\boldsymbol{c_6}$	0.0058	-1.69 10^{-6}	1.25 10^{-14}	-4.32 10^{-12}	5.77 10^{-10}	-3.7 10^{-8}	1.56 10^{-6}
$\boldsymbol{c_5}$	-0.246	7 10^{-5}	$-4.8\ 10^{-13}$	1.61 10^{-10}	-2.11 10^{-8}	1.32 10^{-6}	$-5.79\ 10^{-5}$
$\boldsymbol{c_4}$	4.036	-1.14 10^{-3}	-6.98 10^{-12}	-2.26 10^{-9}	2.87 10^{-7}	-1.69 10^{-5}	8.13 10^{-4}
$\boldsymbol{c_3}$	-32.11	0.009	-5.07 10^{-11}	1.54 10^{-8}	$-1.84\ 10^{-6}$	9.82 10^{-5}	-0.0054
$\boldsymbol{c_2}$	133.7	-0.031	2.11 10^{-10}	-5.96 10^{-8}	6.37 10^{-6}	-2.96 10^{-4}	0.015
$\boldsymbol{c_1}$	117.1	-1.43	-3.8 10^{-12}	2.31 10^{-8}	-1.15 10^{-5}	0.0011	0.6926

A.2. μ=-2 analytical model

Table A.2: Analytical Model for $\mu = -2$

$\mu = -2$	$\boldsymbol{\tau = aA^b}$						
Model	$\boldsymbol{a = a_1 f^{a_2}}$		$\boldsymbol{b = b_1 f^4 + b_2 f^3 + b_3 f^2 + b_4 f + b_5}$				
	a_1	a_2	b_1	b_2	b_3	b_4	b_5
	$\sum_{j=1}^{j=6} c_j L_H^{j-1}$	$\sum_{j=1}^{j=6} c_j L_H^{j-1}$	$\sum_{j=1}^{j=6} c_j L_H^{j-1}$	$\sum_{j=1}^{j=6} c_j L_H^{j-1}$	$\sum_{j=1}^{j=6} c_j L_H^{j-1}$	$\sum_{j=1}^{j=6} c_j L_H^{j-1}$	$\sum_{j=1}^{j=6} c_j L_H^{j-1}$
$\boldsymbol{c_6}$	0.0055	$4.16\,10^{-6}$	$3.59\,10^{-15}$	$-2.71\ 10^{-12}$	$5.36\,10^{-10}$	$-4.25\,10^{-8}$	$1.68\,10^{-6}$
$\boldsymbol{c_5}$	-0.236	$-1.5\,10^{-4}$	$-2.01\,10^{-13}$	1.1510^{-10}	$2.09\,10^{-8}$	$1.53\,10^{-6}$	$-6.22\,10^{-5}$
$\boldsymbol{c_4}$	3.874	0.0019	$4.33\,10^{-12}$	$-1.92\ 10^{-9}$	$3.12\ 10^{-7}$	$-2.02\,10^{-5}$	$8\ 10^{-4}$
$\boldsymbol{c_3}$	-30.73	-0.01	$-4.4\,10^{-11}$	$1.58\,10^{-8}$	$-2.23\,10^{-6}$	$1.2\,10^{-4}$	-0.0057
$\boldsymbol{c_2}$	123.3	0.0357	$2.11\,10^{-10}$	$-6.5\,10^{-8}$	$7.75\,10^{-6}$	$-3.65\,10^{-4}$	0.0165
$\boldsymbol{c_1}$	137.9	-1.502	$-3.4\,10^{-9}$	$8.44\,10^{-7}$	$-8.49\,10^{-5}$	0.0019	0.6708

A.3. μ=-1 analytical model

Table A.3: Analytical Model for $\mu = -1$

$\mu = -1$	$\boldsymbol{\tau = aA^b}$						
Model	$\boldsymbol{a = a_1 f^{a_2}}$		$\boldsymbol{b = b_1 f^4 + b_2 f^3 + b_3 f^2 + b_4 f + b_5}$				
	a_1	a_2	b_1	b_2	b_3	b_4	b_5
	$\sum_{j=1}^{j=6} c_j L_H^{j-1}$	$\sum_{j=1}^{j=6} c_j L_H^{j-1}$	$\sum_{j=1}^{j=6} c_j L_H^{j-1}$	$\sum_{j=1}^{j=6} c_j L_H^{j-1}$	$\sum_{j=1}^{j=6} c_j L_H^{j-1}$	$\sum_{j=1}^{j=6} c_j L_H^{j-1}$	$\sum_{j=1}^{j=6} c_j L_H^{j-1}$
$\boldsymbol{c_6}$	0.008	1.6910^{-6}	$-1.35\,10^{-14}$	1.5210^{-12}	$1.58\,10^{-10}$	$-3.05\,10^{-8}$	$1.65\,10^{-6}$
$\boldsymbol{c_5}$	-0.35	$-5.91\,10^{-5}$	$3.73\,10^{-13}$	$-2.84\,10^{-11}$	$-8.18\,10^{-9}$	$1.13\,10^{-6}$	$-6.13\,10^{-5}$
$\boldsymbol{c_4}$	5.799	$6.8\,10^{-4}$	$-2.26\,10^{-12}$	$-2.53\,10^{-10}$	$1.64\,10^{-7}$	$-1.57\,10^{-5}$	$8.63\,10^{-4}$
$\boldsymbol{c_3}$	-45.58	-0.003	$-1.41\,10^{-11}$	$8.21\,10^{-9}$	$-1.56\,10^{-6}$	$1.02\,10^{-4}$	-0.0057
$\boldsymbol{c_2}$	181.7	0.009	$1.55\,10^{-10}$	$-7.09\,10^{-9}$	$6.41\,10^{-6}$	-3.2410^{-4}	0.01
$\boldsymbol{c_1}$	196.5	-1.584	$-7.09\,10^{-9}$	$1.69\,10^{-6}$	$-1.6\,10^{-4}$	0.0044	0.6736

A.4. μ=0 analytical model

Table A.4: Analytical Model for $\mu = 0$

$\mu = 0$	$\boldsymbol{\tau = aA^b}$						
Model	$\boldsymbol{a = a_1 f^{a_2}}$		$\boldsymbol{b = b_1 f^4 + b_2 f^3 + b_3 f^2 + b_4 f + b_5}$				
	a_1	a_2	b_1	b_2	b_3	b_4	b_5
	$\sum_{j=1}^{j=6} c_j L_H^{j-1}$	$\sum_{j=1}^{j=6} c_j L_H^{j-1}$	$\sum_{j=1}^{j=6} c_j L_H^{j-1}$	$\sum_{j=1}^{j=6} c_j L_H^{j-1}$	$\sum_{j=1}^{j=6} c_j L_H^{j-1}$	$\sum_{j=1}^{j=6} c_j L_H^{j-1}$	$\sum_{j=1}^{j=6} c_j L_H^{j-1}$
$\boldsymbol{c_6}$	0.0142	-1.61 10^{-6}	-2.05 10^{-14}	3.6 10^{-12}	-7.6 10^{-11}	-1.9 10^{-8}	1.56 10^{-6}
$\boldsymbol{c_5}$	-0.589	6.5 10^{-5}	6.09 10^{-13}	-9.82 10^{-11}	-2.68 10^{-11}	7.4 10^{-7}	$-5.78\ 10^{-5}$
$\boldsymbol{c_4}$	9.456	-1.04 10^{-3}	-4.87 10^{-12}	5.36 10^{-10}	6.75 10^{-8}	-1.1 10^{-5}	8 10^{-4}
$\boldsymbol{c_3}$	-73.44	0.008	-4.45 10^{-12}	4.95 10^{-9}	$-1.1\ 10^{-6}$	8.1 10^{-5}	-0.0055
$\boldsymbol{c_2}$	292.5	-0.026	1.46 10^{-10}	-4.6 10^{-8}	5.51 10^{-6}	-2.7 10^{-4}	0.0155
$\boldsymbol{c_1}$	305.7	-1.686	-9 10^{-9}	2.13 10^{-6}	-2 10^{-4}	0.005	0.696

A.5. μ=1 analytical model

Table A.5: Analytical Model for $\mu = 1$

$\mu = 1$	$\boldsymbol{\tau = aA^b}$						
Model	$\boldsymbol{a = a_1 f^{a_2}}$		$\boldsymbol{b = b_1 f^4 + b_2 f^3 + b_3 f^2 + b_4 f + b_5}$				
	a_1	a_2	b_1	b_2	b_3	b_4	b_5
	$\sum_{j=1}^{j=6} c_j L_H^{j-1}$	$\sum_{j=1}^{j=6} c_j L_H^{j-1}$	$\sum_{j=1}^{j=6} c_j L_H^{j-1}$	$\sum_{j=1}^{j=6} c_j L_H^{j-1}$	$\sum_{j=1}^{j=6} c_j L_H^{j-1}$	$\sum_{j=1}^{j=6} c_j L_H^{j-1}$	$\sum_{j=1}^{j=6} c_j L_H^{j-1}$
$\boldsymbol{c_6}$	0.024	-3.74 10^{-6}	-1.48 10^{-14}	3.6 10^{-12}	- 10^{-10}	-1.31 10^{-8}	1.44 10^{-6}
$\boldsymbol{c_5}$	-0.98	1.4 10^{-4}	4.09 10^{-13}	-7.34 10^{-11}	8.45 10^{-10}	5.39 10^{-7}	$-5.36\ 10^{-5}$
$\boldsymbol{c_4}$	15.49	-0.002	-2.21 10^{-12}	1.85 10^{-10}	5.82 10^{-8}	-8.73 10^{-5}	7 10^{-4}
$\boldsymbol{c_3}$	-117.8	0.015	-2.08 10^{-11}	7.33 10^{-9}	$-1.08\ 10^{-6}$	6.91 10^{-5}	-0.005
$\boldsymbol{c_2}$	458.8	-0.048	1.81 10^{-10}	-5.07 10^{-8}	5.39 10^{-6}	-2.4 10^{-4}	0.014
$\boldsymbol{c_1}$	498.1	-1.81	-9.71 10^{-9}	2.32 10^{-6}	-2 10^{-4}	0.006	0.725

A.6. μ=2 analytical model

Table A.6: Analytical Model for $\mu = 2$

$\mu = 2$	$\boldsymbol{\tau = aA^b}$						
Model	$\boldsymbol{a = a_1 f^{a_2}}$		$\boldsymbol{b = b_1 f^4 + b_2 f^3 + b_3 f^2 + b_4 f + b_5}$				
	a_1	a_2	b_1	b_2	b_3	b_4	b_5
	$\sum_{j=1}^{j=6} c_j L_H^{j-1}$	$\sum_{j=1}^{j=6} c_j L_H^{j-1}$	$\sum_{j=1}^{j=6} c_j L_H^{j-1}$	$\sum_{j=1}^{j=6} c_j L_H^{j-1}$	$\sum_{j=1}^{j=6} c_j L_H^{j-1}$	$\sum_{j=1}^{j=6} c_j L_H^{j-1}$	$\sum_{j=1}^{j=6} c_j L_H^{j-1}$
$\boldsymbol{c_6}$	0.039	$-4.54\ 10^{-6}$	$-5.68\ 10^{-15}$	$1.31\ 10^{-12}$	$-4.19\ 10^{-11}$	$-1.02\ 10^{-8}$	$1.32\ 10^{-6}$
$\boldsymbol{c_5}$	-1.59	$1.7\ 10^{-4}$	$9.15\ 10^{-14}$	$-1.88\ 10^{-11}$	$-1.05\ 10^{-9}$	$4.3\ 10^{-7}$	$-4.9\ 10^{-5}$
$\boldsymbol{c_4}$	24.73	$-2.5\ 10^{-3}$	$1.72\ 10^{-12}$	-4.9210^{-10}	$7.97\ 10^{-8}$	$-7.3\ 10^{-6}$	$6.9\ 10^{-4}$
$\boldsymbol{c_3}$	-184.8	0.017	$-4.18\ 10^{-11}$	$1.09\ 10^{-8}$	$-1.17\ 10^{-6}$	$6.07\ 10^{-5}$	-0.0046
$\boldsymbol{c_2}$	705.6	-0.055	$2.21\ 10^{-10}$	$-5.66\ 10^{-8}$	$5.39\ 10^{-6}$	$-2.19\ 10^{-4}$	0.0133
$\boldsymbol{c_1}$	846.8	-1.948	$-9.38\ 10^{-9}$	$2.26\ 10^{-6}$	$-1.98\ 10^{-4}$	0.0058	0.7559

A.7. μ=3 analytical model

Table A.7: Analytical Model for $\mu = 3$

$\mu = 3$	$\boldsymbol{\tau = aA^b}$						
Model	$\boldsymbol{a = a_1 f^{a_2}}$		$\boldsymbol{b = b_1 f^4 + b_2 f^3 + b_3 f^2 + b_4 f + b_5}$				
	a_1	a_2	b_1	b_2	b_3	b_4	b_5
	$\sum_{j=1}^{j=6} c_j L_H^{j-1}$	$\sum_{j=1}^{j=6} c_j L_H^{j-1}$	$\sum_{j=1}^{j=6} c_j L_H^{j-1}$	$\sum_{j=1}^{j=6} c_j L_H^{j-1}$	$\sum_{j=1}^{j=6} c_j L_H^{j-1}$	$\sum_{j=1}^{j=6} c_j L_H^{j-1}$	$\sum_{j=1}^{j=6} c_j L_H^{j-1}$
$\boldsymbol{c_6}$	0.054	-4.18 10^{-6}	2.56 10^{-15}	-1.92 10^{-13}	2.24 10^{-11}	-8 10^{-9}	1.2 10^{-6}
$\boldsymbol{c_5}$	-2.16	1.5 10^{-4}	$-1.82\ 10^{-13}$	3.07 10^{-11}	-2.99 10^{-9}	3.44 10^{-7}	$-4.45\ 10^{-5}$
$\boldsymbol{c_4}$	32.93	-2.2 10^{-3}	4.83 10^{-12}	-1.04 10^{-19}	9.74 10^{-8}	-6.01 10^{-6}	6 10^{-4}
$\boldsymbol{c_3}$	-241.1	0.0157	-5.51 10^{-11}	1.31 10^{-8}	$-1.19\ 10^{-6}$	8.1 10^{-5}	-0.004
$\boldsymbol{c_2}$	894.8	-0.0494	2.29 10^{-10}	-5.64 10^{-8}	5 10^{-6}	-1.83 10^{-4}	0.012
$\boldsymbol{c_1}$	1263	-2.05	-8.33 10^{-9}	2.05 10^{-6}	-1.7 10^{-4}	0.005	0.784

A.8. μ=4 analytical model

Table A.8: Analytical Model for $\mu = 4$

$\mu = 4$	$\boldsymbol{\tau = aA^b}$						
Model	$\boldsymbol{a = a_1 f^{a_2}}$		$\boldsymbol{b = b_1 f^4 + b_2 f^3 + b_3 f^2 + b_4 f + b_5}$				
	a_1	a_2	b_1	b_2	b_3	b_4	b_5
	$\sum_{j=1}^{j=6} c_j L_H^{j-1}$	$\sum_{j=1}^{j=6} c_j L_H^{j-1}$	$\sum_{j=1}^{j=6} c_j L_H^{j-1}$	$\sum_{j=1}^{j=6} c_j L_H^{j-1}$	$\sum_{j=1}^{j=6} c_j L_H^{j-1}$	$\sum_{j=1}^{j=6} c_j L_H^{j-1}$	$\sum_{j=1}^{j=6} c_j L_H^{j-1}$
$\boldsymbol{c_6}$	0.067	$-3.18\ 10^{-6}$	$7.39\ 10^{-15}$	$-1.07\ 10^{-12}$	$-5.25\ 10^{-11}$	$-5.5\ 10^{-9}$	$1.07\ 10^{-6}$
$\boldsymbol{c_5}$	-2.658	$1.2\ 10^{-4}$	$-3.34\ 10^{-13}$	$5.77\ 10^{-11}$	$-3.69\ 10^{-9}$	$2.44\ 10^{-7}$	$-3.98\ 10^{-5}$
$\boldsymbol{c_4}$	39.78	$-1.7\ 10^{-3}$	$6.30\ 10^{-12}$	$-1.28\ 10^{-9}$	$9.77\ 10^{-8}$	$-4.48\ 10^{-6}$	$5.6\ 10^{-4}$
$\boldsymbol{c_3}$	-284.6	0.016	$-5.85\ 10^{-11}$	$1.34\ 10^{-8}$	$1.11\ 10^{-6}$	$4.02\ 10^{-5}$	-0.0037
$\boldsymbol{c_2}$	1019	-0.035	$2.18\ 10^{-10}$	$-5.26\ 10^{-8}$	$4.41\ 10^{-6}$	$-1.4\ 10^{-4}$	0.0010
$\boldsymbol{c_1}$	1787	-2.144	$-6.9\ 10^{-9}$	$1.74\ 10^{-6}$	$-1.5\ 10^{-4}$	0.004	0.8127

A.9. μ=5 analytical model

Table A.9: Analytical Model for $\mu = 5$

$\mu = 5$	$\boldsymbol{\tau = aA^b}$						
Model	$\boldsymbol{a = a_1 f^{a_2}}$		$\boldsymbol{b = b_1 f^4 + b_2 f^3 + b_3 f^2 + b_4 f + b_5}$				
	a_1	a_2	b_1	b_2	b_3	b_4	b_5
	$\sum_{j=1}^{j=6} c_j L_H^{j-1}$	$\sum_{j=1}^{j=6} c_j L_H^{j-1}$	$\sum_{j=1}^{j=6} c_j L_H^{j-1}$	$\sum_{j=1}^{j=6} c_j L_H^{j-1}$	$\sum_{j=1}^{j=6} c_j L_H^{j-1}$	$\sum_{j=1}^{j=6} c_j L_H^{j-1}$	$\sum_{j=1}^{j=6} c_j L_H^{j-1}$
$\boldsymbol{c_6}$	0.076	-2.0110^{-6}	5.12 10^{-15}	-4.91 10^{-13}	-5.86 10^{-12}	-2.05 10^{-9}	9.63 10^{-7}
$\boldsymbol{c_5}$	-2.963	7.42 10^{-5}	$-$2.35 10^{-13}	3.310^{-11}	-1.28 10^{-9}	1.12 10^{-7}	$-$3.54 10^{-5}
$\boldsymbol{c_4}$	43.79	-1.05 10^{-3}	4.59 10^{-12}	-8.74 10^{-10}	5.88 10^{-8}	-2.52 10^{-6}	4.98 10^{-4}
$\boldsymbol{c_3}$	-308.2	0.0071	-4.51 10^{-11}	1.02 10^{-8}	$-$8.2 10^{-6}	2.66 10^{-5}	-0.0033
$\boldsymbol{c_2}$	1075	-0.02	1.93 10^{-10}	-4.66 10^{-8}	3.76 10^{-6}	-1.07 10^{-4}	0.0094
$\boldsymbol{c_1}$	2368	-2.22	-4.75 10^{-9}	1.27 10^{-6}	-1.11 10^{-4}	0.003	0.8381

A.10. μ=6 analytical model

Table A.10: Analytical Model for $\mu = 6$

$\mu = 6$	$\boldsymbol{\tau = aA^b}$						
Model	$\boldsymbol{a = a_1 f^{a_2}}$		$\boldsymbol{b = b_1 f^4 + b_2 f^3 + b_3 f^2 + b_4 f + b_5}$				
	a_1	a_2	b_1	b_2	b_3	b_4	b_5
	$\sum_{j=1}^{j=6} c_j L_H^{j-1}$	$\sum_{j=1}^{j=6} c_j L_H^{j-1}$	$\sum_{j=1}^{j=6} c_j L_H^{j-1}$	$\sum_{j=1}^{j=6} c_j L_H^{j-1}$	$\sum_{j=1}^{j=6} c_j L_H^{j-1}$	$\sum_{j=1}^{j=6} c_j L_H^{j-1}$	$\sum_{j=1}^{j=6} c_j L_H^{j-1}$
$\boldsymbol{c_6}$	0.077	$-5.95\ 10^{-7}$	$9.12\ 10^{-15}$	$-1.35\ 10^{-12}$	$-2.86\ 10^{-11}$	$3.46\ 10^{-11}$	$8.55\ 10^{-7}$
$\boldsymbol{c_5}$	-2.97	$1.94\ 10^{-5}$	$-3.51\ 10^{-13}$	$5.8\ 10^{-11}$	$-2.10\ 10^{-19}$	$2.68\ 10^{-8}$	$-3.15\ 10^{-5}$
$\boldsymbol{c_4}$	43.49	$-2.5\ 10^{-4}$	$5.37\ 10^{-12}$	$-1.04\ 10^{-9}$	$5.83\ 10^{-9}$	$-1.14\ 10^{-6}$	$4.4\ 10^{-4}$
$\boldsymbol{c_3}$	-300.9	0.0018	$-4.04\ 10^{-11}$	$9.33\ 10^{-9}$	$-6.76\ 10^{-7}$	$1.52\ 10^{-5}$	-0.0029
$\boldsymbol{c_2}$	1018	-0.026	$1.25\ 10^{-10}$	$-3.19\ 10^{-8}$	$2.56\ 10^{-6}$	$-6.09\ 10^{-5}$	0.0083
$\boldsymbol{c_1}$	2946	-2.27	$-3.6\ 10^{-9}$	$1.04\ 10^{-6}$	$-9.64\ 10^{-5}$	0.002	0.8585

A.11. μ=7 analytical model

Table A.11: Analytical Model for $\mu = 7$

$\mu = 7$	$\boldsymbol{\tau = aA^b}$						
Model	$\boldsymbol{a = a_1 f^{a_2}}$		$\boldsymbol{b = b_1 f^4 + b_2 f^3 + b_3 f^2 + b_4 f + b_5}$				
	a_1	a_2	b_1	b_2	b_3	b_4	b_5
	$\sum_{j=1}^{j=6} c_j L_H^{j-1}$	$\sum_{j=1}^{j=6} c_j L_H^{j-1}$	$\sum_{j=1}^{j=6} c_j L_H^{j-1}$	$\sum_{j=1}^{j=6} c_j L_H^{j-1}$	$\sum_{j=1}^{j=6} c_j L_H^{j-1}$	$\sum_{j=1}^{j=6} c_j L_H^{j-1}$	$\sum_{j=1}^{j=6} c_j L_H^{j-1}$
$\boldsymbol{c_6}$	0.07295	$4.84\,10^{-7}$	$1.2\,10^{-14}$	$-2.11\ 10^{-12}$	$8.05\,10^{-11}$	$1.47\,10^{-10}$	$7.66\,10^{-7}$
$\boldsymbol{c_5}$	-2.8	$-2.13\,10^{-5}$	$-4.48\,10^{-13}$	8.3510^{-11}	$-3.81\,10^{-19}$	$1.82\,10^{-8}$	$-2.81\,10^{-5}$
$\boldsymbol{c_4}$	40.726	$3.2\,10^{-4}$	$6.42\,10^{-12}$	$-1.33\ 10^{-9}$	$7.67\ 10^{-8}$	$-9.06\,10^{-7}$	310^{-4}
$\boldsymbol{c_3}$	-280.8	-0.002	$-4.43\,10^{-11}$	$1.05\,10^{-8}$	$-7.43\,10^{-7}$	$1.24\,10^{-5}$	-0.026
$\boldsymbol{c_2}$	944.4	-0.0085	$1.304\ 10^{-10}$	$-3.39\,10^{-8}$	$2.61\,10^{-6}$	$-4.86\,10^{-5}$	0.0074
$\boldsymbol{c_1}$	3523	-2.31	$-3.1\ \ 10^{-9}$	$9.55\,10^{-7}$	$-8.86\,10^{-5}$	0.002	0.875

A.12. μ=8 analytical model

Table A.12: Analytical Model for $\mu = 8$

$\mu = 8$	$\boldsymbol{\tau = aA^b}$						
Model	$\boldsymbol{a = a_1 f^{a_2}}$		$\boldsymbol{b = b_1 f^4 + b_2 f^3 + b_3 f^2 + b_4 f + b_5}$				
	a_1	a_2	b_1	b_2	b_3	b_4	b_5
	$\sum_{j=1}^{j=6} c_j L_H^{j-1}$	$\sum_{j=1}^{j=6} c_j L_H^{j-1}$	$\sum_{j=1}^{j=6} c_j L_H^{j-1}$	$\sum_{j=1}^{j=6} c_j L_H^{j-1}$	$\sum_{j=1}^{j=6} c_j L_H^{j-1}$	$\sum_{j=1}^{j=6} c_j L_H^{j-1}$	$\sum_{j=1}^{j=6} c_j L_H^{j-1}$
$\boldsymbol{c_6}$	0.0632	1.4510^{-6}	$1.044\,10^{-14}$	$-1.79\ 10^{-12}$	$4.42\,10^{-11}$	$2.82\,10^{-9}$	$6.87\,10^{-7}$
$\boldsymbol{c_5}$	-2.41	$-5.85\,10^{-5}$	$-3.78\,10^{-13}$	$6.96\,10^{-11}$	$-2.30\,10^{-9}$	$-8.27\,10^{-8}$	$-2.52\,10^{-5}$
$\boldsymbol{c_4}$	34.87	$8.5\,10^{-4}$	$5.17\,10^{-12}$	$-1.07\ 10^{-9}$	$5.12\ 10^{-8}$	$5.71\,10^{-7}$	$3.5\ 10^{-4}$
$\boldsymbol{c_3}$	-238.5	-0.0055	$-3.33\,10^{-11}$	$8.21\ \ 10^{-9}$	$-5.29\,10^{-7}$	$2.09\,10^{-6}$	-0.0023
$\boldsymbol{c_2}$	788.4	0.026	$9.17\ \ 10^{-11}$	$-2.545\,10^{-8}$	$1.87\,10^{-6}$	$-1.8\,10^{-5}$	0.0067
$\boldsymbol{c_1}$	3793	-2.328	$-2.03\ \ 10^{-9}$	$7.29\,10^{-7}$	$-7\,10^{-5}$	0.0014	0.8888

B | Appendix B

In this appendix, we include the validation results for both approaches for the cases $\mu = -2$ et $\mu = 2$ since they are the most probable ones .

B.1. $\mu = -2$ error analysis

The analytical model linking attenuation to delay can be found in table A.2 .

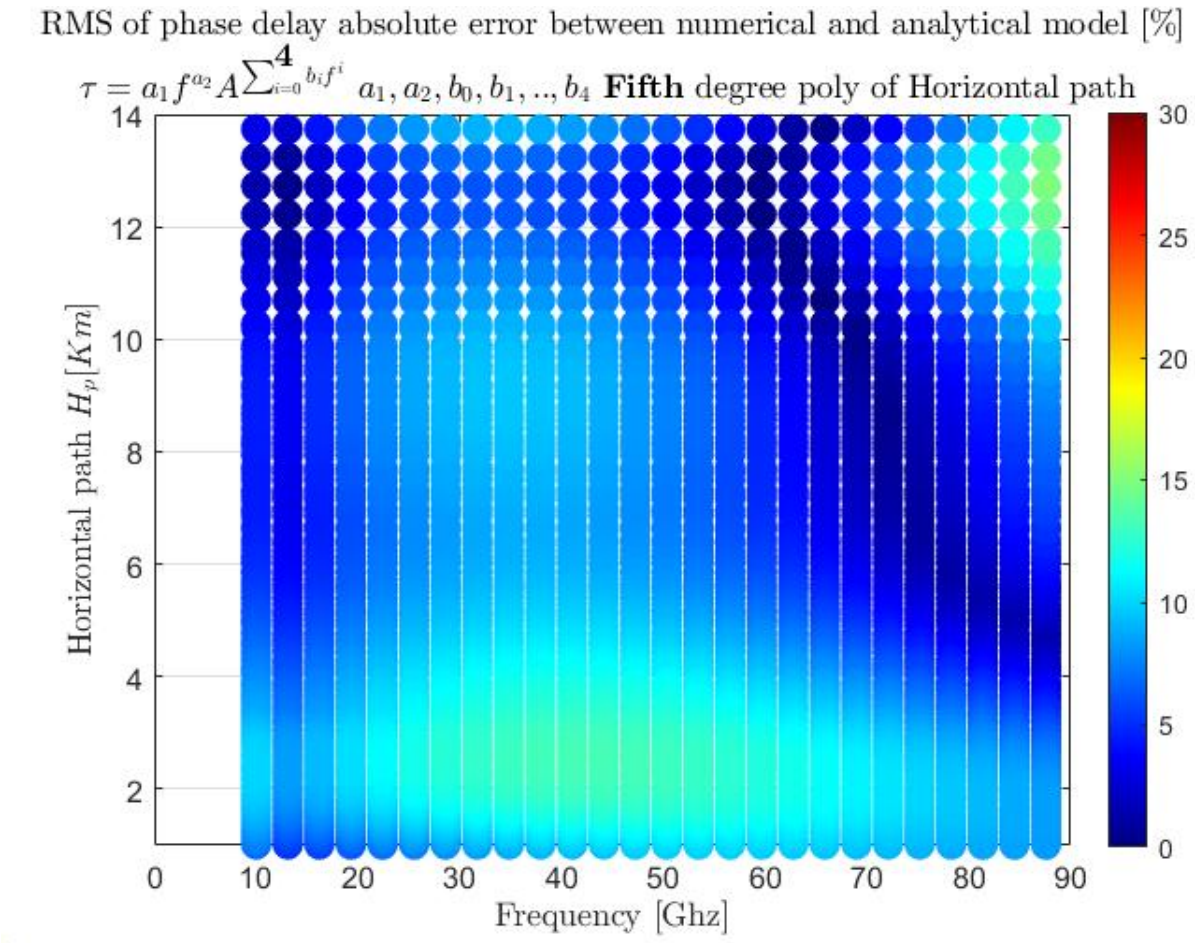

Figure B.1: Rms of the error between Analytical and experimental phase delay

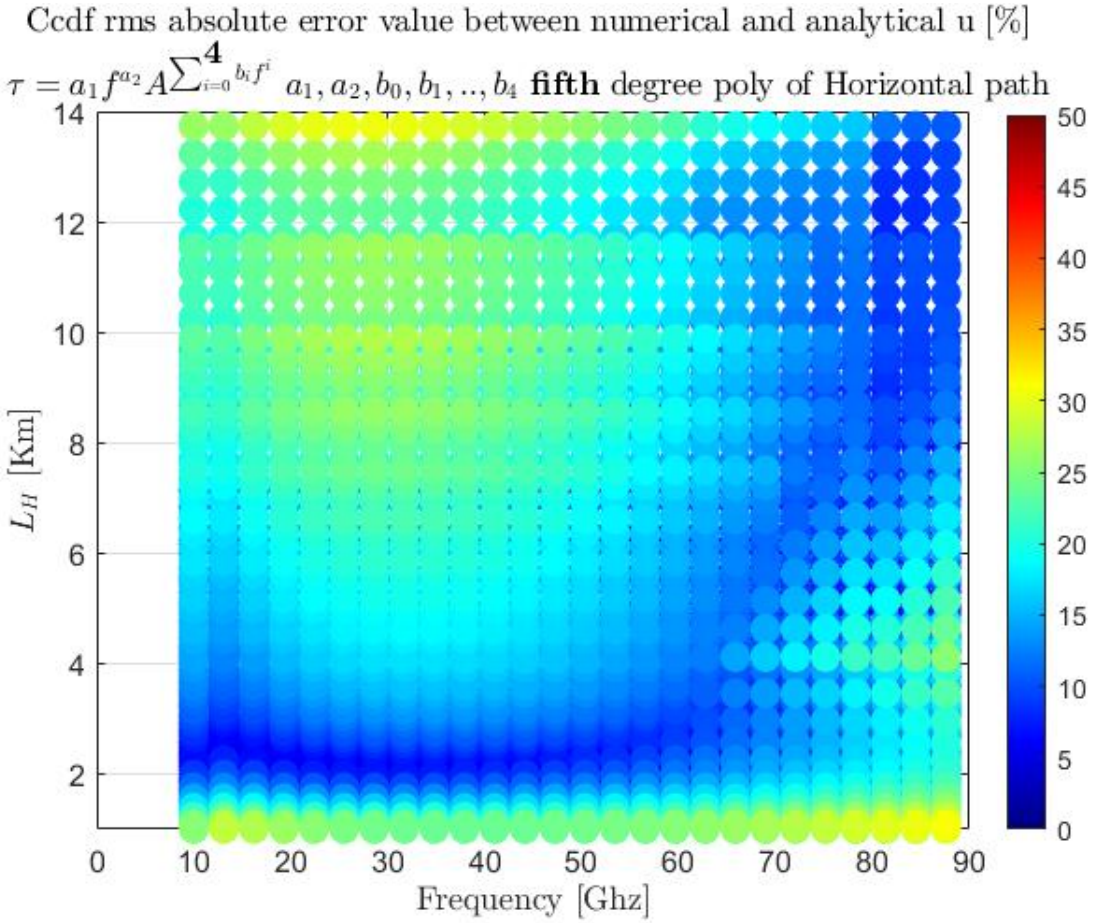

Figure B.2: CCDF rms of the error between Analytical and experimental phase delay

Table B.1: Error between the analytical model and data

	Theoretical Approach			**Ccdf Approach**		
	Mean Value	Min	Max	Mean Value	Min	Max
$\mu = -2$ Model	**8.66**%	0.13 %	24.56 %	**11.06**%	1.16%	30.92%

Comments

- Note that the results shown already include limits for frequency and horizontal path , we recall :
  - 10 GHz $\leq$f $\leq$ 90 GHz
  - $L_H \geq 1$ Km
- Looking at fig. B.2 ,we can confirm that the theoretical rms of the error is satisfying , it's not that good as the original model $\mu = 0$ but with a mean value of 8.66 %, the model still works perfectly
- Concerning the experimental validation fig. B.2 , we have a slighly higher value than the original model ($\mu = 0$) whose mean value is 8.19% .

B.2. $\mu = 2$ error analysis

The analytical model linking attenuation to delay can be found in table A.6 .

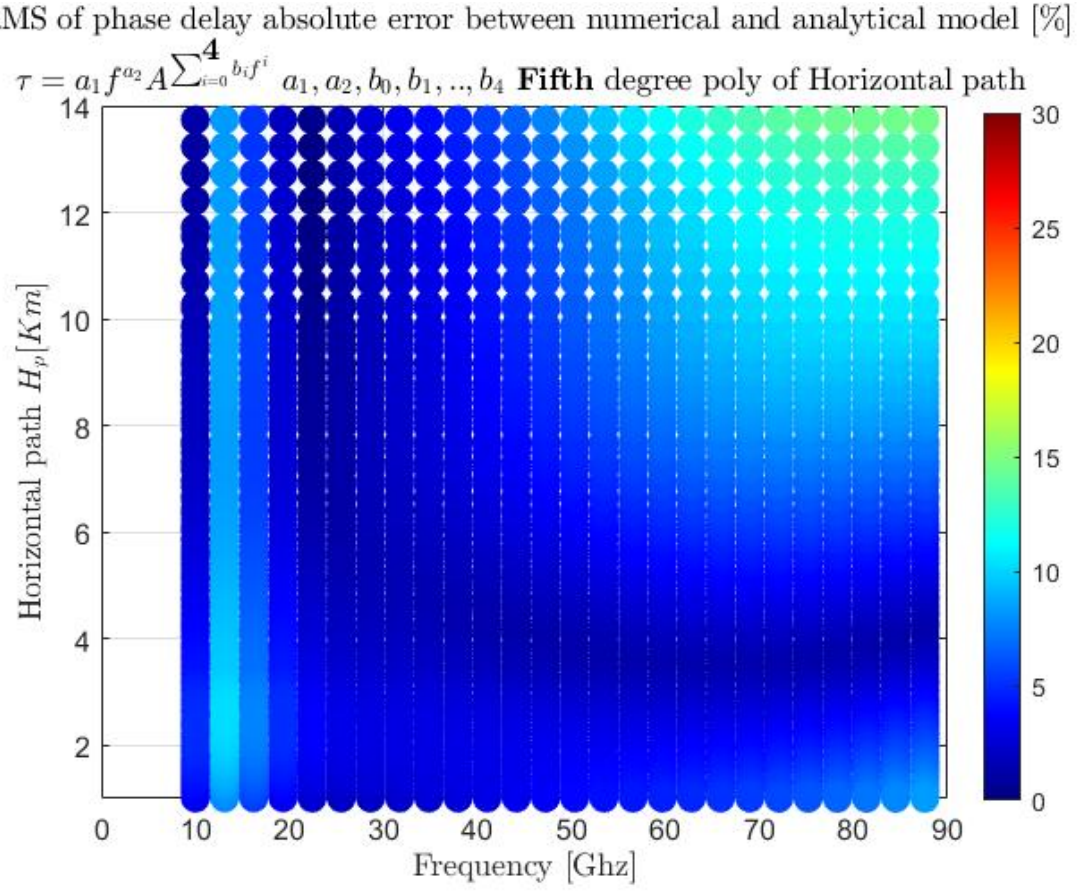

Figure B.3: Rms of the error between Analytical and experimental phase delay

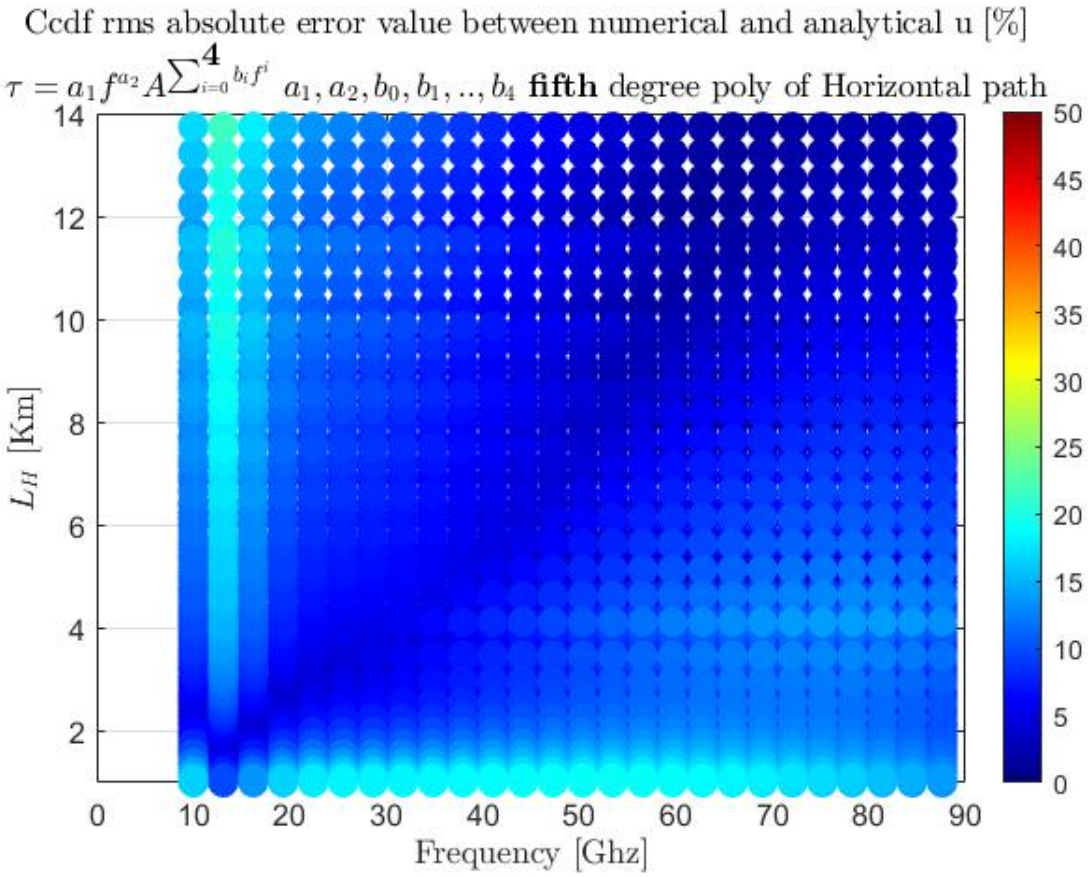

Figure B.4: CCDF rms of the error between Analytical and experimental phase delay

Table B.2: Error between the analytical model and data

	Theoretical Approach			**Ccdf Approach**		
	Mean Value	Min	Max	Mean Value	Min	Max
$\mu = 2$ Model	**3.76**%	0.08 %	14.61 %	**6.48**%	0.63%	21.77%

Comments

- Looking at fig. B.4, we can confirm that the theoretical rms of the error is very satisfying, it's much better than the original model $\mu = 0$ with a mean value of 3.76 %, the model is very accurate
- Concerning the experimental validation fig. B.4, we have very good results with an error mean value of only 6.5%,also much better than the original model $\mu = 0$.

We conclude finally that our analytical model: eq. (3.40) shows that among the three studied cases ($\mu = 0$,$\mu = \pm 2$), the best fitting is for $\mu = +2$